27639

NATIONAL LIBRARY
OTTAWA

CANADA

BIBLIOTHÈQUE NATIONALE
OTTAWA

NAME OF AUTHOR... RALPH A. DiCAPRIO

TITLE OF THESIS... ELECTRICAL COUPLING BETWEEN CELLS OF EARLY XENOPUS EMBRYOS.

UNIVERSITY... UNIVERSITY OF ALBERTA

DEGREE FOR WHICH THESIS WAS PRESENTED... Ph.D.

YEAR THIS DEGREE GRANTED... 1976

Permission is hereby granted to THE NATIONAL LIBRARY OF CANADA to microfilm this thesis and to lend or sell copies of the film.

The author reserves other publication rights, and neither the thesis nor extensive extracts from it may be printed or otherwise reproduced without the author's written permission.

(Signed) Ralph A. DiCapr

PERMANENT ADDRESS:

Dept. of Physiology
Univ. of Alberta
Edmonton, Alberta

DATED April 12, 1976

NL-91 (10-68)

INFORMATION TO USERS

THIS DISSERTATION HAS BEEN
MICROFILMED EXACTLY AS RECEIVED

This copy was produced from a microfiche copy of the original document. The quality of the copy is heavily dependent upon the quality of the original thesis submitted for microfilming. Every effort has been made to ensure the highest quality of reproduction possible.

PLEASE NOTE: Some pages may have indistinct print. Filmed as received.

Canadian Theses Division
Cataloguing Branch
National Library of Canada
Ottawa, Canada K1A ON4

AVIS AUX USAGERS

LA THESE A ETE MICROFILMEE
TELLE QUE NOUS L'AVONS RECUE

Cette copie a été faite à partir d'une microfiche du document original. La qualité de la copie dépend grandement de la qualité de la thèse soumise pour le microfimage. Nous avons tout fait pour assurer une qualité supérieure de reproduction.

NOTA BENE: La qualité d'impression de certaines pages peut laisser à désirer. Microfilmée telle que nous l'avons reçue.

Division des thèses canadiennes
Direction du catalogage
Bibliothèque nationale du Canada
Ottawa, Canada K1A ON4

THE UNIVERSITY OF ALBERTA

ELECTRICAL COUPLING BETWEEN CELLS OF EARLY *Xenopus* EMBRYOS

by

Ralph A. DiCaprio

(C)

A THESIS

SUBMITTED TO THE FACULTY OF GRADUATE STUDIES AND RESEARCH

IN PARTIAL FULFILMENT OF THE REQUIREMENTS FOR THE DEGREE

OF DOCTOR OF PHILOSOPHY

IN

PHYSIOLOGY

DEPARTMENT OF PHYSIOLOGY

EDMONTON, ALBERTA

SPRING, 1976

THE UNIVERSITY OF ALBERTA

FACULTY OF GRADUATE STUDIES AND RESEARCH

The undersigned certify that they have read, and recommend to the Faculty of Graduate Studies and Research, for acceptance, a thesis entitled "Electrical coupling between cells of early *Xenopus* embryos" submitted by R.A. DiCaprio in partial fulfilment of the requirements for the degree of Doctor of Philosophy in Physiology.

A.B. Arnold
(Supervisor)

M. Lipovsky

E.J. Sander

A.N. Spencer

R. Smith

J. Segundo
(External Examiner)

DATE February 25, 1976

ABSTRACT

The electrical coupling between cells of early *Xenopus laevis* embryos was studied using the techniques of linear systems analysis and intracellular recording. Frequency response measurements were made between pairs of cells in two-, four- and eight-cell embryos and theoretical electrical models of these systems were constructed and analyzed using a circuit analysis program on a digital computer. These experiments showed that, in the stages studied, each blastomere was coupled pairwise to all of the other cells in the embryo.

The cell membrane properties were studied during the first cleavage by monitoring the changes in cell membrane resistance and junctional coupling resistance as functions of time. These experiments, as well as investigations using fluorescent tracers and the direct determination that the blastocoel was not electrically isolated from the bathing medium, indicated that the coupling was most probably mediated by specialized intercellular junctions and not by closely apposed cell membranes which have a low specific resistance.

The concentrations of free calcium ions in the external solution and in the interior of individual cells were altered in order to disrupt the electrical coupling. The intracellular injection of calcium did not cause the cells to uncouple, while the lowering of external free calcium ions produced some decrease in the coupling ratio while also affecting the properties of the non-junctional cell membrane.

ACKNOWLEDGEMENTS

I would like to express my gratitude to Doctor A.S. French for his supervision throughout this work. In addition, I would like to thank Doctor E.J. Sanders and Doctor K.G. Pearson for their assistance, advice and encouragement.

I am also grateful to Mrs. Ortella White for her excellent typing and to Mr. Fred Loeffler and Mr. Ken Burt for their production of the photographs used in this work.

TABLE OF CONTENTS

CHAPTER		PAGE
1	INTRODUCTION	1
2	LINEAR SYSTEMS THEORY	5
	2.1 Definition of a linear system	5
	2.2 Application to linear, noise-free systems	6
3	ANALYTICAL TECHNIQUES	13
	3.1 Spectral estimation	13
	3.2 Sampling of continuous signals	14
	3.3 The discrete Fourier transform	15
4	MATERIALS AND METHODS	18
	4.1 Preparation of embryos	18
	4.2 Electrical measurements	18
	4.3 Electrical modelling	21
	4.4 Membrane potentials and sealing	22
	4.5 Staging of embryos	25
	4.6 Electrical properties of the vitelline membrane	26
5	ELECTRICAL COUPLING IN THE TWO-CELL EMBRYO	31
	5.1 Analysis of the two-cell embryo	31
	5.2 Conclusions	42
6	ELECTRICAL COUPLING IN THE FOUR-CELL EMBRYO	46
	6.1 Analysis of the four-cell embryo	46
	6.2 Conclusions	58
7	ELECTRICAL COUPLING IN THE EIGHT-CELL EMBRYO	61
	7.1 Analysis of the eight-cell embryo	61
	7.2 Conclusions	76

CHAPTER		PAGE
8	ELECTRICAL MEMBRANE PROPERTIES DURING FIRST CLEAVAGE	79
	8.1 Introduction	79
	8.2 Resistance measurements	80
	8.3 Frequency response measurements	87
	8.4 Membrane capacitance measurements	91
	8.5 Effects of membrane folding	93
	8.6 Dye diffusion into the blastocoel	95
	8.7 Electrical recording from the blastocoel	98
	8.8 Conclusions	105
9	EFFECTS OF CALCIUM ION CONCENTRATION ON COUPLING	113
	9.1 Introduction	113
	9.2 Effects of low external free calcium concentration	114
	9.3 Effects of intracellular calcium injection	120
	9.4 Conclusions	120
10	DISCUSSION	123
	APPENDIX I	134
	APPENDIX II	139
	BIBLIOGRAPHY	153

LIST OF TABLES

TABLE		PAGE
I	Summary of calculated membrane parameters for two-cell embryos	41
II	Summary of calculated membrane parameters for four-cell embryos	59
III	The connectivity of the seven proposed models for the eight-cell embryo	67
IV	Predicted and measured cell membrane resistance and capacitance of *Xenopus* embryos during the first two cleavages	96
V	Measurements of early blastocoel diameter	97
VI	Summary of results obtained from experiments performed in solutions containing low free calcium	115

LIST OF FIGURES

FIGURE		PAGE
3.1	Flow chart of principle computation routes of spectral analysis package	17
4.1	Basic experimental arrangement for the injection of current into one cell of an embryo while recording the voltage in the injected and adjacent cells	20
4.2	Recorded membrane potentials for embryos at different cleavage stages	23
4.3	The change in cellular input resistance accompanying membrane sealing which follows penetration with a microelectrode	24
4.4	Schematic representation of two-cell embryo incorporating a significant vitelline membrane resistance	28
4.5	Demonstration of vitelline membrane electrical properties	29
5.1	The simplest electrical model of the two-cell embryo	32
5.2	Frequency response and coherence functions between the input and cell 1 of a two-cell embryo	33
5.3	Frequency response and coherence functions between cell 1 and cell 2 of the two-cell embryo used for Fig. 5.2	34
5.4	Reduction of the resistive network model of the two-cell embryo	36
5.5	AC circuit of the two-cell embryo	39
5.6	Two alternative hypothetical models for the two-cell embryo	43
5.7	Reduction of two-cell model containing a junctional resistance to ground	45
6.1	Two possible recording arrangements of a four-cell embryo assuming that the cells are electrically identical	47
6.2	Simplest electrical model of the four-cell embryo	48

FIGURE		PAGE
6.3	Predicted frequency response measurements for the network of Fig. 6.2	49
6.4	Frequency response and coherence functions between two adjacent cells in a four-cell embryo	51
6.5	Frequency response and coherence functions between two diagonally opposed cells in a four-cell embryo	52
6.6	Frequency response and coherence functions between input and cell 1 for the four-cell embryo used in Fig. 6.4	53
6.7	The simplest electrical network capable of explaining the behaviour of a four-cell embryo	54
6.8	Perspective view of the six junctional resistances of Fig. 6.7, arranged in the form of a regular tetrahedron	55
6.9	Electrical network of the four-cell network	57
7.1	Diagrammatic view of an eight-cell embryo, viewed from the animal pole	62
7.2	Two of the seven models (A and G) which were proposed as possibly describing the electrical properties of the eight-cell embryo	64
7.3	The coherence function measured between two recording electrodes while a noise signal was injected into cell 1 of an eight-cell embryo	69
7.4	Experimentally determined frequency response functions between the seven pairs of cells	70
7.5	Theoretical predictions of the frequency response functions of each of the seven pairs of cells with noise injected into cell 1	72-75
8.1	Direct current electrical models of cleaving single-cell embryo	81
8.2	Changes in R_M and R_J during cleavage	83
8.3	Plot of $1/R_M$ vs time data obtained from the value of $R_M(t)$ in Fig. 8.2	85

FIGURE		PAGE
8.4	Gain characteristic of frequency response during first cleavage	88
8.5	Phase characteristic of frequency response during first cleavage	89
8.6	Coherence of frequency response during first cleavage	90
8.7	A.C. electrical model of cleaving single-cell embryo	92
8.8	Fluorescent micrograph of the eight-cell embryo	100
8.9	Fluorescent micrograph of the eight-cell embryo	102
8.10	Measurement of the blastocoel potential	104
8.11	Scanning electron micrographs of the eight-cell embryo used in the experiment of Fig. 8.10	107
8.12	Two higher power views of the half embryo shown at the bottom of Fig. 8.11	109
9.1	Effect of 10^{-5} M free external calcium on intracellular voltage and coupling ratio	117
9.2	Effect of 10^{-5} M free external calcium on intracellular voltage and coupling ratio	118
9.3	Effect of varying external free calcium concentration on sealing rate	119
A.1	Electron micrograph of a section through the cortical region of a *Xenopus laevis* embryo showing the vitelline membrane *in situ*, the perivitelline space and the plasma membrane	142
A.2	Scanning electron micrograph of the animal pole of a four-cell embryo	144
A.3	Light micrograph of a section through the vegetal hemisphere of a four-cell embryo	146
A.4	Scanning electron micrograph of an eight-cell embryo from which one cell has been removed	148
A.5	Scanning electron micrograph of the cell which was removed from the embryo in Fig. A.4	148

FIGURE		PAGE
A.6	An enlargement of the blastocoel cavity of Fig. A.4	150
A.7	Scanning electron micrograph of vegetal pole cells of an eight-cell embryo showing a process from one cell making contact with two other cells by pushing between them	150
A.8	Light micrographs of sections through an eight-cell embryo, cut in a vertical plane	152

CHAPTER 1

INTRODUCTION

The individual cells which make up multicellular organisms do not function in isolation. They may be grouped together to form different tissues and structures which in turn become the component parts of the organism. Cellular interactions may be mediated by intercellular contacts which serve to mechanically anchor the cells to one another, such as tight junctions and desmosomes, or by the intertwining of different cells to form a sturdier overall structure, such as glial-nerve cell interactions. Another degree of cooperation between cells may be achieved by the transfer of information between them via substances released from one cell and received at specific sites on another cell. This is true in the case of hormones which may affect numerous cells and in the case of chemical synapses between neurons, where the interaction is more localized.

If the development and overall activity of the organism is to be coordinated, then there must be a means of communication available in order to achieve these ends. One mechanism for intercellular communication occurs when the interiors of cells are directly connected to each other so that an electric current applied to one cell spreads to an adjacent cell and the amount of spread is too great to be explained by the cells being in the same volume conductor (Bennett, 1966). This type of communication is generally termed electrical coupling. It should be emphasized that although these contacts facilitate the flow of electric current between cells, this may not necessarily

be their physiological function in every system. The electrical pathway may instead serve to mediate the transfer of various substances, such as ions or small molecules, between cells concerned with the control, signaling or equalization of cellular activities.

There are many types of cells which have been found to be electrically coupled. In excitable cells of adult nerve and muscle the coupling serves to facilitate the transfer of electrical impulses between the cells and this type of transmission has been found in many different organisms (Auerbach and Bennett, 1969; Baker and Llinas, 1971; Bennett, Waxman and Pappas, 1969; Furukawa and Furshpan, 1963; Furshpan and Potter, 1959; Sotelo and Llinas, 1972; Hagiwara and Morita, 1962; Watanabe and Grundfest, 1961; Wilson, 1961; Barr, Dewey and Berger, 1965; Keneko, 1971; Nichols and Purves, 1970). Electrical coupling has also been demonstrated in adult non-excitable cells (Kuffler and Potter, 1964; Loewenstein, Socolar, Higashino, Kanno and Davidson, 1965; Sheridan, 1971; Farquhar and Palade, 1963, 1965), cultured cells (Borek, Hagashino and Loewenstein, 1969; Azarnia, Larsen and Loewenstein, 1973; Goshima, 1969, 1970; Johnson and Sheridan, 1971; Gilula, Reeves and Steinbach, 1972; Michalke and Loewenstein, 1971) and in embryonic cells (Ashman, Kanno and Loewenstein, 1960; Bennett, Spira and Pappas, 1972; Furshpan and Potter, 1968; Sheridan, 1968, 1971; Tupper and Saunders, 1971; Ito and Loewenstein, 1969; Palmer and Slack, 1970).

The functional significance of electrical coupling in excitable cells is readily understandable as these cells normally use electrical signals to process or transfer information between cells or to trigger mechanical activity in a group of cells. The function of coupling in

non-excitable cells and particularly embryonic cells is not yet clear although there has been considerable speculation (Loewenstein, 1968; Bennett, 1973) that the transfer of material between these cells via the electrical pathway may serve to control the growth, division and differentiation of the embryonic cells.

In many cases where ultrastructural studies have been undertaken on various cell types, a correlation has been found between the presence of gap junctions and the existence of electrical coupling between the cells (McNutt and Weinstein, 1970, 1973; Rose, 1971). These junctions are characterized by an intercellular gap of 20 Å in thin sections and by a hexagonal array of intramembranous particles in freeze-cleaved preparations. These junctions are also capable of transferring small molecules between cells in adult (Rose, 1971) and embryonic cells (Sheridan, 1971).

A first step in determining the role of intercellular communication in embryonic cells is to investigate the degree of coupling found in developing embryos and how it changes during development. Amphibian embryos have been used for some time as model systems in embryology, and measurements have been made of electrical coupling during their development (Palmer and Slack, 1970; Ito and Hori, 1966; Warner, 1973). The objective of the research presented here was to determine the degree of electrical coupling during the formation of the first three cleavage furrows of *Xenopus laevis* embryos as well as the properties of the junctional and non-junctional membranes during development. These problems were investigated using the techniques of linear systems theory, primarily spectral analysis. These procedures

have been primarily used in the analysis of neurophysiological systems (cf. Terzuolo, 1969; French, Holden and Stein, 1972; French and DiCaprio, 1975) but they may be applied to any biological system which has clearly defined input and output electrical signals. The result of this analysis as applied to the case of electrically coupled embryonic cells is a mathematical description of the input and output properties of the system. The structures that mediate the coupling are treated as "black boxes" and are not accessible via these techniques, although analytical models of the system may be constructed in order to give some information concerning the possible construction of these pathways.

CHAPTER 2

LINEAR SYSTEMS THEORY

2.1 *Definition of a linear system:*

In a linear system, which may be characterized by linear algebraic equations, difference equations or differential equations, the output of the system is directly proportional to the input. In other words, if the input to the system is $x(t)$ and the output is $y(t)$ then:

$$y(t) = f(x(t))$$

and if K is any arbitrary constant:

$$K\,y(t) = K\,f(x(t)) \qquad 2.1$$

Linear systems are also characterized by the principle of superposition, that is, if:

$$y_1(t) = f(x_1(t))$$

and

$$y_2(t) = f(x_2(t))$$

then

$$y_1(t) + y_2(t) = f(x_1(t)) + f(x_2(t)) \qquad 2.2$$

A system is linear if and only if it satisfies Eq. 2.2.

The linear systems discussed here may be further classified as lumped-parameter, time-invariant linear systems. In a lumped-parameter model of an electrical system, the energy in the system is stored or dissipated by distinct elements, resistors, capacitors and inductors. Any disturbance in the system is propagated instantly to all elements of the system and the physical measurements at each element, such as the voltage across and the current through an element, are related by a single physical constant. In a time-invariant system, a response $y(t)$ to an input $x(t)$ will be the same if the input is delayed by a time τ so that if:

$$y(t) = f(x(t)) \ .$$

Then:

$$y(t - \tau) = f(x(t - \tau)) \qquad 2.3$$

2.2 *Application to linear, noise-free systems:*

For a linear, noise-free system with a single input function $x(t)$ and a single output function $y(t)$ the output is related to the input by the convolution integral:

$$y(t) = \int_0^t x(\tau)h(t,\tau)d\tau \qquad 2.4$$

and if the system is time-invariant a function $h(t)$ exists such that:

$$y(t) = \int_0^t x(\tau)h(t - \tau)d\tau \qquad 2.5$$

where $h(t)$ is the impulse response of the system (Lathi, 1965).

The mathematical treatment of the input-output relation given in Eq. 2.5 is greatly simplified if it is transformed to the s domain, where s is a complex variable in the form $\sigma + j\omega$, where $j = \sqrt{-1}$. This may be accomplished by use of the single-sided Laplace transform (Lathi, 1965). The single-sided Laplace transform is a linear operator and is defined by:

$$L\{y(t)\} = Y(s)$$

$$= \int_0^\infty y(t)e^{-st}dt \qquad 2.6$$

and its inverse is given by:

$$L^{-1}\{Y(s)\} = \frac{1}{2\pi j}\int_{\sigma-j}^{\sigma+j} Y(s)e^{ts}ds \qquad 2.7$$

$Y(s)$ and $y(t)$ then form a Laplace transform pair:

$$y(t) \leftrightarrow Y(s) \ .$$

Some useful properties of the Laplace transform are:

a) Linearity

$$K\,y(t) \leftrightarrow K\,Y(s)$$

$$y(t) + z(t) \leftrightarrow Y(s) + Z(s)$$

b) Scaling

For $a > 0$

$$y(at) \leftrightarrow \frac{1}{a} Y(\frac{s}{a})$$

c) Time shift

For $t_0 > 0$

$$y(t - t_0) \leftrightarrow Y(s)e^{-st_0}$$

d) Real convolution

$$\int_0^t y(t - \tau)f(\tau)d\tau \leftrightarrow Y(s)F(s) \ .$$

When the convolution property of the Laplace transform is applied to Eq. 2.5 the result is:

$$Y(s) = H(s)X(s) \qquad 2.8$$

If the input function $x(t)$ is a unit impulse or Dirac delta function $\delta(t)$ defined as:

$$\int_{-\infty}^{\infty} \delta(t)dt = 1$$

$$\delta(t) = \begin{cases} 0 \text{ if } t \neq 0 \\ \infty \text{ if } t = 0 \end{cases} \qquad 2.9$$

Then the Laplace transform of $x(t)$ is unity so that Eq. 2.8 becomes:

$$Y(s) = H(s)$$

The Laplace transform of the response to a unit impulse input is the Laplace transform of the weighting function $h(t)$. $H(s)$ is also called the transfer function of the system and is only defined for linear, time-invariant, noise-free systems. The transfer function will completely characterize the input-output relations of such a system.

An alternative representation of the transfer function is the frequency response function, $H(f)$, given by the single-sided Fourier transform of $h(t)$:

$$H(f) = \int_0^\infty h(t)e^{-j2\pi ft}dt \qquad 2.10$$

The frequency response $H(f)$ is generally a complex function which may be separated into two real functions:

$$G(f) = |H(f)| \qquad 2.11$$

and

$$P(f) = \arctan H(f) \qquad 2.12$$

where $G(f)$ is the gain and $P(f)$ the phase of the frequency response function.

When the input $x(t)$ to the system is a stationary stochastic

process, the autocovariance function $\rho_{xx}(\tau)$ of $x(t)$ is defined as (Jenkins and Watts, 1968):

$$\rho_{xx}(\tau) = \lim_{T\to\infty} \frac{1}{2T} \int_{-T}^{T} x(t)x(t+\tau)dt \qquad 2.13$$

and the autocovariance $\rho_{yy}(\tau)$ of the output $y(t)$ as:

$$\rho_{yy}(\tau) = \lim_{T\to\infty} \frac{1}{2T} \int_{-T}^{T} y(t)y(t+\tau)dt \qquad 2.14$$

and the forward cross-covariance $\rho_{xy}(\tau)$ from the input to the output as:

$$\rho_{xy}(\tau) = \lim_{T\to\infty} \frac{1}{2T} \int_{-T}^{T} x(t)y(t+\tau)dt \qquad 2.15$$

The power spectra of the input and the output and the cross power spectrum can be obtained from the Fourier transforms of the corresponding input, output and cross-covariance functions according to the Wiener-Kinchine theorem (Carlson, 1968).

The Fourier transform $X(f)$ of a function $f(t)$ is defined by:

$$X(f) = \int_{-\infty}^{\infty} f(t)e^{-j2\pi ft} \qquad 2.16$$

and the inverse transform by:

$$x(t) = \frac{1}{2\pi} \int_{-\infty}^{\infty} X(f)e^{j2\pi ft}dt \qquad 2.17$$

The input power spectrum $S_{xx}(f)$, the output power spectrum

$S_{yy}(f)$ and the cross-power spectrum $S_{xy}(f)$ are therefore given by:

$$S_{xx}(f) = \int_{-\infty}^{\infty} \rho_{xx}(\tau) e^{-j2\pi f\tau} d\tau$$

$$S_{yy}(f) = \int_{-\infty}^{\infty} \rho_{yy}(\tau) e^{-j2\pi f\tau} d\tau \qquad 2.18$$

$$S_{xy}(f) = \int_{-\infty}^{\infty} \rho_{xy}(\tau) e^{-j2\pi f\tau} d\tau$$

The frequency response function can then be obtained from the above power spectra using the following relations:

$$H(f) = \frac{S_{xy}(f)}{S_{xx}(f)} \qquad 2.19$$

and

$$S_{yy} = |H(f)|^2 S_{xx}(f) \qquad 2.20$$

One additional function which may be computed from the power spectra is the coherence function, $\gamma^2(f)$, given by:

$$\gamma^2(f) = \begin{cases} \dfrac{|S_{xy}(f)|^2}{S_{xx}(f) \cdot S_{yy}(f)} \; ; \; S_{xx}(f) \cdot S_{yy}(f) > 0 \\ 0 \; ; \; S_{xx}(f) \cdot S_{yy}(f) = 0 \end{cases} \qquad 2.21$$

The coherence function is a normalized measure of the extent to which the linear frequency response function predicts the input-output behaviour of the system (Bendat and Piersol, 1966). Coherence varies over the range

$0 \leq \gamma^2(f) \leq 1$ and the coherence of a linear, noise-free system would be unity at all frequencies.

CHAPTER 3

ANALYTICAL TECHNIQUES

3.1 *Spectral estimation*

The power spectra defined by Eq. 2.18 are in practice obtained for finite time functions $f_T(t)$ where:

$$f_T(t) = \begin{cases} f(t) & 0 \leq t \leq T \\ 0 & T < 0,\ t > T \end{cases} \qquad 3.1$$

In place of the power spectra, an estimate of the power spectrum is defined as the sample spectrum $\hat{S}_{xx}(f)$ (Jenkins and Watts, 1968). Then, in place of Eq. 2.18 the sample spectrum is given by:

$$\hat{S}_{xx}(f) = \int_{-T}^{T} \hat{\rho}_{xx}(\tau) e^{-2\pi f \tau} d\tau \qquad 3.2$$

where $\hat{\rho}_{xx}(\tau)$ is the sample autocovariance given by:

$$\hat{\rho}_{xx}(\tau) = \frac{1}{2T} \int_{-T}^{T} x(t)x(t+\tau)dt \qquad 3.3$$

An alternative definition of $S_{xx}(f)$ is given by:

$$\hat{S}_{xx}(f) = \frac{1}{T} \int_0^T X_T(t) e^{-j2\pi ft} dt \int_0^T X_T(t') e^{j2\pi ft'} dt'$$

$$= \frac{1}{T} X_T(f) \cdot X^*(f)$$

$$= \frac{1}{T} |X_T(f)|^2 \qquad 3.4$$

where $X_T(f)$ is the Fourier transform of $x(t)$ and $X_T^*(f)$ is its complex conjugate.

The direct method of spectral estimation using Eq. 3.4 has only been computationally efficient since the rediscovery of the fast Fourier transform (FFT) algorithm by Cooley and Tukey (1965) which makes possible the economical computation of the discrete Fourier transform. This method has been used for the computation of all the spectra in this work.

3.2 *Sampling of continuous signals:*

To compute $S_{xx}(f)$ using a digital computer and the FFT algorithm, the continuous time function $\{x(t), -\infty < t < \infty\}$ must be transformed to a discrete time process $\{X_{(\Delta t)}(n) : n = 0, \pm 1, \pm 2 \ldots\}$ which is formed by setting:

$$X_{(\Delta t)}(n) = X(n\Delta t) \qquad 3.5$$

where Δt is determined from the Nyquist sampling theorem (Lathi, 1965). If $x(t)$ is a signal of finite energy band-limited by W Hz, then $x(t)$ can only be recovered error-free from $X_{(\Delta t)}(n)$ if:

$$1/\Delta t \geq 2W .$$

Half the sampling rate, $1/2\Delta t$, is called the Nyquist frequency, f_N. If there is any power in $S_{xx}(f)$ for $f > f_N$ then this power will alias as power at frequencies $f < f_N$ which will result in an incorrect estimate

of $\hat{S}_{xx}(f)$. When taking regular samples, Δt must therefore be chosen so that $f_N > f$ where $S_{xx}(f) \neq 0$ for all f.

3.3 *The discrete Fourier transform:*

Use of the regular sampling technique discussed above on the input and output finite time records $X_T(t)$ and $Y_T(t)$ results in a series of N numbers, $X_{T(\Delta t)}(n)$ and $Y_{T(\Delta t)}(n)$ for $n = 0, 1, \ldots N-1$. A discrete set of numbers may be associated with the time function:

$$x'(t) = \sum_{n=0}^{N-1} x(n\Delta t)\delta(t - n\Delta t)$$

whose Fourier transform is given by:

$$X'(f) = \int_{-\infty}^{\infty} x'(t)e^{-j2\pi ft}dt$$

$$= \sum_{n=0}^{N-1} x(n\Delta t)e^{-j2\pi ft}dt \qquad 3.6$$

This method of obtaining the Fourier transform of $x(n\Delta t)$ provides a means of defining the discrete Fourier transform of a set of N numbers $x(n)$, $n = 0, 1, \ldots N-1$ as:

$$X(m) = \sum_{n=0}^{N-1} x(n)e^{-j2\pi nm/N} \qquad 3.7$$

and the inverse transform by:

$$x(n) = \frac{1}{N} \sum_{n=0}^{N-1} X(m)e^{j2\pi nm/N} \qquad 3.8$$

Applying Eq. 3.7 to a series of alias-free samples of $x(t)$ taken at regular intervals Δt from a record of length $T = N\Delta t$ gives the Fourier coefficients of $X(n\Delta t)$, $X(m\Delta f)$ where the coefficients are complex and given by:

$$X(m\Delta f) = A_m + jB_m \qquad 3.9$$

The power spectra of Eq. 2.18 can thus be calculated as in Eq. 3.4 from the Fourier coefficients of the sampled time series given in Eq. 3.9. The principal computational routines are shown in Fig. 3.1 and have been fully described elsewhere (French and Holden, 1971a, b; French, 1973).

Frequency response functions are presented in the form of Bode plots (d'Azzo and Houpis, 1966) which consist of the logarithm of the gain, $G(f)$, in decibels, and the phase, $P(f)$, in degrees, plotted against the logarithm of frequency.

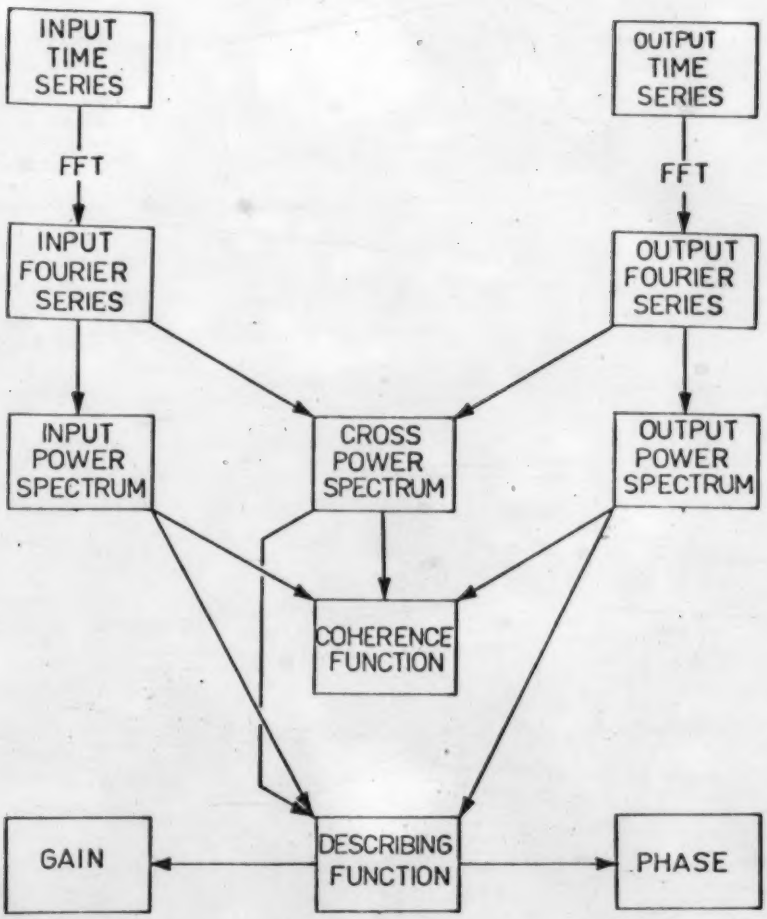

Fig. 3.1 Flow chart of principle computation routes of spectral analysis package.

CHAPTER 4

MATERIALS AND METHODS

4.1 *Preparation of embryos:*

Embryos of *Xenopus laevis* were obtained by subcutaneous injection of adult animals with gonadotrophic hormone (Parke-Davis and Co., Antuitrin-S). Males and females received 500 and 1,000 IU of the hormone respectively. Embryos were kept in Steinberg's solution (Hamburger, 1960) made up as follows: 17 g NaCl was dissolved in 100 ml of distilled water; 250 mg KCl in 50 ml; 400 mg $Ca(NO_3)_2$ 4 H_2O in 50 ml; 1,025 mg $MgSO_4$ in 50 ml; 2,800 mg Tris was added to the mixture of the four different solutions described above. The final volume was made up to 5,000 ml with distilled water and the pH of the final solution was adjusted to 7.4 with 1 N HCl. Embryos were then partially de-jellied for 2 minutes at room temperature in a solution of fresh Papain-cysteine solution made by dissolving 1 g of L-cysteine hydrochloride hydrate in 3 ml of 10% NaOH; final volume was made up to 1,000 ml with Steinberg's solution; 1 g of Papain was added to obtain the final reagent. The enzyme mixture was not allowed to completely remove the jelly coat, in order to avoid damage to the vitelline or plasma membranes. The embryos were then washed a minimum of six times in Steinberg's solution to remove all traces of the enzyme mixture. The embryos were then stored at 4°C until the time of the experiments, which were performed at room temperature.

4.2 *Electrical measurements:*

The basic recording arrangement used for investigating the

electrical properties of *Xenopus* embryos is illustrated in Fig. 4.1. The embryos were placed on a layer of paraffin wax in a Petri dish filled with Steinberg's solution. In all experiments glass microelectrodes, filled with 3 M KCl, were used for the recording of intracellular voltage and injection of stimulation currents. The electrodes were pulled from glass capillary tubes of 0.9-1.1 mm ID (Kimak No. 34507) on a vertical electrode puller (Narishige, PE-2). The recording electrodes were interfaced to resistance and capacitance compensated bridge electrometers (W.P. Instruments, M4-A) by Ag/AgCl junctions and the bathing solution was returned to electrical ground via a 3 M KCl-Agar bridge and an Ag/AgCl junction. The resistance of the microelectrodes used was in the range 3-5 $\times$ 10^6 Ω. In each experiment, three electrodes were used, two for recording intracellular voltage, and one for injection of intracellular current. A 10^8 Ω resistance was placed in series with the current injection electrode so as to allow current measurement independent of electrode resistance. Sinusoidal stimulating currents were obtained from a function generator (Hewlett Packard, 3301A) and white noise stimulation from a diode noise generator (French, 1974) with a flat power bandwidth from 1 to 400 Hz. The white noise was band-limited to the desired frequency by three cascaded three-pole Butterworth low-pass active filters, giving a total attenuation of 54 dB/octave above the corner frequency. Voltage and current measurements were recorded at the time of the experiment on a four-channel paper chart recorder (Beckman R411) and monitored on an oscilloscope (Tektronix 565).

The input and output signals from two- and four-cell experiments were first recorded on a four-channel FM tape recorder (Thermionics,

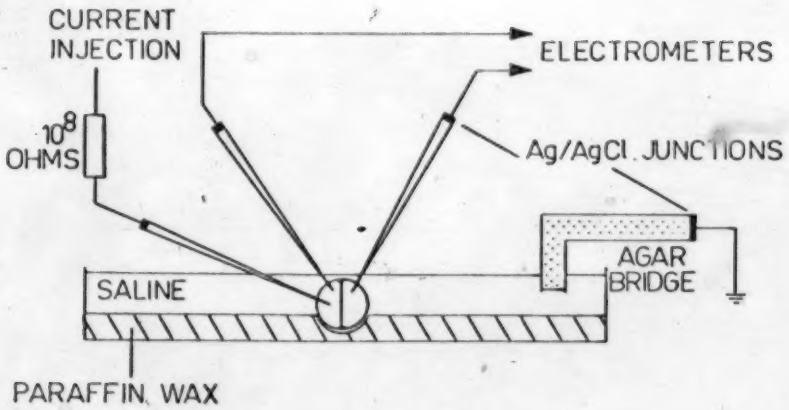

Fig. 4.1 Basic experimental arrangement for the injection of current into one cell of an embryo while recording the voltage in the injected and adjacent cells.

T3000). These records were later replayed and sampled by a ten-bit analog to digital converter and stored in digital form on a DEC-tape. The spectral analysis was then performed using a standard record length of 512 complex numbers. Using a sampled time series of 512 points, the resolution of the spectral estimate obtained from the transform will be $1/(512\ t_0)$, where t_0 is the sample interval. Successive input and output spectra were then averaged to produce the final estimate of the spectrum, from which the cross-spectrum and coherence function were calculated. The frequency response plots from the two- and four-cell experiments were computed from 50 averaged spectra. Other experiments were performed by sampling the experimental data on-line with a ten-bit analog to digital converter and storing the sampled values on a magnetic disc using a PDP 11/40 computer. Spectral estimates were then computed at the end of each experiment in the same manner as described above.

4.3 *Electrical modelling:*

Electronic circuit models of the systems under study were initially analyzed with a computer simulation program (IBM application program GH 20-0170-2, electronic circuit analysis program [ECAP]).using the University of Alberta IBM 360/67 computer. Later a circuit simulation program was written in FOCAL for the PDP 11/40 computer (*F*ocal *C*ircuit *A*nalysis *P*rogram, FCAP). This program was adapted from a similar program written in BASIC (Digital Equipment Computer Users Society No. 11-12, see Appendix I). These programs enabled the user to simulate an electrical network containing resistors, capacitors,

inductors and independent voltage sources. The programs describe the electrical behaviour of the network by specifying the node voltages of the network when a voltage source is applied between any two nodes. An excellent review of computer-aided circuit analysis is contained in McCalla and Pederson (1971).

4.4 *Membrane potentials and sealing:*

The penetration of a recording microelectrode into the embryo was detected by observing the transmembrane potential as the electrode was inserted into a cell. The membrane potentials were measured and used to establish the correct stage of the embryo (Fig. 4.2). These data were also compared with previous measurements made by other investigators (Palmer and Slack, 1970; de Laat *et al.*, 1973). Correct positioning of the current injection electrode was monitored by connecting a slow sinusoidal voltage (0.5 Hz) with an amplitude of 1 V peak-to-peak to the electrode before impalement. When the electrode was successfully inserted into the embryo, a sinusoidal modulation of the membrane potential could be detected by the recording electrodes.

After the electrodes have penetrated the cell membrane, a sealing process occurs which initially alters the observed properties of the embryo. This sealing process has been reported before in *Xenopus* (Palmer and Slack, 1970; Bluemink, 1972) and other tissues (Oliveira-Castro and Loewenstein, 1971) and produces an apparent increase in the cell membrane resistance. This process is relatively slow, as shown in Fig. 4.3. There is a period from about 4-6 minutes after the insertion of the electrode where the measured input resistance of the embryo rises

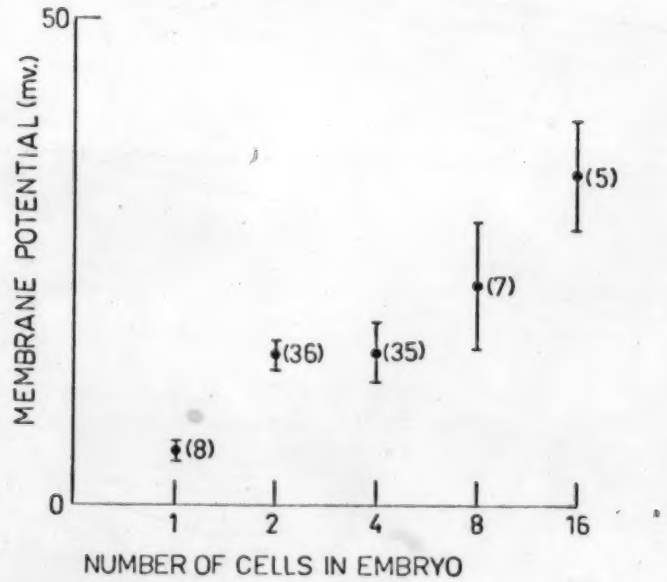

Fig. 4.2 Recorded membrane potentials for embryos at different cleavage stages. The upper and lower limits on each measurement are the standard deviations, and the figures in parentheses next to each result are the total number of observations used.

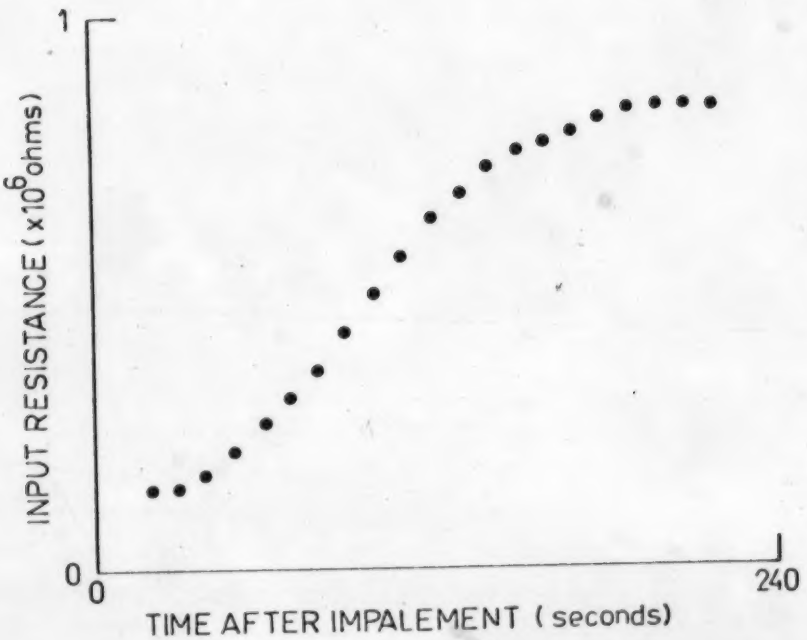

Fig. 4.3 The change in cellular input resistance accompanying membrane sealing which follows penetration with a microelectrode. This sealing reaction is also indicated by the formation of a heavily pigmented ring around the electrode. This data was obtained from a two-cell embryo.

and then stabilizes. The sealing process is accompanied by the formation of a pigmented ring around the microelectrode at the point where it penetrates the cell membrane.

In all experiments the input resistance was monitored to ensure that complete membrane sealing had occurred before the experiment was allowed to proceed.

4.5 *Staging of embryos:*

For all experiments on early *Xenopus* embryos it was important to correctly determine the stage of an embryo before continuing with the experiment since it was not possible to judge from the external appearance alone whether a cleavage had completely divided a cell into two daughter cells. The second embryonic cleavage always started before the completion of the first, making it impossible to define a cleavage stage solely on external morphology. In categorizing embryos as two-cell or four-cell stages, four separate criteria were used. Each of these criteria had to be satisfied throughout the experiment before the result was accepted as being typical of that embryonic stage. The criteria were as follows:

(1) External morphology of the embryo. In order to distinguish a complete two-cell embryo the data of Bluemink (1971) was used which indicates that the first cleavage is complete approximately 35 minutes after its initial appearance as a shallow groove. This has been confirmed by scanning electron microscopy of the internal surfaces (Sanders and Singal, 1973) which indicates that the first cleavage is complete by the time the second cleavage is a shallow groove. Four-cell

embryos were not used until after the appearance of the third cleavage furrow.

(2) Membrane potential. As illustrated earlier, the membrane potential of the embryonic cells varies substantially with the stage. Although this is not a good criterion for the separation of two- and four-cell stages, it is useful for rejecting one- and eight-cell stages.

(3) Coupling ratio. This parameter can be measured immediately after the cells are penetrated and allows a clear distinction between single cells, with a coupling ratio of unity, and other embryos.

(4) Frequency response function. This was a retrospective selector because it was not available until after the experiment had been completed. However, a result which was clearly outside the normal limits of variation was rejected as probably having changed stage during the experiment.

4.6 *Electrical properties of the vitelline membrane:*

The fertilized *Xenopus* embryo is surrounded by a fertilization or vitelline membrane. As a first step in the study of the electrical properties of these embryos, the electrical characteristics of the vitelline membrane were determined. Previous investigators (Slack and Palmer, 1969; Palmer and Slack, 1970) have left the vitelline membrane intact, but if this membrane possesses a significant resistance or capacitance, it would seriously bias the measurement of the electrical properties of the cell membrane. Measurements of the degree of electrical coupling between cells could also be affected if the resistance of the vitelline membrane was of the same order of magnitude as

the plasma membrane. Some coupling between cells would then be measured relative to external medium even if there were no specialized contacts providing a pathway between the cells. This situation is illustrated in Fig. 4.4. If a current is injected into cell 1 then the voltage observed in the perivitelline space is given by:

$$V_X = V_A \cdot \frac{R_V}{R_A + R_V} \qquad 4.1$$

In the absence of direct electrical coupling between the cells no current flows in the resistor R_B, the voltage $V_B = V_X$ and the observed coupling ratio will be:

$$V_B/V_A = V_X/V_A = \frac{R_V}{R_A + R_V} \qquad 4.2$$

The apparent coupling ratio will therefore approach 1 if $R_V >> R_A$. An analogous situation has been described in the morula surface of *Triturus* which has a high resistance and increases the apparent coupling between blastomeres (Ito and Loewenstein, 1969).

It was possible to make direct measurements of the vitelline membrane resistance by placing a microelectrode into the perivitelline space. The recording arrangement and a record from a typical experiment are shown in Fig. 4.5. A current injecting electrode was placed in one cell of a two-cell embryo and a recording electrode was inserted into the adjacent cell. A second recording electrode was then placed next to the embryo above the cleavage furrow and slowly driven through the vitelline membrane into the perivitelline space. A small hyper-

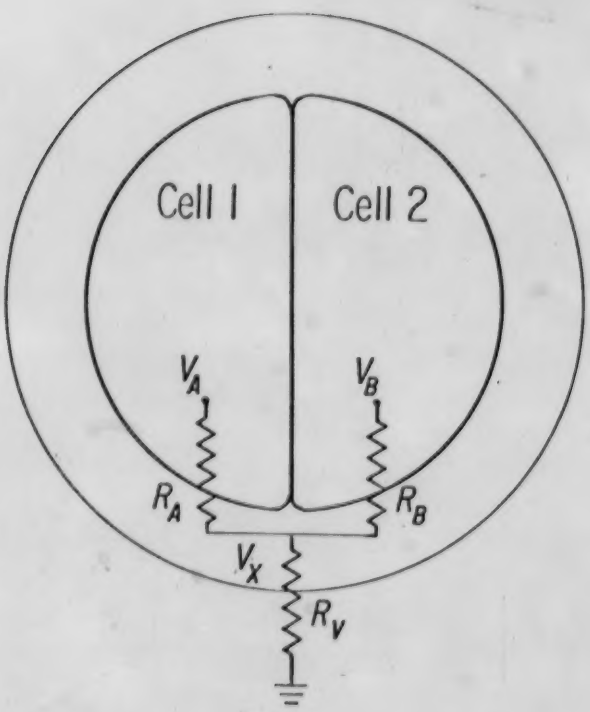

Fig. 4.4 Schematic representation of two-cell embryo incorporating a significant vitelline membrane resistance.

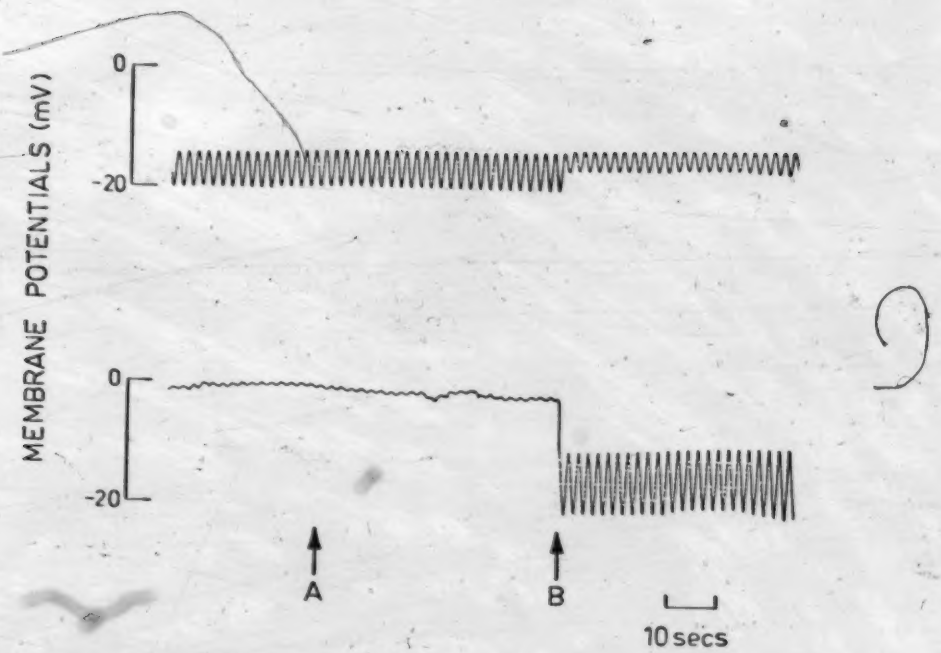

Fig. 4.5 Demonstration of vitelline membrane electrical properties. A microelectrode has been inserted into one cell of a two-cell embryo and is injecting sinusoidal current. A second electrode has been placed in the adjacent cell and is recording the coupled modulation (upper trace). A third electrode is positioned just outside the embryo in the saline medium and is recording some unavoidable pickup of the stimulating voltage (lower trace). At time A, the third electrode is pushed through the vitelline membrane into the perivitelline space and records a small negative membrane potential, but no increase in sinusoidal modulation. At time B, the electrode is pushed further into the embryo and through the first cell membrane, at which point a normal membrane potential with a large sinusoidal modulation is observed. At the same time, the physical movement causes the electrode in the adjacent cell to become somewhat unsealed and its modulation level decreases. The absence of modulation in the vitelline membrane potential is interpreted to mean that it has very low resistance.

polarizing membrane potential was seen but there was no detectable modulation of the potential in the perivitelline space. This indicates that the vitelline membrane resistance is much smaller than the plasma membrane resistance.

Another experiment provided evidence that the resistance of the vitelline membrane is small compared to the cell membrane resistance. It is possible at the two-cell stage to remove the vitelline membrane with forceps, although this is a very delicate procedure and the embryo may be easily damaged. However, in eight experiments where the vitelline membrane was removed without visible damage to the embryo, there were three instances where the embryo had identical electrical properties before and after removal of the vitelline membrane.

Electron micrographs of the vitelline membrane also indicate that it possesses a loose fibrillar structure which is compatible with its low ionic resistance (see Appendix II). In light of these indications that the vitelline membrane resistance was negligible compared with the plasma membrane resistance of the cells, all succeeding experiments were conducted with the vitelline membrane intact.

CHAPTER 5

ELECTRICAL COUPLING IN THE TWO-CELL EMBRYO

5.1 *Analysis of the two-cell embryo:*

The simplest electrical model of a two-cell *Xenopus* embryo is shown in Fig. 5.1. This is a lumped-parameter model with R_M and C_M denoting the cell membrane resistance and capacitance respectively and with R_J being the junctional, or coupling, resistance. The plasma membrane components R_M and C_M for each cell are assumed to be identical. In addition, the 10^8 Ω resistance used for current injection is included in the circuit so that all calculations may be done in terms of voltage ratios. The parameters that may be obtained experimentally for this network are the input voltage, V_i, the intracellular voltage of cell 1, V_1, and the intracellular voltage of cell 2, V_2, all measured with respect to ground. In order to calculate R_M, R_J and C_M, it was necessary to compute one of two frequency response functions from these voltages, that is, between the input and cell 1, or between cell 1 and cell 2. A D.C. measurement of the embryo's input resistance was also required.

Typical measurements of these frequency response functions are shown in Figs. 5.2 and 5.3. The value of the coherence function for both plots is high (> 0.9) indicating that a linear model is a good predictor of the system's behaviour. The low frequency asymptotes of the gain curves in Figs. 5.2 and 5.3 provide a value for the D.C. voltage ratios, V_1/V_i and V_2/V_1. Since under direct current conditions the impedance of the capacitance elements in Fig. 5.1 approach a value

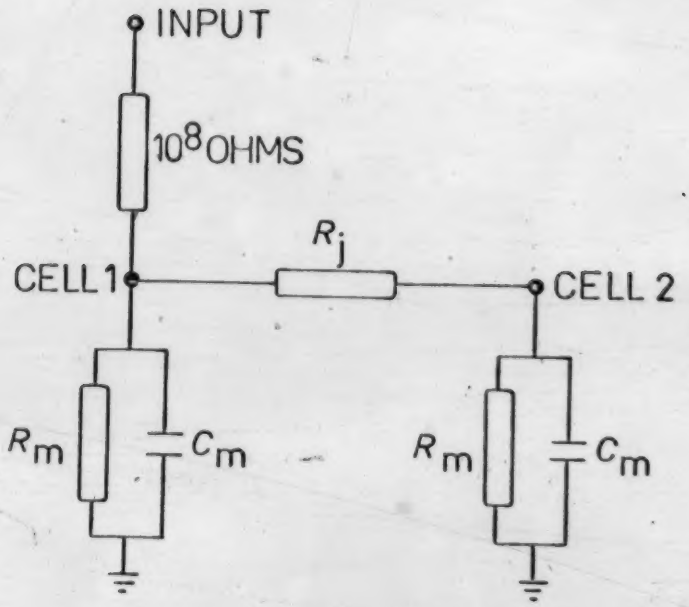

Fig. 5.1 The simplest electrical model of the two-cell embryo. R_M and C_M are the cell membrane resistances and capacitances respectively while R_J is the junctional resistance. The fixed input resistance of 10^8 Ω which was used for current injection is included to allow all calculations to be made in voltage ratios.

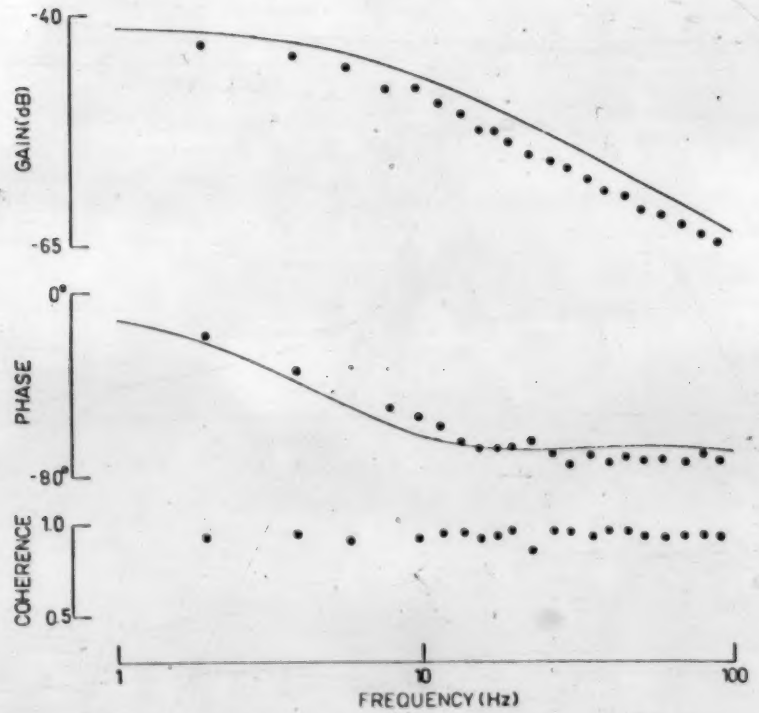

Fig. 5.2 Frequency response and coherence functions between the input and cell 1 of a two-cell embryo. Filled circles are experimental results and solid lines are theoretical predictions based upon the network of Fig. 5.1.

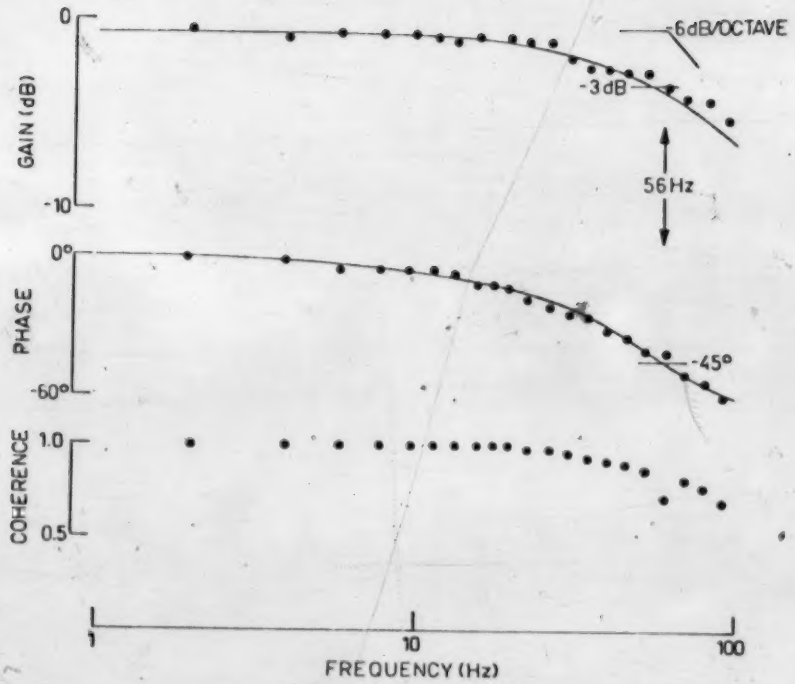

Fig. 5.3 Frequency response and coherence functions between cell 1 and cell 2 of the two-cell embryo used for Fig. 5.2. Filled circles are experimental results and solid lines are theoretical predictions based upon the network in Fig. 5.1. The corner frequency, f_c, is determined by the intersection of the gain asymptotes, the passage of the phase curve through -45° and the passage of the gain curve through -3 dB relative to the low frequency asymptote. In this example f_c is approximately 56 Hz.

of ∞, a simplified circuit consisting solely of resistive elements may be analyzed (Fig. 5.4a). This circuit can be rearranged (Fig. 5.4b), and the input resistance of the two-cell mode, R_I, derived as:

$$R_I = R_M \,||\, (R_J + R_M) \tag{5.1}$$

$$= \frac{R_M(R_J + R_M)}{2R_M + R_J} \tag{5.2}$$

The voltage ratio V_1/V_i may then be calculated from the simple voltage divider circuit shown in Fig. 5.4c:

$$V_1/V_i = \frac{R_M}{R_M + R_J} \tag{5.3}$$

The voltage ratio V_2/V_1 may be obtained from inspection of the circuit in Fig. 5.4a:

$$V_2/V_1 = \frac{R_M}{R_M + R_J} \tag{5.4}$$

The voltage ratio V_2/V_1 has also been referred to as the coupling ratio, CR (Palmer and Slack, 1970; Rose, 1970). Solving Eq. 5.4 for R_J gives:

$$R_J = \frac{R_M(1 - \mathrm{CR})}{\mathrm{CR}} \tag{5.5}$$

and substituting Eq. 5.5 into Eq. 5.2 yields an expression for R_I in terms of R_M and the coupling ratio:

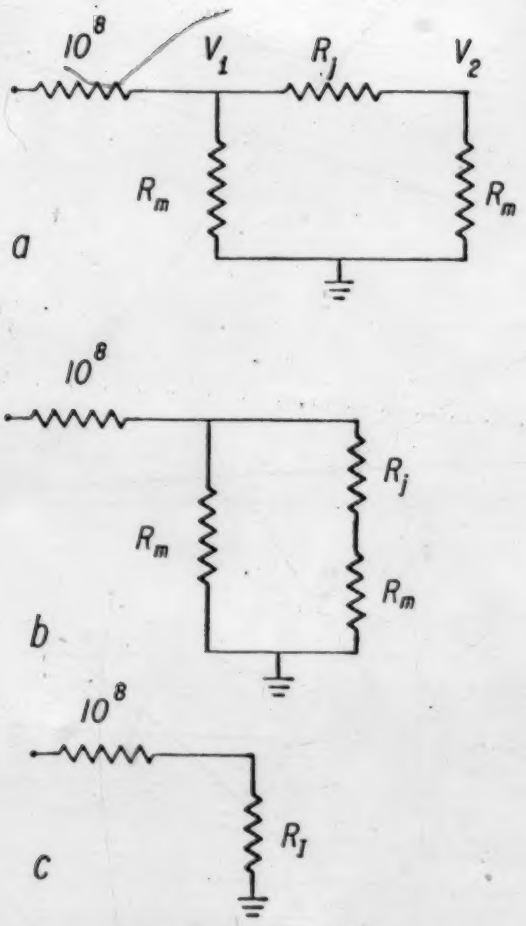

Fig. 5.4 Reduction of the resistive network model of the two-cell embryo.

$$R_I = \frac{R_M\left(R_M + \frac{R_M(1 - CR)}{CR}\right)}{2R_M + \frac{R_M(1 - CR)}{CR}} \qquad 5.6$$

$$= \frac{CR \cdot R_M \cdot R_M(1 - CR)}{1 + CR} \qquad 5.7$$

$$= \frac{R_M}{1 + CR} \qquad 5.8$$

Therefore:

$$R_M = R_I(1 + CR) \qquad 5.9$$

Substituting the value of R_I from Eq. 5.8 into Eq. 5.3 gives an expression for R_M in terms of the known quantities, V_i, V_1 and CR:

$$R_M = \frac{10^8\ V_1/V_i}{1 - V_1/V_i} \cdot (1 + CR) \qquad 5.10$$

Once that R_M has been calculated, this value may be substituted into Eq. 5.5, which yields a value for R_J.

When the membrane and junctional resistances have been determined, the value of C_M may be computed from data given by the cell-to-cell frequency response (Fig. 5.3). This is a first-order linear function as shown by a high frequency gain amplitude of -6 dB/octave and a phase asymptote of -90°. The network characteristics are determined by the voltage divider formed by R_J and the parallel combination of R_M and C_M.

In order to calculate C_M, the corner frequency (f_c) of the gain-phase plot must be determined. There are three methods of obtaining

f_c: (1) If the low and high frequency gain asymptotes of 0 dB/octave and -6 dB/octave respectively are extended, they will intersect at the corner frequency. (2) The gain curve should pass through a point 3 dB below the low frequency asymptote at f_c. (3) The phase curve should pass through -45° at the corner frequency. For the example shown in Fig. 5.3, it can be seen that there is excellent agreement between these three criteria, and they coincide at approximately 56 Hz.

To predict the ratio, V_2/V_1, as a function of frequency, f, it is necessary to consider the impedances of the junctional and membrane elements (Z_J, Z_M) of the circuit shown in Fig. 5.5. Therefore:

$$V_2/V_1(f) = Z_M(f)/[Z_M(f) + Z_J(f)] \qquad 5.11$$

where

$$Z_J(f) = R_J \qquad 5.12$$

$$Z_M(f) = R_M/(1 + j2\pi f\, C_M\, R_M) \qquad 5.13$$

Substituting Eq. 5.12 and Eq. 5.13 into Eq. 5.11 gives:

$$V_2/V_1(f) = R_M/[R_M + R_J(1 - j2\pi f\, C_M\, R_M)] \qquad 5.14$$

Eq. 5.14 may be separated into real and imaginary parts by inverting:

$$V_1/V_2(f) = [1 + (R_J/R_M)] + j(2\pi f\, R_J\, C_M) \qquad 5.15$$

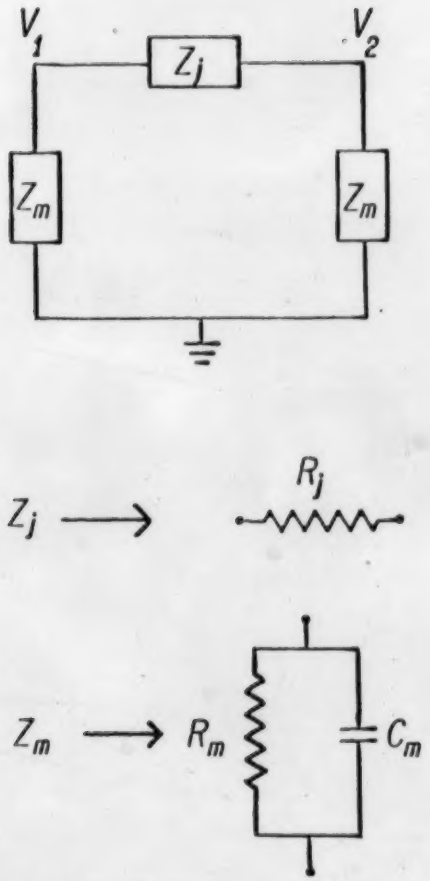

Fig. 5.5 AC circuit of the two-cell embryo.

The phase angle of the ratio V_2/V_1 is therefore given by:

$$P(f) = \arctan \left(\frac{2\pi f\, R_J\, C_M}{1 + R_J/C_M}\right) \qquad 5.16$$

At the corner frequency, f_c, the phase passes through -45° and given that tan(-45°) = -1, Eq. 5.16 becomes:

$$-1 = - \frac{2\pi f_c\, R_J\, C_M}{1 + R_J\, R_M} \qquad 5.17$$

Therefore:

$$C_M = (1 + R_J/R_M)\, 2\pi f_c\, R_J \qquad 5.18$$

Using Eqs. 5.5, 5.10 and 5.18 and the data obtained from the experiment shown in Fig. 5.3, the calculated values of R_J, R_M and C_M for this experiment were: $1.46 \times 10^5\ \Omega$, $1.67 \times 10^6\ \Omega$ and 0.0215 μf respectively. These values were used as the parameters for the model shown in Fig. 5.1 and the ECAP program was used to predict the two frequency response curves, shown as solid lines in Figs. 5.2 and 5.3. The predicted characteristics are in excellent agreement with the experimental curves.

The electrical characteristics of the two-cell embryo are given in Table I. The calculations of specific membrane resistance and capacitance are based on the assumption that each cell is a perfect hemisphere. The measured diameter of the embryos were all in the range 1.25-1.31 mm and the mean value of 1.28 mm was used for all calculations.

TABLE I

SUMMARY OF CALCULATED MEMBRANE PARAMETERS FOR TWO-CELL EMBRYOS

Where applicable the figures are expressed as the mean value ± the standard deviation. The maximum variation in embryonic diameter was less than 3% of the mean value so that the accuracies of the specific membrane properties are similar to the whole membrane measurements from which they were derived.

	First cleavage stage (2 cells)	Units
Membrane potential	15.5 ± 1.6	mV
Diameter of embryo	1.28	mm
Coupling ratio	0.772 ± 0.058	
Membrane resistance (R_M)	1.05 ± 0.16	MΩ
Specific membrane resistance	0.041	MΩcm^2
Membrane capacitance (C_M)	0.0239 ± 0.0035	μf
Specific membrane capacitance	0.62	μf/cm^2
Junctional resistance (R_J)	0.286 ± 0.071	MΩ
Membrane time constant	25	ms
Number of experiments	9	

5.2 *Conclusions:*

The increase in magnitude of the membrane potential of embryonic cells during cleavage has been observed in several other amphibians (Ito and Hori, 1966; Woodward, 1968) including *Xenopus* (Palmer and Slack, 1970; de Laat, Luchtel and Bluemink, 1973). The membrane potential data presented in Fig. 4.2 is in good agreement with these previous results, although the plateau in potential observed between the two- and four-cell stages has not been clearly demonstrated before. The reasons for this increasing polarization are not clear as the membrane potential of the normally cleaving embryo has been found to be insensitive to the concentration of K^+, Na^+ and Cl^- in the external medium (Slack and Warner, 1973; de Laat, Buwalda and Habets, 1974). It has been suggested that the new membrane which is inserted in the cleavage furrows has a higher K^+ permeability than the pre-existing membrane (Slack and Warner, 1973; de Laat *et al.*, 1974; de Laat and Bluemink, 1974).

The electrical measurements made here on the two-cell embryo do not provide any information about the detailed electrical characteristics of the junctional mechanism which exists between the cells. Fig. 5.6 illustrates two alternate networks for the junctional elements. It is based on speculation made by various authors (McNutt and Weinstein, 1970; Bennett, 1972; Ito and Loewenstein, 1969) on the structure of electrical junctions where relatively large areas of membrane are apposed, with a closely-packed two-dimensional array of subunits within the membranes and a hydrophilic channel passing through each subunit.

Fig. 5.6a shows a model where an additional RC network (R_{JM} C_{JM})

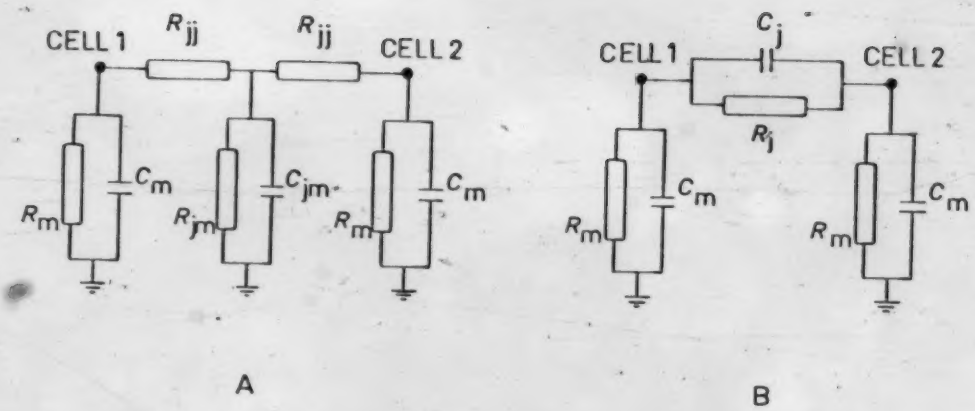

Fig. 5.6 Two alternative hypothetical models for the two-cell embryo. In A, the junctional system is modelled by a "T" network of resistances, R_{jj} and R_{jm}, with a junctional membrane capacitance, C_M. This arrangement would be expected if the junction behaves as a membranous cable. In B, a direct junctional capacitance, C_j, might be produced by the close apposition of the cell membranes in the junctional region.

is inserted between the two cells to account for the cable-like properties of the proposed intercellular channels. The frequency response functions measured for this system do not suggest that this additional network is present, as it would place another first-order filter between the two cells, resulting in an overall second-order response. This still does not rule out the presence of these elements as C_{JM} could be quite small relative to C_M and would therefore only have an effect on the frequency response at frequencies higher than have been used for the previous measurements.

The value of a junctional resistance to ground, R_{JM}, also cannot be determined from the present measurements as the T network formed by R_{JJ}, R_{JM} and R_{JJ} may be transformed to a π network as shown in Fig. 5.7A. The resistive elements of the two-cell network of Fig. 5.1 would then be transformed as shown in Fig. 5.7B. The behaviour of these two networks would be identical, the only difference being that the measured value of R'_M would not be the true value of the membrane resistance.

The second possible modification to the two-cell network is the insertion of a junctional coupling capacitance, C_J. This element can be justified due to the close apposition of the cell membranes at the site of junctional coupling. The presence of a significant capacitance in this position would introduce a high-pass filter between the two cells which would produce high frequency gain and phase asymptotes of 0 dB/octave and 0° respectively. As this type of behaviour is not observed, it must be concluded that if C_J exists, it is too small to be detected in the frequency range that has been used.

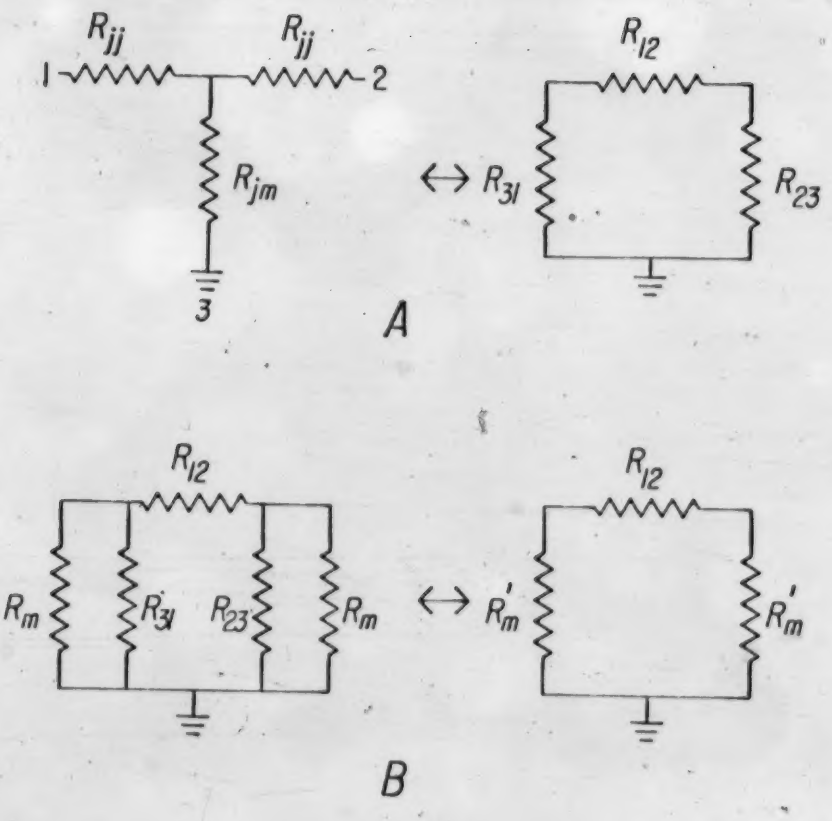

Fig. 5.7 Reduction of two-cell model containing a junctional resistance to ground.

CHAPTER 6

ELECTRICAL COUPLING IN THE FOUR-CELL EMBRYO

6.1 *Analysis of the four-cell embryo:*

The second cleavage of *Xenopus laevis* embryos divides the embryo into four approximately equally-sized cells. Given the assumption that the four cells are electrically identical, then two recording arrangements must be used to investigate the electrical properties of the embryo (Fig. 6.1). The first recording scheme measures the frequency response function between two adjacent cells while current is injected into one cell. The second procedure determines the frequency response function between diagonally opposed pairs of cells as current is injected into one of them.

The simplest model of the four-cell embryo is shown in Fig. 6.2. It consists of four parallel RC networks representing the lumped membrane resistance and capacitance of each cell, and four junctional resistances which link pairs of cells whose membranes are apposed. Theoretical analysis of this network produces two types of frequency response functions, one for the adjacent cell measurement and another for the diagonal cell measurement. The theoretical predictions for the network shown in Fig. 6.2 are shown in Fig. 6.3. It can be seen that the adjacent cell frequency response is characteristic of a first-order system while the diagonal measurement is characteristics of a second-order system. The second-order behaviour is produced by the two cascaded first-order systems in each possible current path between the cells.

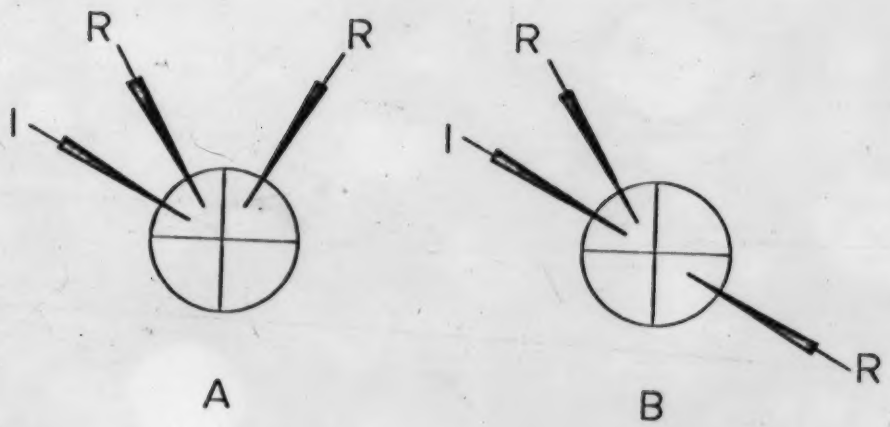

Fig. 6.1 Assuming that the cells of a four-cell embryo are electrically identical, there are two possible recording arrangements: A, The second recording electrode is placed in the cell adjacent to the stimulated cell. B, The second electrode is placed in the cell diagonally opposite to the stimulated cell. R = Recording electrode and I = Current injecting electrode.

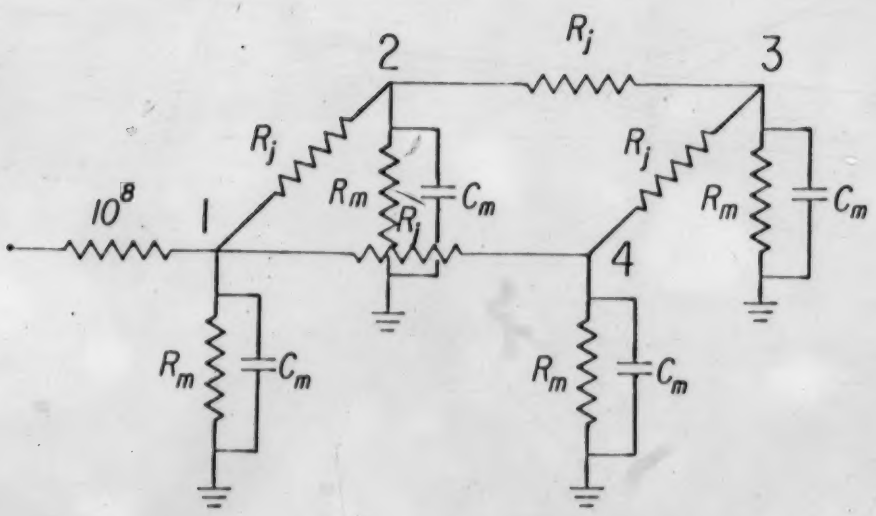

Fig. 6.2 Simplest electrical model of the four-cell embryo. Junctional resistances, R_J, only appear between directly apposed cells. R_M and C_M are the plasma membrane resistances and capacitances.

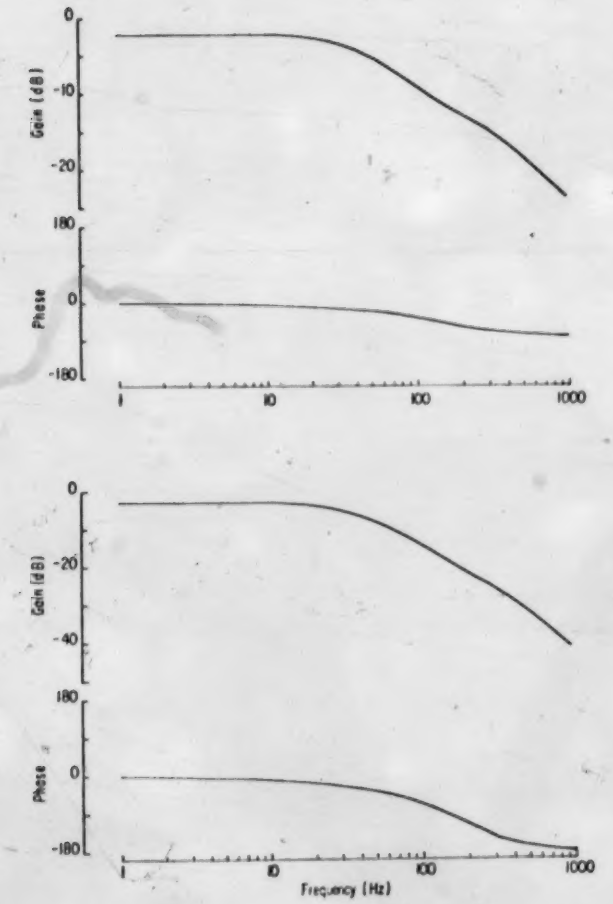

Fig. 6.3 Predicted frequency response measurements for the network of Fig. 6.2. The upper graph is the predicted frequency response for adjacent cells and the lower graph is the predicted frequency response between diagonally opposed cells.

The experimental measurements of the frequency response functions did not exhibit the behaviour predicted by the model in Fig. 6.2. Instead, the adjacent and diagonal cell-to-cell measurements were similar in that both were first-order responses, and no second-order behaviour was observed for the diagonal response. Fig. 6.4 illustrates the experimentally determined adjacent cell-to-cell frequency response for a four-cell embryo and Fig. 6.5 is the response obtained from a different embryo for diagonally opposed cells. It proved to be technically difficult to determine both frequency response functions in the same embryo as there was the possibility of damaging the embryo when the position of one voltage recording electrode was changed. The frequency response for the input - cell 1 measurement is shown in Fig. 6.6.

The model shown in Fig. 6.2 is clearly not adequate to explain the experimental results. The alternate network shown in Fig. 6.7 was therefore considered. It contains the same four membrane resistor-capacitor networks but in contrast to Fig. 6.2, junctional resistances, R_J, are located between all pairs of cells. The two additional junctional coupling elements produce a network of high symmetry which greatly facilitates its electrical analysis. This symmetry is best illustrated in a spatially rearranged view of the junctional elements shown in Fig. 6.8. The non-junctional cell membrane components have been omitted since they are assumed to have identical values. It can be seen that the pathways between any one cell and all the others are identical and the load seen by any cell due to the rest of the network is also identical. Therefore, no matter which cell is used for current

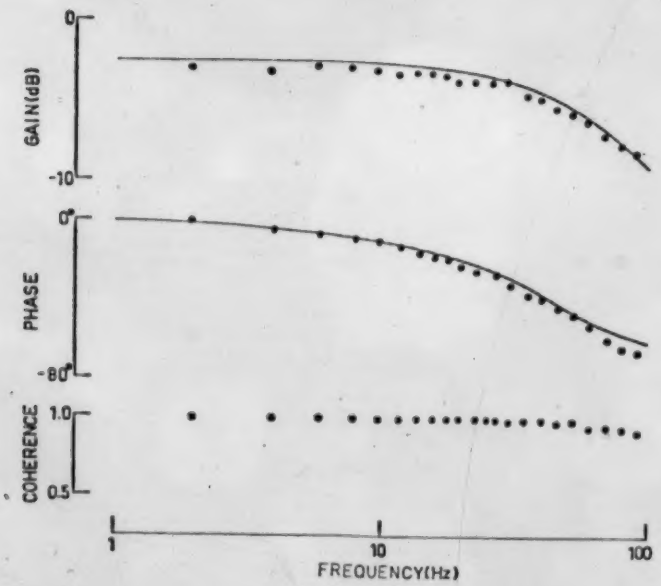

Fig. 6.4 Frequency response and coherence functions between two adjacent cells in a four-cell embryo. Filled circles are experimental results and solid lines are theoretical predictions based upon the network of Fig. 6.7.

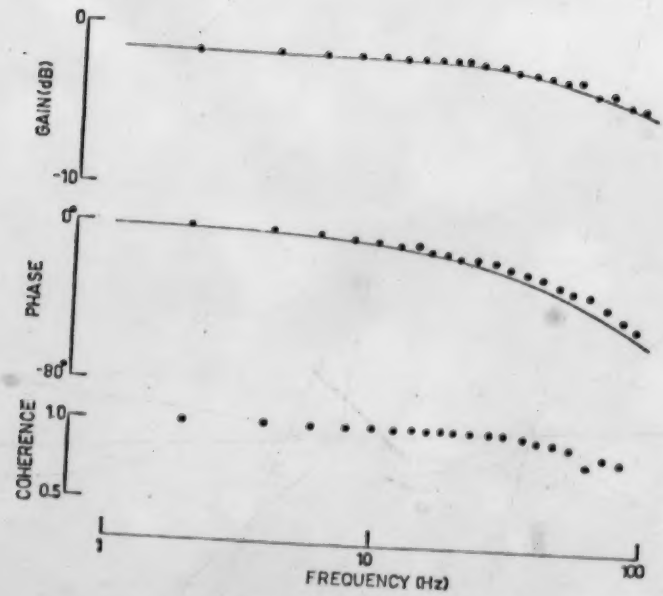

Fig. 6.5 Frequency response and coherence functions between two diagonally opposed cells in a four-cell embryo. Filled circles are experimental results and solid lines are theoretical predictions based upon the network of Fig. 6.7. Note the very close similarity between this frequency response and that illustrated in Fig. 6.4 for the adjacent cells.

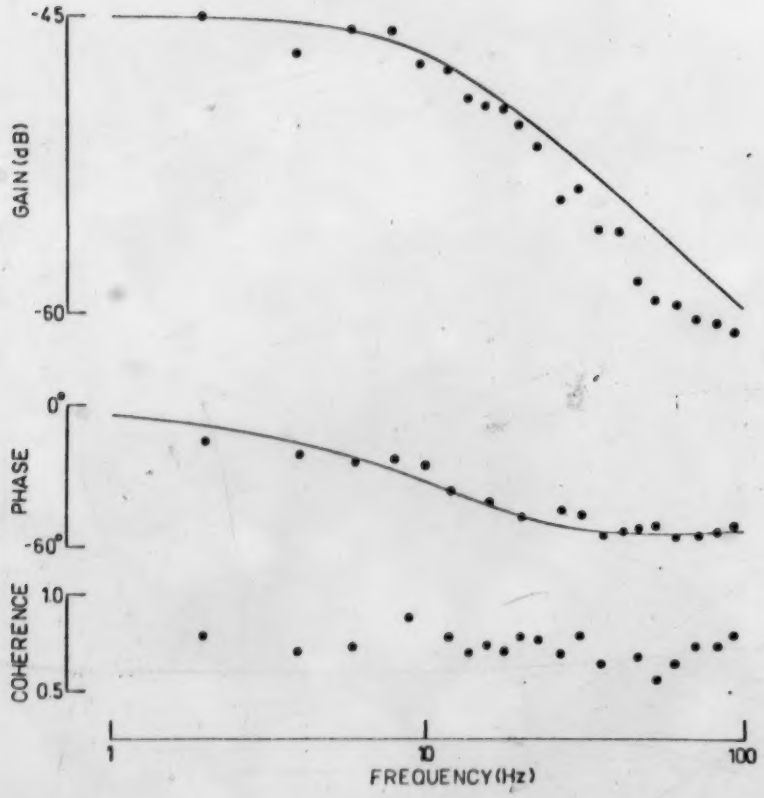

Fig. 6.6 Frequency response and coherence functions between input and cell 1 for the four-cell embryo used in Fig. 6.4. Filled circles are experimental results and solid lines are theoretical predictions based upon the network of Fig. 6.7.

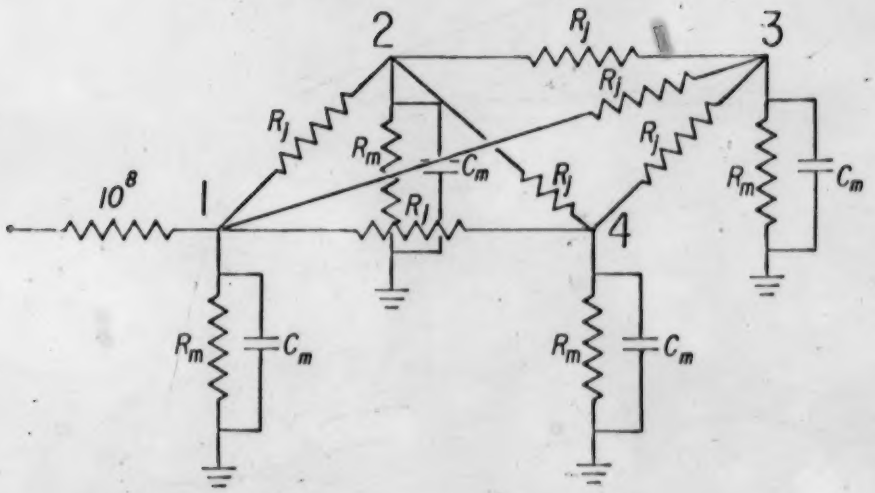

Fig. 6.7 The simplest electrical network capable of explaining the behaviour of a four-cell embryo. R_M and C_M are the plasma membrane resistances and capacitances and R_J are the intercellular junction resistances.

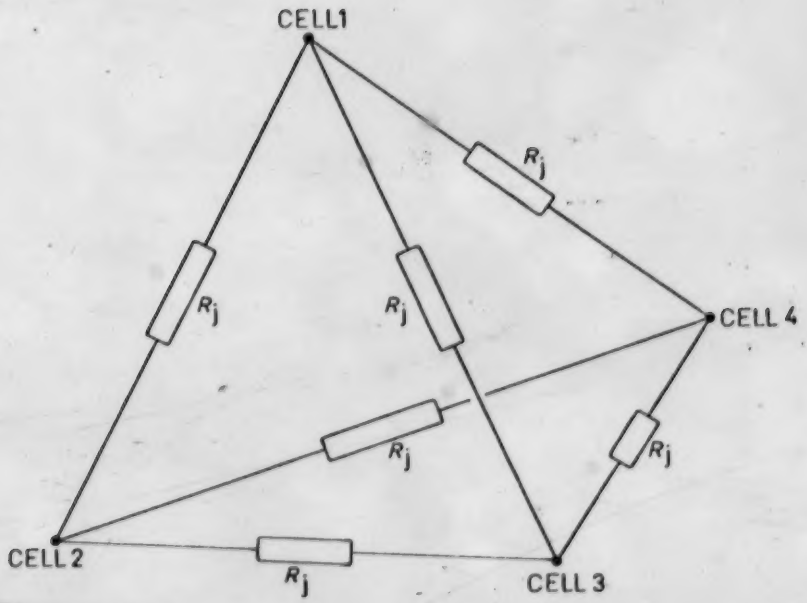

Fig. 6.8 Perspective view of the six junctional resistances of Fig. 6.7, arranged in the form of a regular tetrahedron. In this spatial rearrangement it is clear that the cells are electrically identical with each cell connected to all of its neighbors.

injection, the voltage in the three other cells will be identical. If the voltages in these cells are the same there will be no current flow between them, and the components along these current paths may be omitted in order to simplify the analysis. According to the nomenclature of Fig. 6.7, the junctional resistances between cell 2 - cell 3, cell 3 - cell 4 and cell 2 - cell 4 may be ignored, leaving three identical independent current paths from cell 1 to the others. Each pathway consists of a junctional coupling resistance, R_J, in series with the parallel combination of the membrane elements, R_M and C_M (Fig. 6.9).

The lumped input resistance at cell 1 is given as:

$$R_I = [R_M(R_M + R_J)]/(4R_M + R_J) \qquad 6.1$$

and given that:

$$V_1/V_i = R_L/(R_L + 10^8) \qquad 6.2$$

$$V_2/V_1 = V_3/V_1 = V_4/V_1 = CR = R_M/(R_M + R_J) \qquad 6.3$$

Substituting Eq. 6.3 into Eq. 6.1 and solving for R_M:

$$R_M = R_I(1 + 3CR) \qquad 6.4$$

The value of R_M may then be substituted into Eq. 6.3 to calculate R_J. Since Eq. 6.3 is identical to Eq. 5.4 which defines the coupling ratio

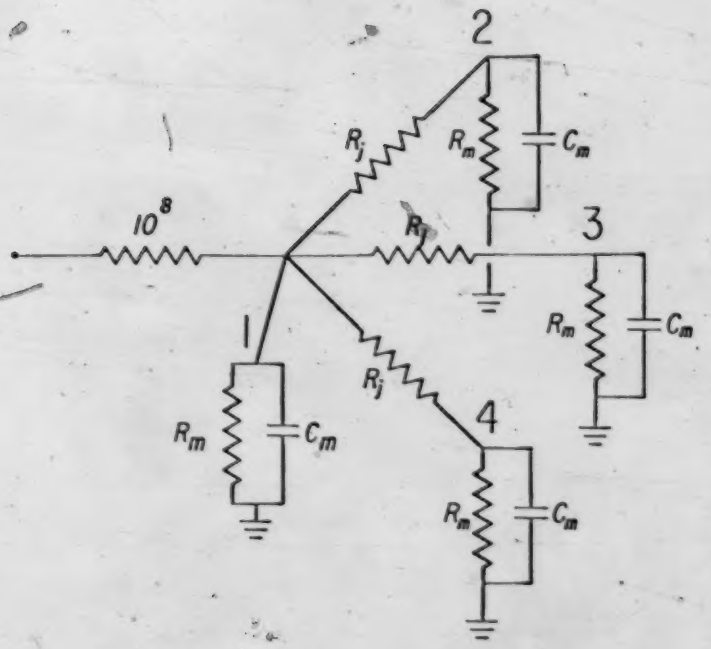

Fig. 6.9 Electrical network of the four-cell network. The junctional resistances have been eliminated where no current flows through these elements.

for the two-cell model, Eq. 5.18 may be used to determine C_M for the four-cell model. The values of R_M, R_J and C_M for the embryo used in Figs. 6.4 and 6.6 are 2.10×10^6 Ω, 4.18×10^5 Ω and .0057 μf respectively. The same parameters for the embryo of Fig. 6.5 are $R_M = 1.52 \times 10^6$ Ω, $R_J = 5.02 \times 10^5$ Ω and $C_M = .0076$ μf. These parameters were used to model the network of Fig. 6.7 with the ECAP program and the calculated gain and phase curves are superimposed as solid lines on the experimental data of Figs. 6.4 - 6.6. Comparison of these curves with the experimental results indicates that the four-cell network model of Fig. 6.7 is adequate to account for the electrical characteristics of the embryo.

The electrical characteristics of the four-cell embryo are summarized in Table II. As in the two-cell case, the embryo is assumed to be perfectly spherical with a mean diameter of 1.28 mm with each cell being a perfect quarter sphere.

6.2 *Conclusions:*

The most interesting feature of electrical coupling in the four-cell embryo is the fact that the four cells are identically connected to each other. The finding that the junctional resistances, R_J, are identical in the network model that accurately predicts the behaviour of the system, implies that the coupling mechanism is relatively independent of the area of contact between the cells as the adjacent cells have a much larger non-junctional membrane area in mutual apposition than the diagonally apposed cells. Similar results in *Triturus* embryos have been obtained by Ito and Loewenstein (1969) where

TABLE II

SUMMARY OF CALCULATED MEMBRANE PARAMETERS FOR FOUR-CELL EMBRYOS

Where applicable the figures are expressed as the mean value ± the standard deviation. The maximum variation in embryonic diameter was less than 3% of the mean value so that the accuracies of the specific membrane properties are similar to the whole membrane measurements from which they were derived.

	Second cleavage stage (4 cells)	Units
Membrane potential	16.0 ± 2.4	mV
Diameter of embryo	1.28	mm
Coupling ratio	0.808 ± 0.026	
Membrane resistance (R_M)	1.80 ± 0.20	MΩ
Specific membrane resistance	0.046	MΩcm^2
Membrane capacitance (C_M)	0.0106 ± 0.0047	μf
Specific membrane capacitance	0.41	μf/cm^2
Junctional resistance (R_J)	0.421 ± 0.061	MΩ
Membrane time constant	19	ms
Number of experiments	10	

the junctional resistance is relatively independent of the area of membrane apposition as well as in various electrically-coupled adult tissues (Loewenstein *et al.*, 1965). The investigation of coupling in four-cell embryos using electrophysiological techniques did not provide any further information concerning the detailed structure of the junctions. The possible models for the electrical network of the junctional resistance already discussed for the two-cell embryo may also apply in this case.

Morphological investigations of the four-cell embryo support the existence of coupling between diagonally apposed cells (see Appendix II). These studies indicate that the geometry of the four-cell embryo is not simply a sphere divided into four quarter spheres, but rather that two hemispheres are rotated parallel to the cleavage plane to produce an area of contact between two pairs of cells at the animal pole. This situation is reversed at the vegetal pole, so that the pairs of cells that are separated at the animal pole are closely apposed at the vegetal pole.

CHAPTER 7

ELECTRICAL COUPLING IN THE EIGHT-CELL EMBRYO

7.1 *Analysis of the eight-cell embryo:*

Investigation of the electrical properties of the eight-cell embryo is complicated by the fact that the third cleavage divides the embryo into two classes of cells. The four animal pole cells are smaller than the four vegetal pole cells and therefore the membrane resistances and capacitances of the two groups of cells are different. While it would be possible to determine the exact value of each element in the eight-cell network by linear systems analysis, this would be a formidable task. An alternate approach is to measure the connectivity of the cells in the embryo, since this is the property of the embryo which is of most interest. Connectivity used in this context will be defined as the degree to which the cells are directly coupled, permitting the direct flow of current between one cell and another without passing through an intermediate cell. The connectivity can be determined by measuring the frequency response functions between specific pairs of cells.

In order to systematize the analysis of the eight-cell embryo, the numbering scheme shown in Fig. 7.1 was used, which shows the embryo as viewed from directly above the animal pole. The cells were unambiguously numbered by reference to the grey crescent, a more lightly pigmented patch on the surface of the animal pole cells. The condition where two diagonally opposite animal pole cells are in contact at the apex of the embryo is preserved from the four-cell embryo. Fig. 7.1

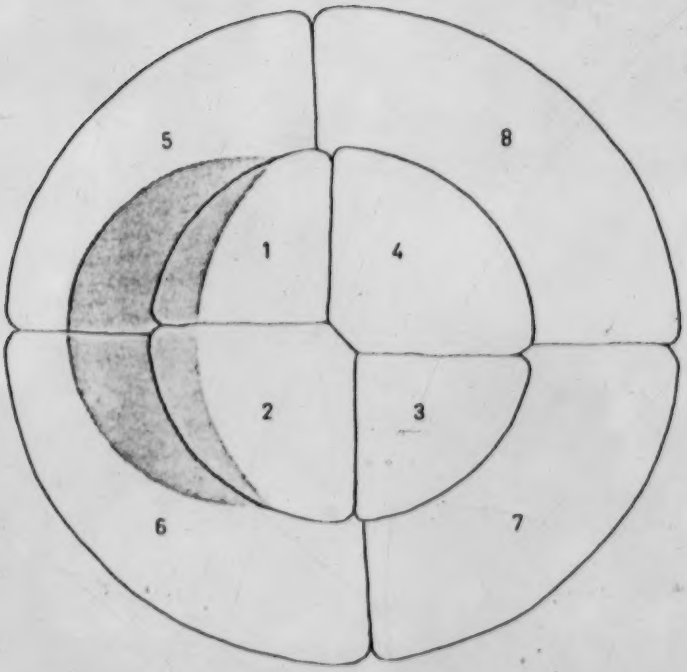

Fig. 7.1 Diagrammatic view of an eight-cell embryo, viewed from the animal pole. The difference in size between the four animal pole cells (1-4) and the four vegetal pole cells (5-8) has been exaggerated. The numbering scheme is based on the grey crescent (stippled area) covering portions of the surfaces of cells 1 and 2.

illustrates cells 2 and 4 touching one another and separating cells 1 and 3, while investigation of the vegetal hemisphere would indicate that the alternate pair of cells (5-7) was apposed, in the same fashion as the four-cell embryo. However, examination of a large number of embryos indicated that there was no preference for either pair of cells to be in contact (1-3 or 2-4) so that the diagonal apposition is unrelated to the grey crescent and therefore to the numbering scheme.

The approach used to determine the connectivity was to synthesize a range of differently connected models of the embryo and to predict the behaviour of each model. Experimental measurements were then made in attempts to eliminate one or more of the models. Since no attempt was made to evaluate the specific values of the network components, it was necessary to assume values for the membrane resistances, R_M, the membrane capacitances, C_M, and the junctional resistances, R_J. These estimated values are based on the previously determined values for the four-cell embryo and measurements of cell surface areas made from scanning electron micrographs. The animal pole cells were all assumed to have identical surface areas. The vegetal pole cells were also assumed to have equal surface areas, although larger than the animal pole cells by a ratio of approximately 2:1. The actual values used in the models were: R_M (animal pole) = 2.3×10^6 Ω, R_M (vegetal pole) = 1.1×10^6 Ω, C_M (animal pole) = 5×10^{-9} μf, C_M (vegetal pole) = 1×10^{-8} μf and $R_J = 2.5 \times 10^5$ Ω.

Seven possible models with varying connectivity were constructed and will be referred to as models A through G. Models A and G represent the two extreme possibilities and are illustrated in Fig. 7.2.

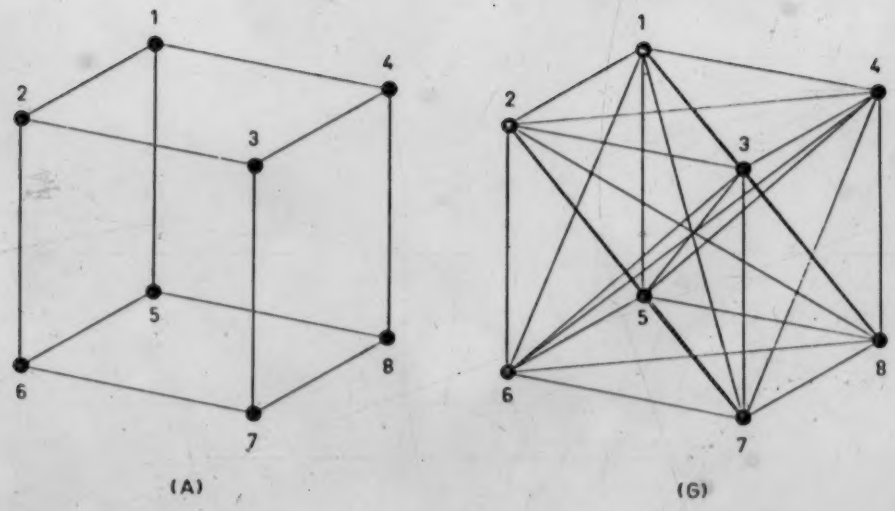

Fig. 7.2 Two of the seven models (A and G) which were proposed as possibly describing the electrical properties of the eight-cell embryo. Solid lines represent junctional resistances and the non-junctional components are omitted for clarity. Details of the connectivity of all the seven models are given in Table III.

Only the junctional elements are shown as solid lines and the cells are numbered according to the convention of Fig. 7.1. Model A is the simplest model that would be predicted on the basis of the embryo geometry. Junctional resistances are only present in this model between cells that are directly apposed along the plane of a cleavage furrow. Model G is the most complicated model, where each cell in the embryo is connected pairwise to every one of the other cells.

Using the minimum connectivity of model A as a base, the number of different models that may be constructed with the remaining 16 possible connections is given by:

$$N = \sum_{k=1}^{16} \binom{16}{k} \qquad 7.1$$

where $\binom{16}{k}$ is the binomial coefficient defined as:

$$\binom{n}{k} = \frac{n!}{k!(n-k)!} \qquad 7.2$$

Solving Eq. 7.1 for N yields a total of 65,536 different models of intermediate connectivity, which therefore precludes the analysis of all models. Five intermediate models have been considered which represent a range of connectivities having the principal groups of connections. Model B includes the two diagonal connections which lie in the plane of the animal pole cells, model C has the two diagonal connections in the vegetal pole plane, and model D combines B and C. Model E is model A plus the four connections running through the interior of the embryo and model F has all adjacent and diagonal exterior connections but omits the

interior pathways. The details of the connections for all the models are listed in Table III.

To further standardize the analysis, the white noise stimulating current was always injected into cell 1. Recording microelectrodes were then placed in any pair of cells in order to measure the frequency response and coherence function. The electrical symmetry of the embryo was first tested by injecting current into cell 1 and measuring the voltage in cells 2 and 4 and cells 6 and 8. It was found that there was no voltage difference between the cells in either pair which would indicate that the embryo is electrically symmetrical about the two vertical cleavage planes. Therefore, if current was injected into cell 1, the possible cell pairs between which distinct signal transfer properties would be observed were: 1 to 2, 1 to 3, 1 to 5, 1 to 6, 1 to 7, 5 to 6 and 5 to 7.

The predicted frequency response functions for each of these seven cell pairs were calculated for each of the seven models. Experimental measurements of the frequency response functions were then made and compared with the theoretical predictions.

An examination of the predicted frequency response functions indicated that an accurate distinction between the various models could only be made by comparing the high frequency portions of the functions, since they diverge with increasing frequency. It is experimentally difficult to make these high frequency measurements for two reasons: (1) Since each cell membrane has a capacitance element, the injected current will be shunted to ground at high frequencies, thereby decreasing the level of the signal which passes through the junctional resistance.

TABLE III

THE CONNECTIVITY OF THE SEVEN PROPOSED MODELS FOR THE EIGHT-CELL EMBRYO

The twenty-eight possible cell pair connections are listed vertically at the left, using the numbering scheme of Figure 7.1. Asterisks indicate the presence of a particular connection in each model.

	MODELS						
CELL PAIR	A	B	C	D	E	F	G
1-2	*	*	*	*	*	*	*
1-3		*		*		*	*
1-4	*	*	*	*	*	*	*
1-5	*	*	*	*	*	*	*
1-6						*	*
1-7					*		*
1-8						*	*
2-3	*	*	*	*	*	*	*
2-4		*		*		*	*
2-5						*	*
2-6	*	*	*	*	*	*	*
2-7						*	*
2-8					*		*
3-4	*	*	*	*	*	*	*
3-5					*		*
3-6						*	*
3-7	*	*	*	*	*	*	*
3-8						*	*
4-5						*	*
4-6					*		*
4-7						*	*
4-8	*	*	*	*	*	*	*
5-6	*	*	*	*	*	*	*
5-7			*	*		*	*
5-8	*	*	*	*	*	*	*
6-7	*	*	*	*	*	*	*
6-8			*	*		*	*
7-8	*	*	*	*	*	*	*

It was therefore necessary to increase the input amplitude of the current signal in order to maintain the accuracy of the measurement at high frequencies. (2) The microelectrodes are capacitively coupled at high frequencies, due to their high impedance and close apposition. Some portion of the high frequency signals would therefore pass between the two electrodes without going through the embryo. An experiment to determine the extent of these effects is illustrated in Fig. 7.3, which shows the coherence function between the signal measured by two recording electrodes when they were inserted in the embryo and when they were placed just outside the embryo in the bathing medium. Three distinct regions can be seen in the trace. From 1 Hz to approximately 500 Hz the coherence function has a value close to 1. In the region from 500 to 1,000 Hz the coherence drops sharply and as the frequency increases past 1,000 Hz the coherence rises and again approaches unity. The coherence function of the electrodes in saline exhibits a slow rise from 0 to 1 in the frequency range of 1 Hz to 1,000 Hz. The interpretation of this data is that measurements made in the frequency range of 0 to 500 Hz accurately reflect the electrical characteristics of the embryo. Between 500 and 1,000 Hz most of the input power is shunted to ground by the cell membrane capacitance and the coherence is therefore low. At frequencies above about 1,000 Hz the electrodes become capacitively coupled and although the value of the coherence function is high it reflects the presence of an electrical pathway outside the embryo. The experimental frequency response measurements are therefore only accurate up to a frequency of about 500 Hz.

Fig. 7.4 shows the frequency response functions measured

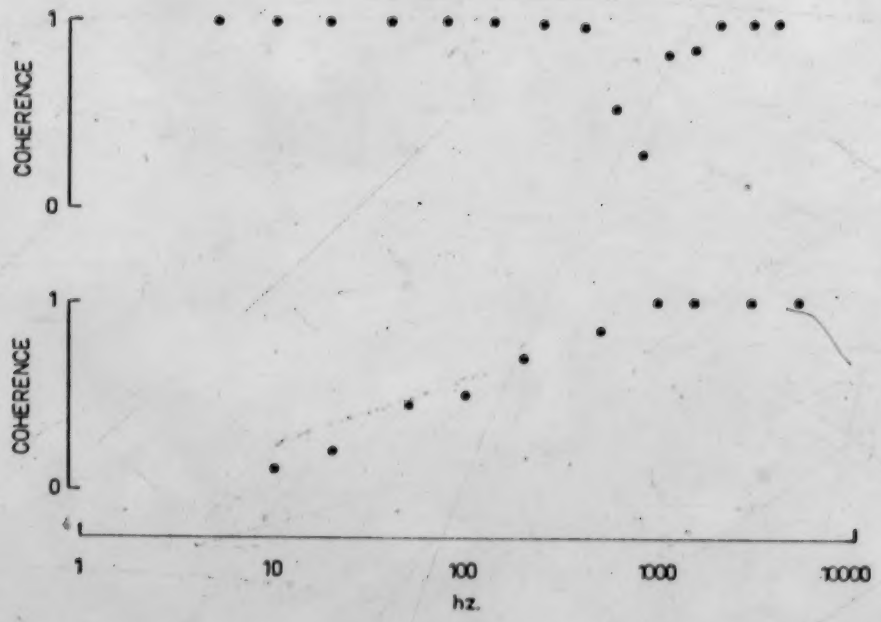

Fig. 7.3 The coherence function measured between two recording electrodes while a noise signal was injected into cell 1 of an eight-cell embryo. In the upper trace the two recording electrodes were located intracellularly in two coupled cells. Similar coherence function curves were observed whichever pair of cells was impaled. In the lower trace the two electrodes have both been raised through the cell membranes so that they are resting with their tips in the bathing solution just outside the embryo.

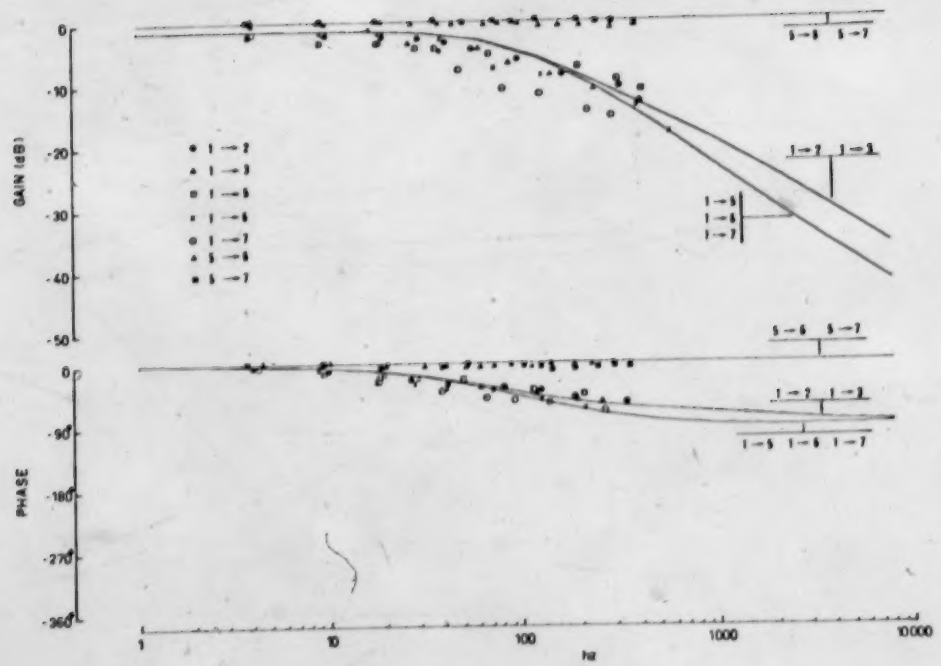

Fig. 7.4 Experimentally determined frequency response functions between the seven pairs of cells. The cells are numbered according to the scheme of Fig. 7.1, and symbols are used to identify the individual pairs. Solid lines are theoretical predictions based upon the network of Model G (Fig. 7.2).

between each of the seven pairs of cells in an eight-cell embryo and it can be seen that the results fall into two groups. All of the pairs which contain cell 1 have first-order characteristics, that is, a high frequency gain asymptote of -6 dB/octave and a high frequency phase asymptote of -90°. The other two pairs of cells, 5-6 and 5-7, have a flat or zero-order response with gain and phase asymptotes of 0 dB and 0° respectively.

The predicted frequency response functions for each of the seven pairs of cells for each of the seven models are shown in Fig. 7.5. Each plot compares the calculations for a single pair of cells for each different model. Inspection of these curves indicates that some of the measurements do not allow distinctions to be made between the various models. For example, Fig. 7.5a shows the curves for the cell 1 - cell 2 measurement, all of which are first-order, and they are so similar that no discrimination between models is possible with this measurement. Fig. 7.5b illustrates the cell 1 - cell 3 measurement and a distinction can be made here between models A and C, which give second-order responses, and the other five which are first-order. Comparison of this prediction with the experimental data presented in Fig. 7.4 for the 1-3 pair indicates that models A and C are not correct.

The remaining curves may be considered in a similar fashion. Fig. 7.5c shows the predictions for cells 1-5 which are all first-order curves and, as in the 1-2 case, allows no distinctions to be made between the models. The curves for cells 1-6 shown in Fig. 7.5d allow a comparison of models A through E, which exhibit second-order behaviour, and models F and G which give first-order responses. Fig. 7.5e shows the

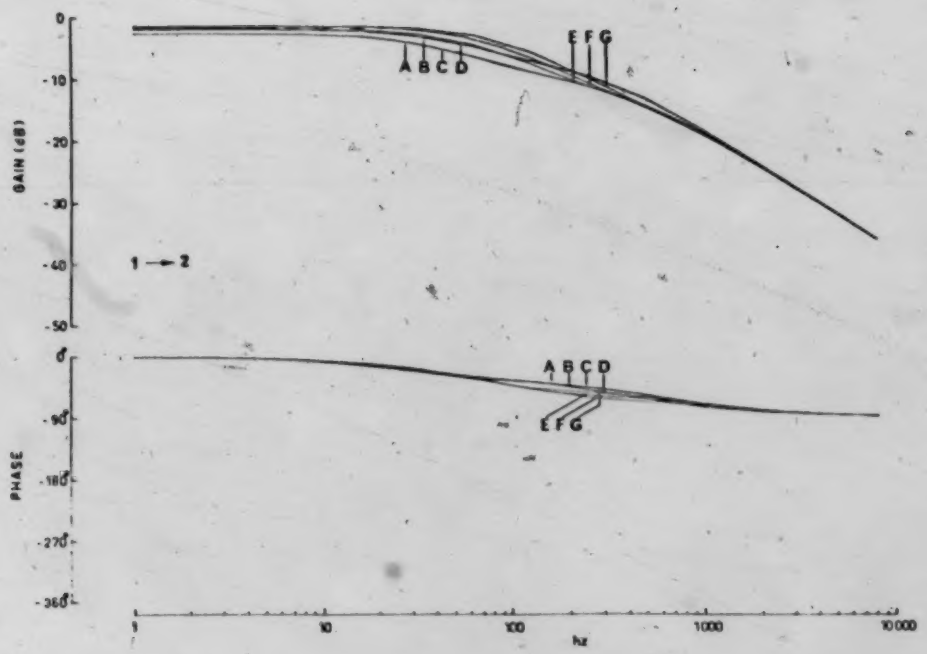

a

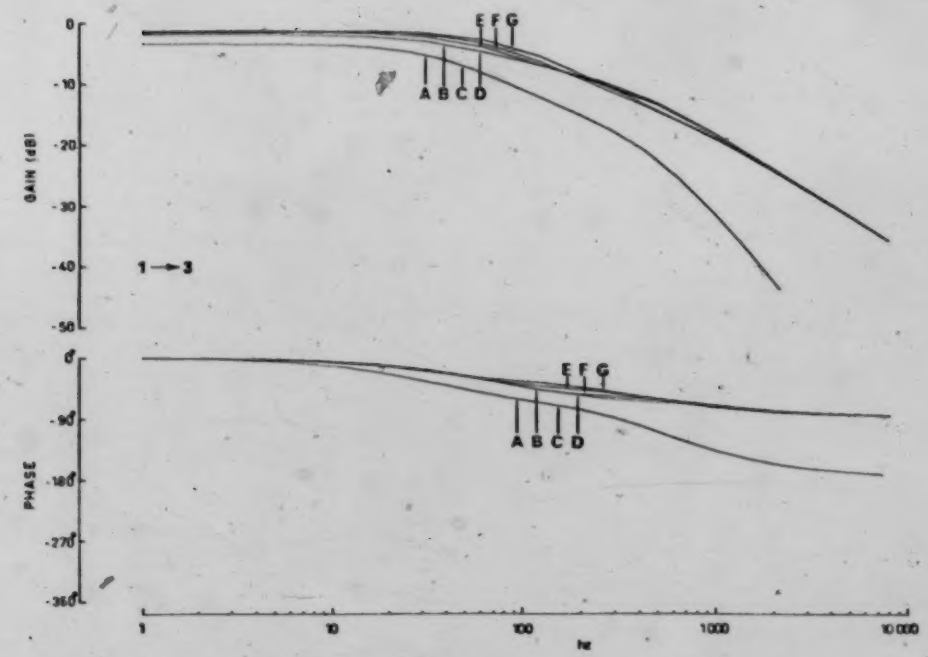

b

Fig. 7.5 a-g Theoretical predictions of the frequency response functions of each of the seven pairs of cells with noise injected into cell 1. Each plot shows seven predicted results corresponding to the seven models, A-G.

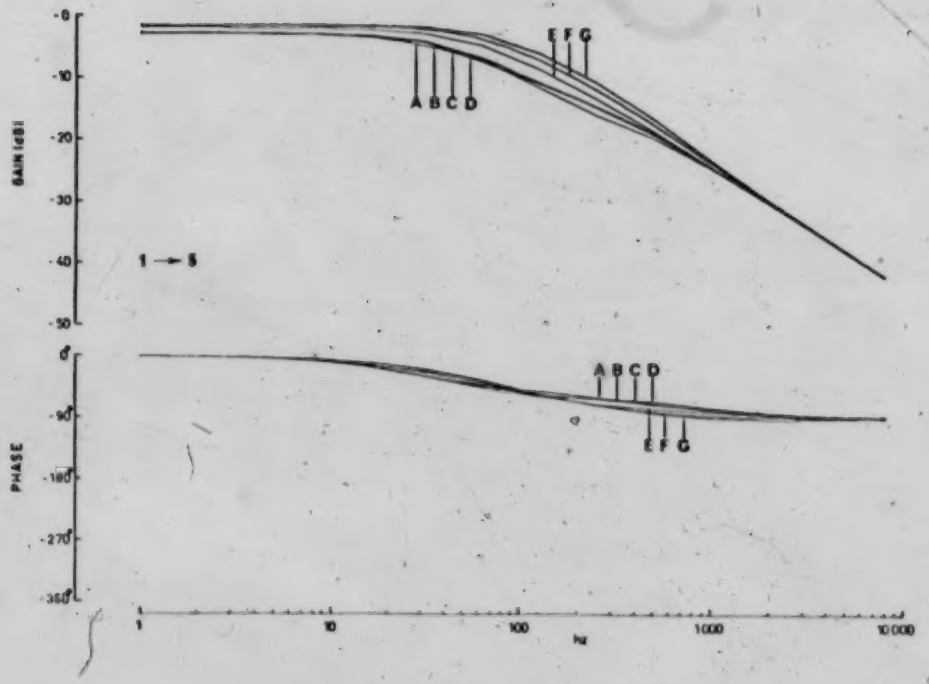
GAIN (dB)
0
-10
-20
-30
-40
-50
1 → 5
A B C D
E F G
PHASE
0
-90
-180
-270
-360
A B C D
E F G
1
10
100
1000
10000
Hz

C

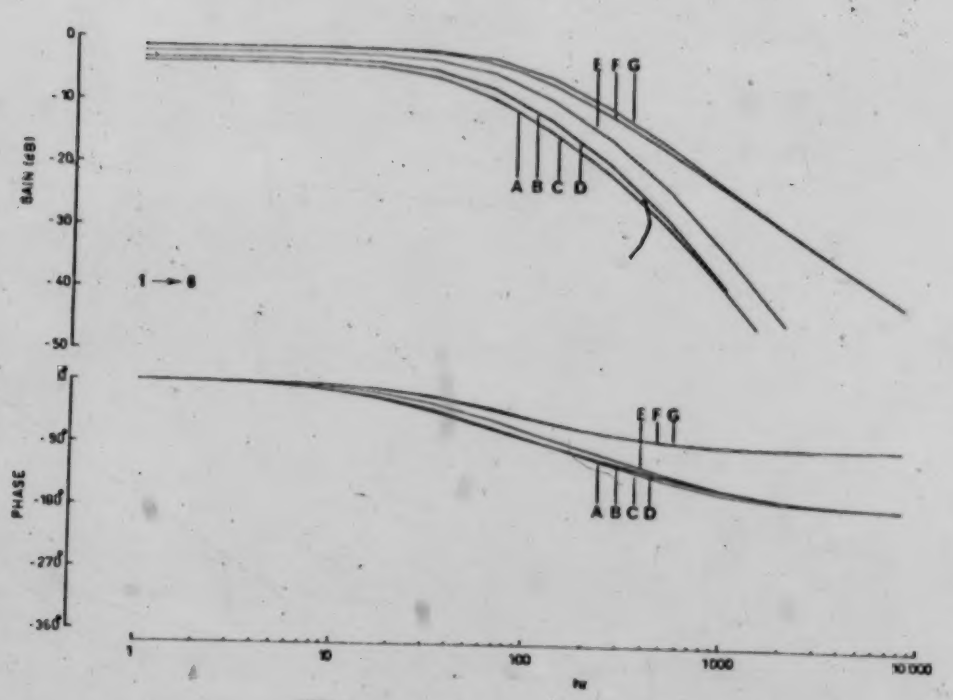
GAIN (dB)
0
-10
-20
-30
-40
-50
1 → 6
A B C D
E F G
PHASE
0
-90
-180
-270
-360
E F G
A B C D
1
10
100
1000
10000
Hz

d

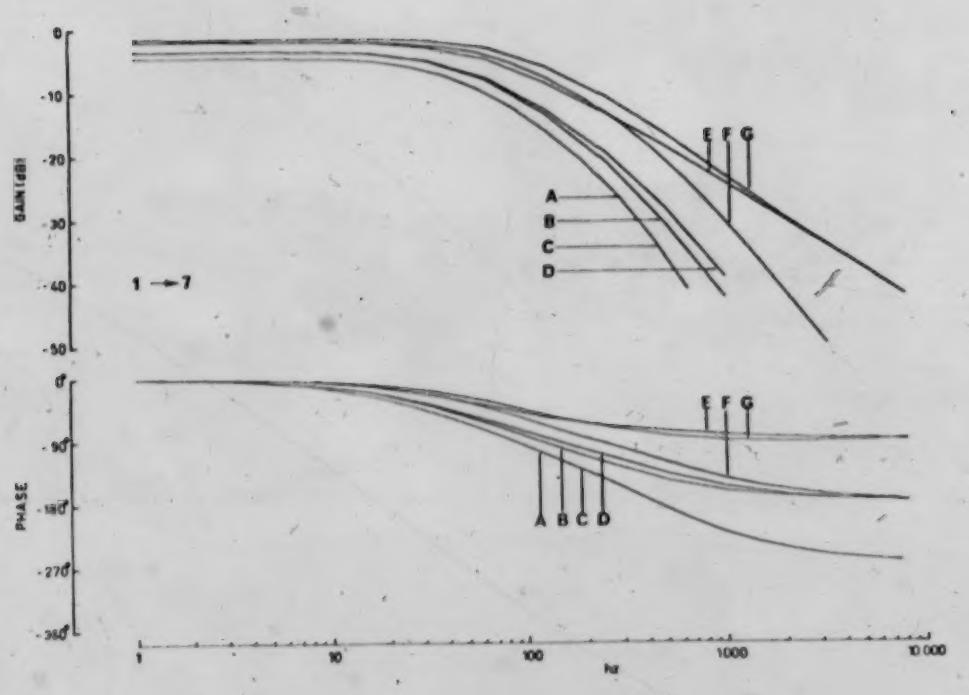
GAIN (dB)
0
-10
-20
-30
-40
-50
1 → 7
A
B
C
D
E F G
PHASE
0°
-90°
-180°
-270°
-360°
1
10
100
1000
10 000
Hz

e

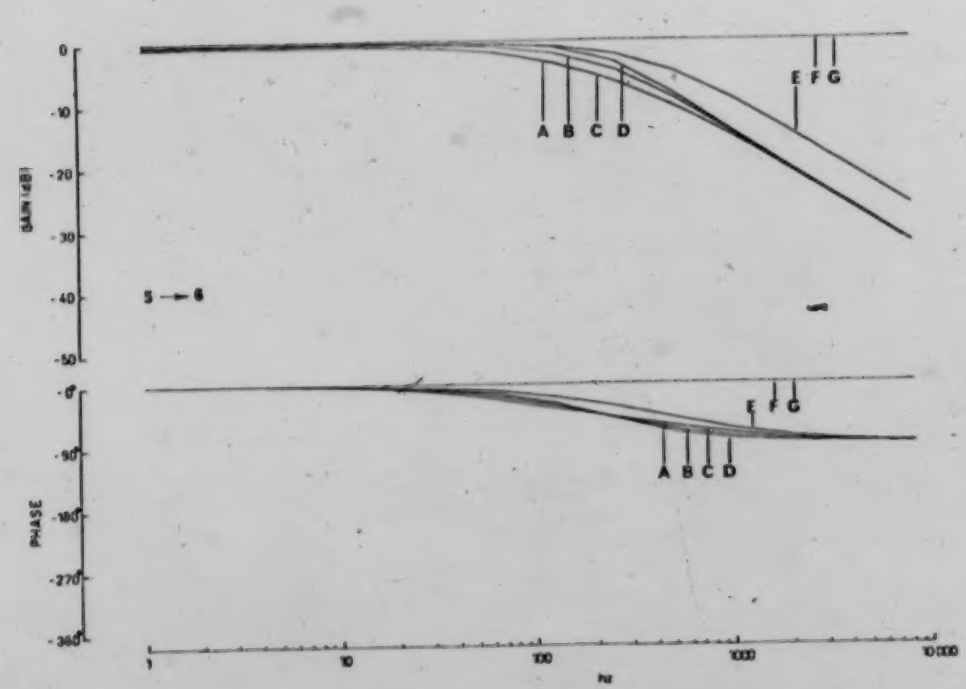
GAIN (dB)
0
-10
-20
-30
-40
-50
5 → 6
A B C D
E F G
PHASE
0°
-90°
-180°
-270°
-360°
1
10
100
1000
10 000
Hz

f

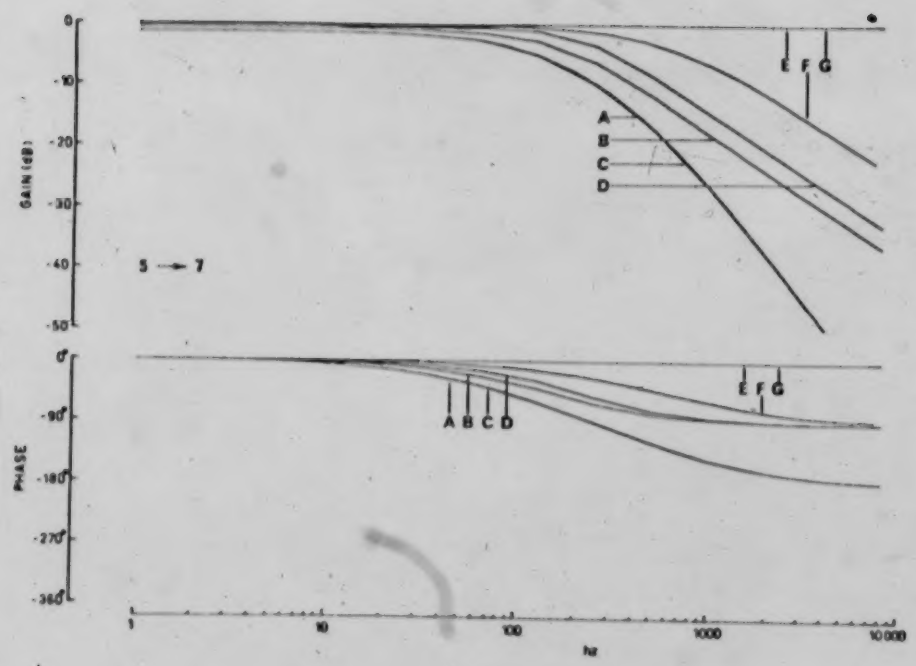
0
-10
-20
-30
-40
-50
GAIN (dB)
5 → 7
A
B
C
D
E F G
0°
-90°
-180°
-270°
-360°
PHASE
A B C D
E F G
1
10
100
1000
10000
hz

g

theoretical curves for cells 1-7, and in this case models E and G have first-order characteristics, B, D and F give second-order, and A and C predict third-order characteristics. At this point the only model which is consistent with the experimental results is model G. The argument that model G is correct is further strengthened by inspection of the curves for cells 5-6 and 5-7 shown in Figs. 7.5f and 7.5g respectively. The experimental results (see Fig. 7.4) indicate that the measurements between these two pairs of cells both displayed zero-order frequency response characteristics. In Fig. 7.5f only models F and G give this behaviour, while in Fig. 7.5g only models E and G give a zero-order response. It therefore seems probable that model G is correct since it alone correctly predicts the frequency response functions for all cell pairs.

The theoretical results using model G are superimposed on the experimental data in Fig. 7.4. The separation into two classes of curves is clearly indicated, with no responses greater than first-order, although the calculated curves do not perfectly overlay the experimental results. This is due to the fact that the parameters for the model have only been estimated, and not calculated analytically. If the connectivity of the model is correct, but the actual component values are different, such a difference is to be expected. These differences would not affect the order of the theoretical responses, but only shift the curves along the frequency and/or gain axes.

7.2 *Conclusions:*

Electrophysiological investigations of electrical coupling in

the eight-cell *Xenopus* embryo have indicated that all cells in the embryo are directly coupled to each other via identical resistive junctions. This appears to be an extension of the pairwise coupling which was found to occur in the four-cell embryo.

The conclusion that the maximum connectivity present in model G is correct is supported by the observation that if any of the intercellular connections in this model are removed, then the frequency response function between the two cells would become second-order, because current between them must flow through an intermediate cell. The order of one of the measured frequency response functions would therefore increase. As the experimental measurements never revealed a frequency response of higher order than that predicted by model G, any models of lower connectivity appear to be invalid.

Morphological investigations of the eight-cell embryo have also supported the high degree of connectivity present in model G (DiCaprio *et al.*, 1975). Scanning electron micrographs of an embryo where one animal pole cell has been removed revealed fine direct contact faces with adjacent cells (see Appendix II), as well as several cytoplasmic processes protruding from the primitive blastocoel. It was not possible to establish the origin of these processes or the details of the pathways that they could provide from scanning electron micrographs. The finest processes observed in these studies are about 10-15 μm in diameter.

Examination of serial light microscope sections (Appendix II, Fig. A.8) provides further evidence for extensive intercellular contact. These investigations have shown that fine processes can extend across

the embryo and between cells to provide a basis for remote contact between two cells. Processes which have diameters as small as 1 μ have been observed.

CHAPTER 8

ELECTRICAL MEMBRANE PROPERTIES DURING FIRST CLEAVAGE

8.1 *Introduction:*

The previous investigations of electrical coupling in early *Xenopus laevis* embryos have revealed that the blastomeres are all directly coupled to each other through the eight-cell stage. Morphological investigations of the early embryo have indicated that the first cleavage furrow is open to the extracellular medium and that intercellular contacts with some of the features of gap junctions are present between the cells of these stages (Sanders and Zalik, 1972; Singal and Sanders, 1974). One reasonable hypothesis for the mechanism of intercellular communication in *Xenopus* would therefore be that gap junctions serve to mediate current flow between the cells. This suggestion has also been made for *Triturus* embryos (Ito and Loewenstein, 1969; Ito and Hori, 1966).

Other authors have offered an alternate mechanism for the electrical coupling in *Xenopus* embryos. They have suggested that the new membrane which is present in the cleavage furrows has a lower specific resistance due to a high permeability to K^+ ions and that the perimeter of the furrow is sealed, thereby electrically isolating it from the external medium. Intercellular current flow would then not require the presence of specialized junctions since the blastocoel and furrow space would act as a common node linking all of the cells (Woodward, 1968; Slack and Warner, 1973; de Laat and Bluemink, 1974).

In order to determine which of these two mechanisms is more

probable, the electrical properties of the embryo were measured before and during the first cleavage. In addition, experiments using fluorescent dye injections and direct measurement of the electrical properties of the blastocoel were performed.

8.2 *Resistance measurements:*

The early *Xenopus* embryo may be modelled as a sphere, with the first cleavage furrow represented as a plane dividing the embryo into two hemispheres. The area of the new membrane in the cleavage furrow is therefore disc-shaped. Deviations from this model are possible due to the roughness of the embryo's surface and are discussed in detail by Bluemink and de Laat (1973). Using this simple model, the surface area of the single-cell embryo will be $4\ \pi r^2$, where r is the radius of the embryo. The first cleavage will then produce two cells with surface areas of $3\ \pi r^2$ each, and at the end of the second cleavage each cell will have a surface area of $2\ \pi r^2$.

The system used to model the membrane resistances as functions of time is shown in Fig. 8.1. The embryo at the single-cell stage may be considered to consist of two parallel identical resistances, R_M, each of which is the resistance of a hemispherical area of membrane, so that the equivalent input resistance of the embryo is $R_M/2$. The two-cell stage contains two membrane resistances, R_M, and the junctional resistance, R_J, which links the two cells. The cleaving embryo can therefore be described by a single electrical network which consists of three time-varying resistive elements: two identical membrane resistances, $R_M(t)$, and the junctional resistance, $R_J(t)$. If a stimulating current is

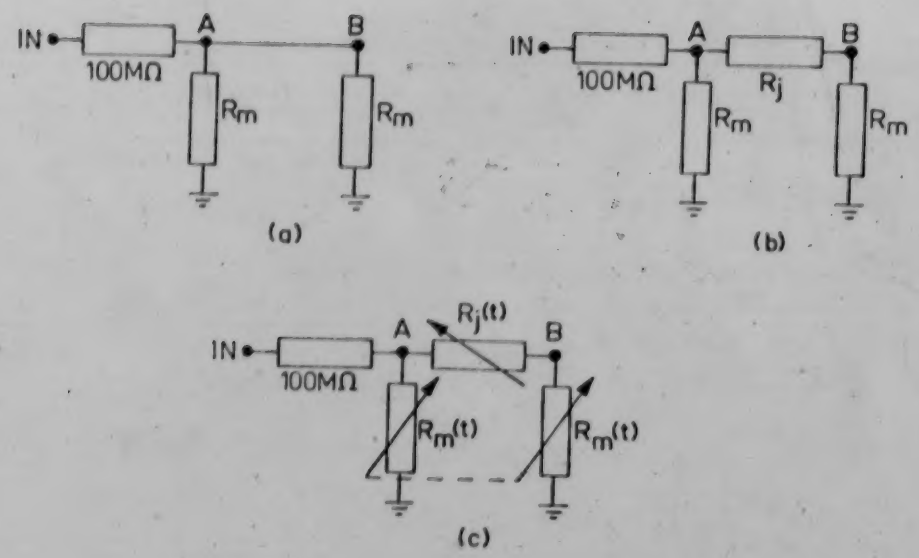

Fig. 8.1 Direct current electrical models of cleaving single cell embryo. (a) D.C. model of uncleaved embryo. (b) D.C. model of two-cell embryo. (c) D.C. model of embryo during first cleavage.

injected into one hemisphere, and the intracellular voltages are recorded in each side, the values of the resistances may be calculated at any time using Eqs. 5.5 and 5.9.

Three microelectrodes were used for each experiment. A stimulating voltage of 1 volt peak-to-peak amplitude at a frequency of 0.5 Hz was connected to one electrode and the two remaining electrodes were placed on opposite sides of the developing cleavage furrow to record the intracellular voltages. These signals were recorded during the experiment on a chart recorder. The values of intracellular voltage were later measured at 1 minute intervals from the chart record.

The results of a typical experiment are shown in Fig. 8.2. Time was measured in minutes from the instant at which the current injection and recording electrodes were inserted into the embryo. There was an initial large increase in apparent membrane resistance due to the sealing process around the electrodes which lasted approximately 6 minutes. Resistance values are therefore plotted from the sixth minute onward, although there was still a slight rise in $R_M(t)$ due to the termination of the sealing process during the seventh minute. During the course of the first cleavage, the membrane resistance, R_M, decreased steadily while the junctional resistance, R_J, was very low at the single-cell stage and did not change until the seventeenth minute, when it increased abruptly to more than 50% of its final value.

The simplest model of membrane formation during the cleavage is that the membrane of the cleavage furrow is produced by addition of new membrane, which is identical to the existing membrane, at a constant rate with time. If the cleavage furrow does not provide a significant

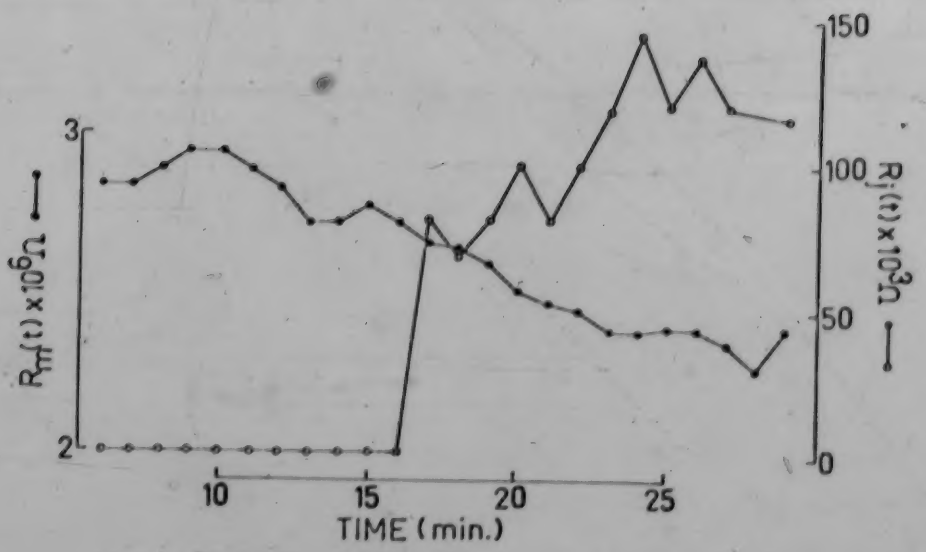

Fig. 8.2 Changes in R_M and R_J during cleavage. $R_M(t)$ and $R_J(t)$ are calculated from measurements of input resistance and coupling ratios using the network model shown in Fig. 8.1(c).

resistance to the flow of electric current, relative to the membrane resistance, all of the cell surfaces will contribute to the measured lumped membrane resistance. This model predicts that the membrane area will increase linearly with time, and since membrane resistance is inversely proportional to membrane area, the reciprocal of the membrane resistance should vary linearly with time. The measured values of membrane resistance from Fig. 8.2 are plotted in Fig. 8.3 as $1/R_M(t)$. The first three data points are not included so as to exclude the effects of the sealing process.

The above experiment was performed twenty times and four experiments met the criteria for normal embryonic development. The conditions which were used to define abnormally cleaving embryos were: (1) reversal of the cleavage furrow after electrode insertion, (2) displacement of the electrodes by the developing furrow, (3) spurious furrows appearing around the electrode, (4) abnormal development following removal of the electrodes. For the last criterion, each embryo was compared with control embryos placed in the same saline solution until the late blastula stage. The four acceptable experiments produced results similar to those illustrated in Figs. 8.2 and 8.3. The slopes of the best-fitting straight lines on the $1/R_M(t)$ plots were in the range of 5.3 to 13.1 $\times 10^{-9}$ mhos per minute. Using the value of 45 KΩcm^2 for specific resistance of surface membrane determined in earlier experiments, the range of slopes gives a range of membrane area addition rates of 2.3 to 5.8 $\times 10^{-4}$ cm^2/minute. This may be compared to the rate of 4×10^{-4} cm^2/minute obtained by de Laat and Bluemink (1974). The linear correlation coefficients for the four plots were in the range 0.971 to

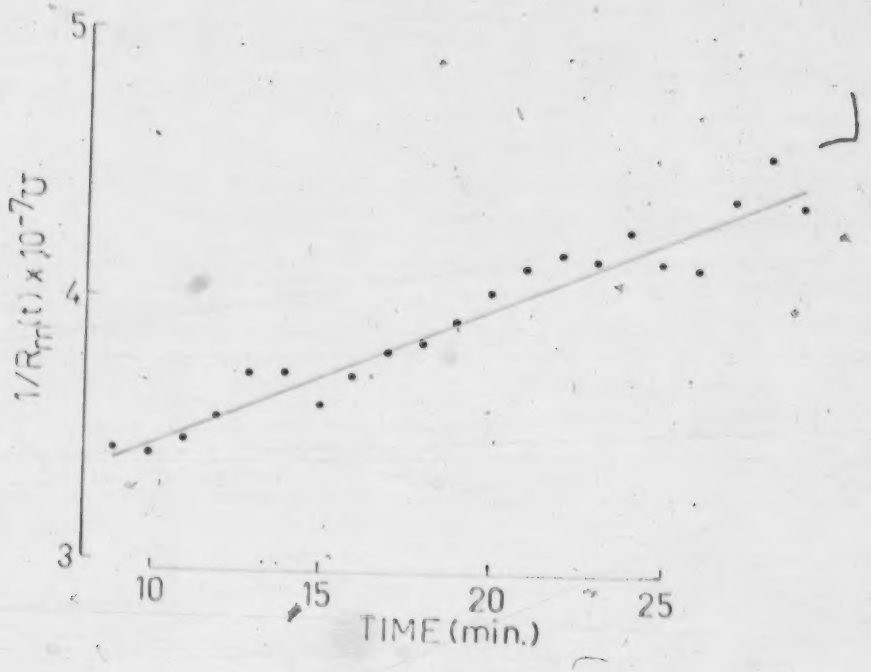

Fig. 8.3 Plot of $1/R_M$ vs time data is obtained from the value of $R_M(t)$ in Fig. 8.2. The first four points from Fig. 8.2 were eliminated to remove the effect of the sealing process.

0.985, indicating that the simple-model of membrane addition is compatible with the results for $R_M(t)$.

A valid model for a cleaving single-cell embryo must account for the rapid rise of the junctional resistance from approximately zero to 50% of its final value in 1 minute. During the early portion of this cleavage process, the resistance, $R_J(t)$, represents the resistance of the cytoplasmic bridge which still joins the two hemispheres of the embryo. After this bridge has closed off, the value of $R_J(t)$ represents the junctional resistance between the two blastomeres. The resistance of the cytoplasmic bridge would initially be very small, remaining undetectable until its diameter was comparable to its length. The sudden rise in $R_J(t)$ for the experiment shown in Fig. 8.2 could therefore be explained by the closure of the cytoplasmic bridge, whose low resistance up to that time would have dominated the observed value even if the junctional resistance between the cells were already established. The embryo used for the experiment of Fig. 8.2 was at the far advanced groove stage (Singal and Sanders, 1974) at the time of electrode insertion, which is 15-18 minutes after the start of cleavage. The normal time course of development would therefore place completion of first cleavage at approximately 36 minutes or at about the eighteenth minute in Fig. 8.2. Using the rates of membrane insertion computed above, the range of times between the onset of cleavage and closure of the cytoplasmic bridge would be 22-25 minutes. The sudden rise in $R_J(t)$ which occurred at about 32-35 minutes after the onset of cleavage is therefore compatible with the observed external morphology during the experiment and with the calculated rates of membrane addition.

8.3 *Frequency response measurements:*

The input frequency response of the dividing embryo was measured as a function of time in order to further investigate the membrane resistance and capacitance during cleavage. The corner frequency of the input response is a function of all the elements in the network model of the embryo, R_J, R_M and C_M. If the changes in R_M and C_M are predicted according to the simple geometric model where the surface area increases by 50% during the first cleavage, the predicted change in corner frequency should agree with the experimental results if this model is correct.

Three electrodes were inserted into an uncleaved embryo, two recording electrodes on either side of the developing furrow, and one current injection electrode. The injected current was white noise with a peak-to-peak amplitude of 1 volt and band-limited to 0-50 Hz. After the electrodes were inserted and the sealing process terminated, the input and output signals were sampled regularly at intervals of 10 msec and stored in digital format on a magnetic disc using the PDP-11/40 computer. Data storage continued until the external morphology of the embryo indicated that the first cleavage was complete. The duration of an entire experiment was approximately 45-50 minutes. The stored data was later analyzed to produce frequency response function plots at 1 minute intervals, using twenty sets of averaged spectral estimates to produce each curve. The results of a typical experiment are plotted in Figs. 8.4-8.6 as three-dimensional views of the gain, phase and coherence curves versus time. The curves are all fairly uniform with only one abrupt change which occurred at the twelfth minute. The discontinuity is

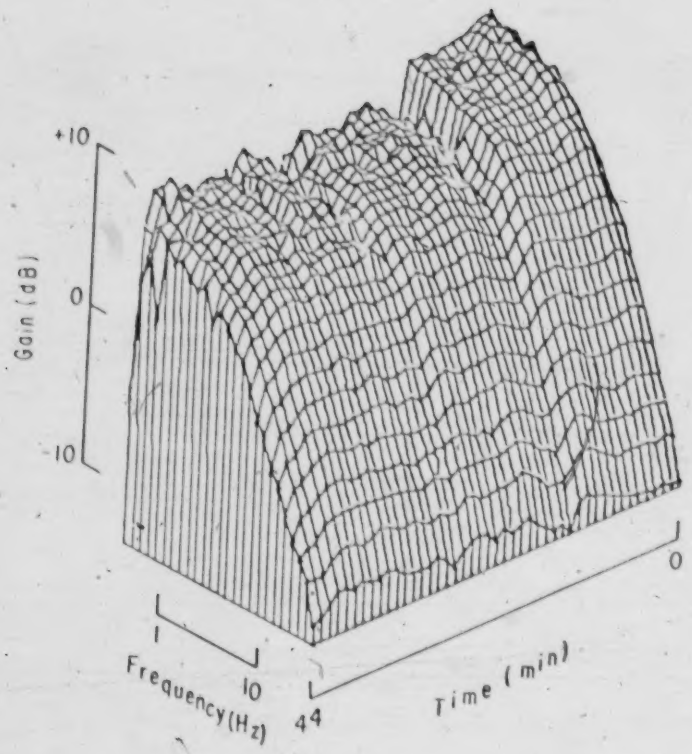

Fig. 8.4. Gain characteristic of frequency response during first cleavage.

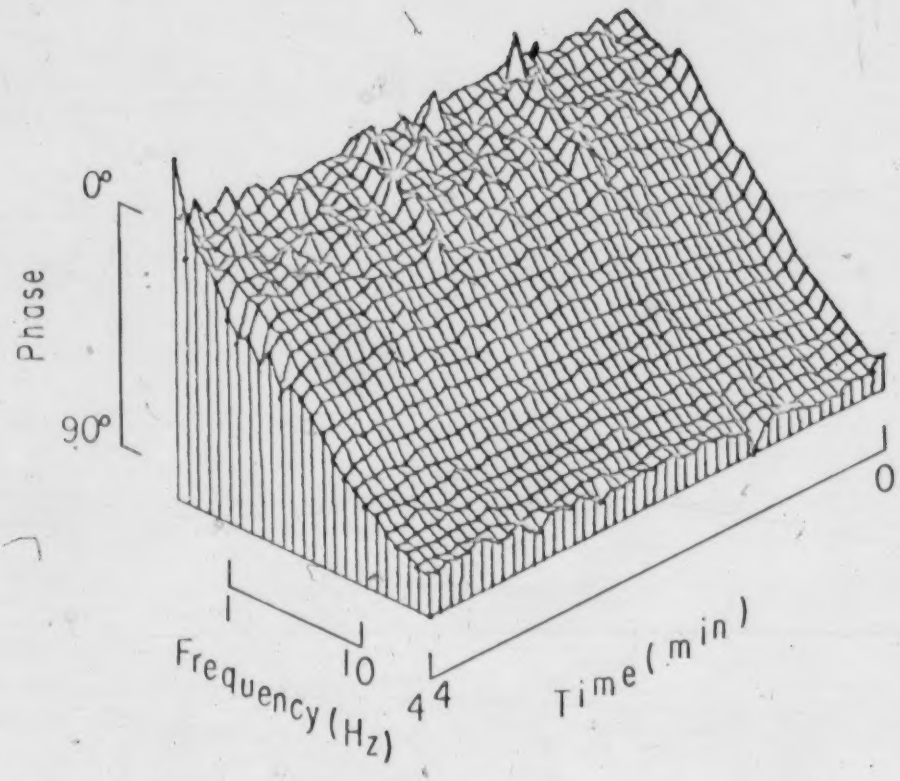

Fig. 8.5 Phase characteristic of frequency response during first cleavage.

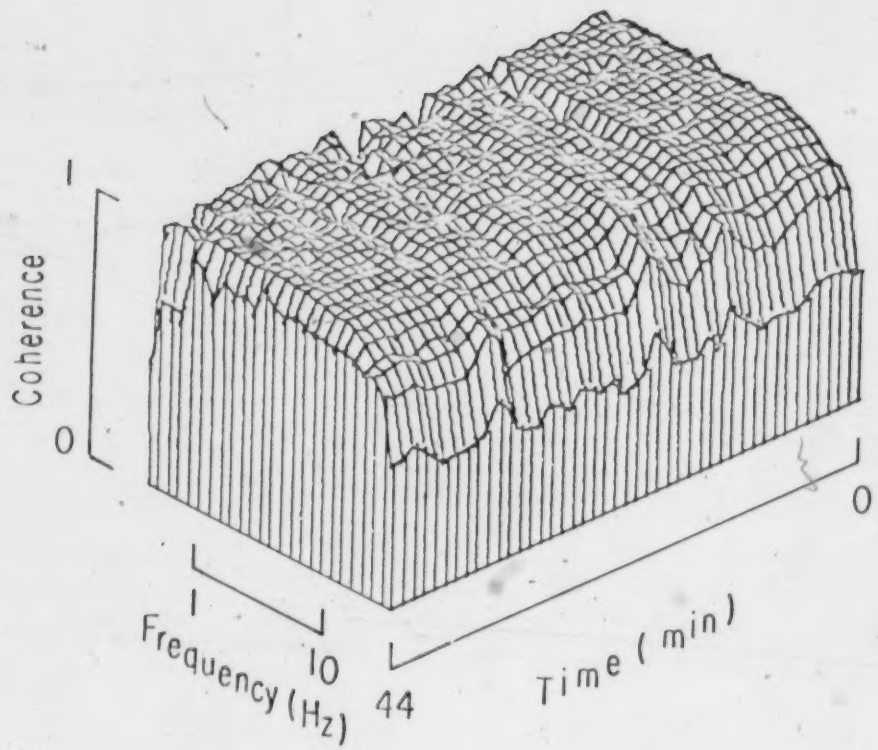

Fig. 8.6 Coherence of frequency response during first cleavage.

seen in the gain, phase and coherence curves, which would indicate that it was probably caused by a mechanical disturbance to the system.

These results may be compared with the theoretical model shown in Fig. 8.7. The values of R_M and C_M before and after cleavage reflect a change in the membrane area from 2 πr^2 to 3 πr^2, where the coupling ratio of 0.9 is taken from the experiment of Fig. 8.4 giving a value of R_J = 140 kΩ. The predicted corner frequency of the input response for the uncleaved embryo is 4.0 Hz and 6.1 Hz after the first cleavage. The experimental data in Fig. 8.5 gives an initial corner frequency of 3.7 Hz, changing to 5.2 Hz after the completion of first cleavage. The changes in corner frequency for the experimental and theoretical curves are not in agreement as the predicted change is 52% while the experimental change is 40%.

8.4 *Membrane capacitance measurements:*

It proved to be technically difficult to measure the membrane capacitance as a function of time from the type of experiment described above. However, an accurate estimate of membrane capacitance for the single-cell embryo was determined using spectral analysis techniques. Two electrodes were inserted into an uncleaved embryo, one for recording and one for current injection. A low frequency measurement of the membrane resistance, R_M, was made using a sinusoidal input current of 0.5 Hz and the input frequency response was measured using a white noise input. The value of C_M was then obtained from:

$$C_M = \frac{1}{2\pi f_c R_M}$$

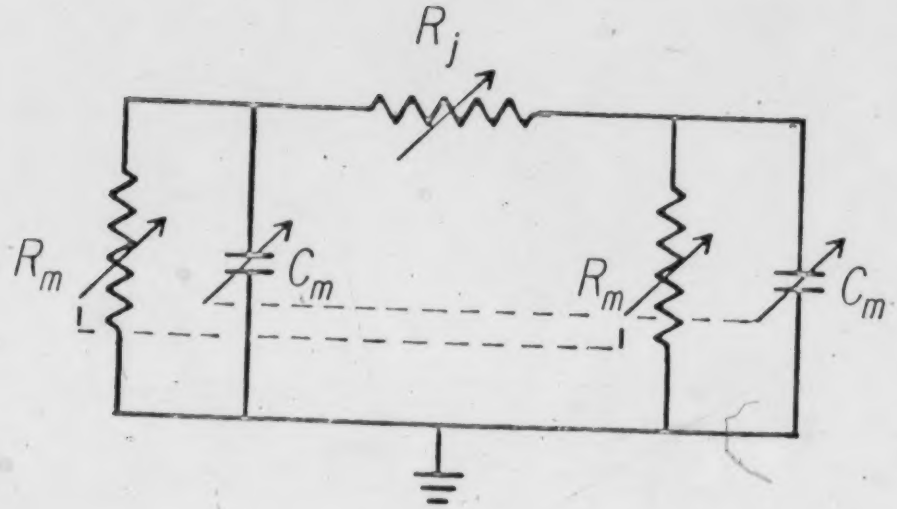

Fig. 8.7 A.C. electrical model of cleaving single-cell embryo.

where f_c is the corner frequency of the input frequency response function. The measured capacitance of the uncleaved embryo was 0.0428 ± 0.0054 μf (mean ± standard deviation for twelve experiments).

Since membrane capacitance is proportional to membrane surface area, there should be a linear relationship between the total surface area of the cells and the capacitance, if the new membrane is of the same specific capacitance as the original membrane and is accessible to the external solution. However, the measured capacitance decreases faster than would be predicted by this model. The simple geometric models of the membrane surface area predict two- and four-cell lumped capacitances of 0.0321 μf and 0.0214 μf respectively based on the single-cell measurement of 0.0428 μf. The values calculated from the experimental measurements were 0.0239 μf and 0.0106 μf. If the furrow membrane and blastocoel were isolated from electrical ground by sealing junctions at the surface of the embryo the expected values of capacitance would be 0.0214 μf and 0.0107 μf for the two- and four-cell stages. The simple model of addition of identical new membrane to an unsealed cleavage furrow therefore does not adequately explain the capacitance measurements.

8.5 *Effects of membrane folding:*

The simple geometric model of cleavage in early *Xenopus* embryos, in which the embryo is modelled as a perfect sphere, does not appear to adequately explain the data from the frequency response and the cell membrane capacitance measurements. This model may be modified by considering the effects of membrane folding on the surface area. Bluemink

and de Laat (1973) have estimated that the surface area of the uncleaved embryo is 69% greater than that of a simple sphere due to the roughness of the 'old' membrane. They also report that the new membrane which is present in the cleavage furrow is smooth compared to the surface membrane, so that no correction for the surface area is required in this region. These findings are also supported by the work of Singal and Sanders (1974).

The surface area of an uncleaved embryo would therefore be approximately 6.8 πr^2 assuming a 70% increase in the area of the rough outer membrane. The area of a cell from a two-cell embryo would be 3.4 πr^2 for the outer surface and πr^2 for the smooth furrow membrane or a total of 4.4 πr^2. In a similar manner the surface area of a cell from a four-cell embryo would be 2.7 πr^2. These changes in membrane surface area cause a change in the calculated rate of membrane addition, the predicted frequency response changes during cleavage and the predicted value of membrane capacitance.

The specific membrane resistance (41 $K\Omega cm^2$) for a two-cell embryo given in Table I becomes 69.7 $K\Omega cm^2$ when the folding of the surface membrane is taken into account. This new value of specific resistance yields a range of membrane area addition rates of 3.7 to 9.1×10^{-4} cm^2/minute based on the slopes of the best-fitting straight lines on the $1/R_M$ versus t plots. The value of 4×10^{-4} cm^2/minute obtained by de Laat and Bluemink (1974) is therefore still in the range determined from the experiments described in section 8.2.

The measurement of the change in corner frequency of the input frequency response is also affected by the modification of the membrane

surface area. The predicted changes in R_M and C_M are not based on a change in membrane surface area from 3.4 πr^2 to 4.4 πr^2 and not from 2 πr^2 to 3 πr^2 as used previously in the previous sections. Using the revised values of R_M and C_M and choosing R_J so that the coupling ratio is 0.9, the FCAP program predicts a change in corner frequency of 37% compared to 40% for the experiment shown in Fig. 8.4, and 52% for the prediction based on the smooth membrane model.

Measurements of R_M and C_M for the uncleaved embryo are given in Table IV. The value for R_M is 0.96 ± 0.25 × 10^6 Ω (26 experiments) which is in agreement with the value of 0.852 × 10^6 Ω obtained by de Laat and Bluemink (1974), and the value of C_M is 0.0428 × 0.0053 μf, determined from fifteen experiments. The predicted values of R_M and C_M for two- and four-cell embryos are given in Table IV based on the rough membrane model. The predicted membrane resistance and capacitance are both higher than the experimental values but all values are within one standard deviation of each other.

8.6 *Dye diffusion into the blastocoel:*

The primitive blastocoel first appears as a small enlargement of the cleavage furrow during first cleavage (Kalt, 1971; Singal and Sanders, 1974). Measurements of blastocoel size made using embryos that had been dehydrated in a critical point dryer and then split along the cleavage furrow are summarized in Table V.

To investigate whether the blastocoel and cleavage furrows are isolated from the external medium, attempts were made to diffuse dye into the blastocoel from the perivitelline space. Glass microelectrodes were

TABLE-IV

PREDICTED AND MEASURED CELL MEMBRANE RESISTANCE AND CAPACITANCE OF *Xenopus* EMBRYOS DURING THE FIRST TWO CLEAVAGES

The measured values for the uncleaved egg are presented here for the first time and the predicted values for the next two stages are based upon the uncleaved egg measurements and open furrow models with rough outside membranes and smooth furrow membranes. The measured values for the two- and four-cell stages are those reported by DiCaprio *et al.* (1974).

STAGE	MEASURED RESISTANCE	MEASURED CAPACITANCE	PREDICTED RESISTANCE	PREDICTED CAPACITANCE
1-cell	$.96 \pm 0.22 \times 10^6$ Ω	0.0428 ± 0.0054 μ	-	-
2-cell	$1.05 \pm 0.16 \times 10^6$ Ω	0.0239 ± 0.0035 μf	1.48×10^6 Ω	0.0276 μf
4-cell	$1.80 \pm 0.20 \times 10^6$ Ω	0.0106 ± 0.0047 μf	1.71×10^6 Ω	0.0146 μf

TABLE V

MEASUREMENTS OF EARLY BLASTOCOEL DIAMETER

Ten embryos were measured at each stage

STAGE	FRACTION OF EMBRYOS WITH DETECTABLE BLASTOCOEL	MEAN BLASTOCOEL DIAMETER
2-cell	25%	< 40 μ
4-cell	75%	146 μ
8-cell	100%	240 μ

filled with a 5% solution of fluorescent dye, Procion yellow M4RAN, in Steinberg's solution. Electrodes were placed in a holder designed for pressure injection and inserted into the perivitelline space. The dye was injected under pressure for a period of 3-5 minutes and the embryos were allowed to remain in the saline solution for 10-15 minutes after the injection and then fixed in Kalt's fixative (Kalt and Tandler, 1971). During the interval between the injection of the dye and fixation of the embryo the dye was observed to be slowly diffusing through the vitelline membrane, but the perivitelline space still contained a high concentration of Procion yellow as indicated by its yellow-orange color. The embryos were not allowed to cleave before fixation and any embryos that sustained any physical damage or deformation during the experiment were discarded.

After fixation the embryos were dehydrated in alcohol and xylene, mounted in wax and sectioned for light microscopy. Figs. 8.8 and 8.9 show fluorescent micrographs obtained from sections of an eight-cell embryo. The Procion has not bound to the plasma membrane on the surface or the interior of the embryo. The only place where there is fluorescence present is where a cell has been damaged in the interior of the embryo and the cytoplasm has been stained (Fig. 8.8). The stain also appears in both the cleavage furrows as seen in Fig. 8.9.

8.7 *Electrical recording from the blastocoel:*

To determine whether current flowing between blastomeres passes through the blastocoel, electrical recordings were made directly from the blastocoel using a microelectrode. Attempts to place an electrode into the primitive blastocoel of two- and four-cell embryos were

Fig. 8.8 Fluorescent micrograph of the eight-cell embryo, section is through the primitive blastocoel and shows Procion yellow staining of cytoplasm which has leaked from one cell.

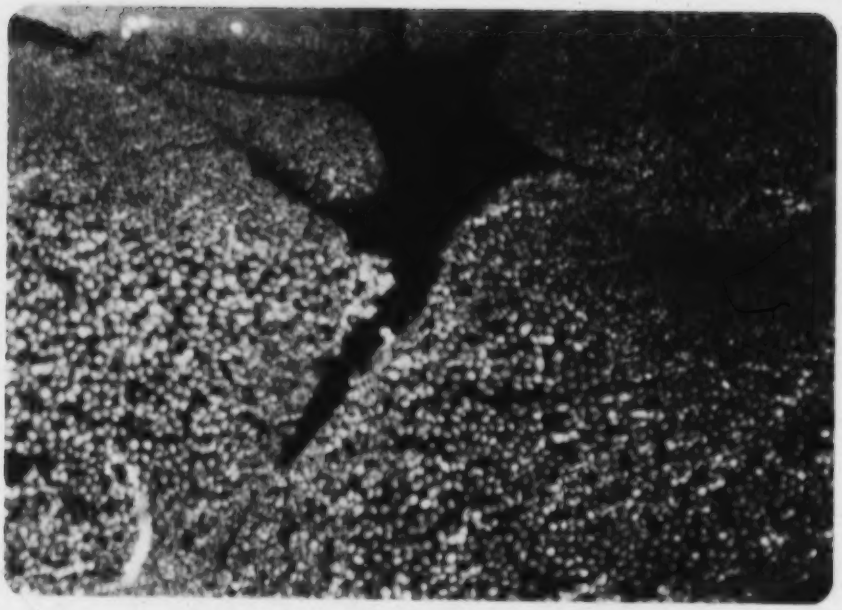

Fig. 8.9 Fluorescent micrograph of the eight-cell embryo, showing the presence of Procion yellow in the cleavage furrow.

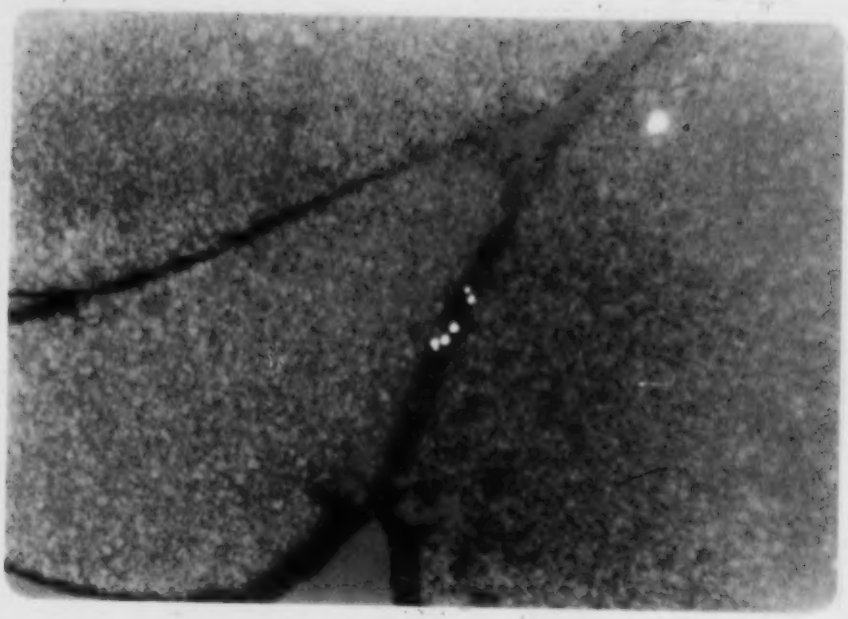

unsuccessful, but experiments on eight-cell embryos produced results similar to that shown in Fig. 8.10. A current injecting electrode was placed in an animal pole cell of an eight-cell embryo and a 0.5 Hz sinusoidal current applied to it. Two recording electrodes were used, one in the cell with the current injection and the other in the diagonally opposite cell. The first recording electrode was positioned by a hydraulic micromanipulator which allowed precise movement of the electrode in one direction with measurement of relative position to a resolution of 1 μ. The electrode was placed to enter the embryo at an angle of 45° to the vertical so that its path would intercept the blastocoel. In Fig. 8.10 the intracellular voltage recorded with this electrode is plotted against time as the electrode was advanced through the embryo. Initially a membrane potential of -15 mV was observed, with the superimposed sine wave being due to the injected current in the adjacent cell. At a depth of 540 μ relative to the surface of the embryo the sinusoidal modulation ceased and the membrane potential changed abruptly to 0 volts. The electrode was then withdrawn and the sinusoidal modulation and hyperpolarized membrane potential again observed until the electrode was removed from the cell. The bottom trace in Fig. 8.10 is a record of the intracellular voltage in the cell diagonally opposite from the cell containing the driven electrode. It can be seen that electrical coupling is maintained in the embryo throughout the course of the experiment with the slight disturbances due to the first electrode being withdrawn from the embryo.

The above experiment is interpreted to mean that the electrode passed through the animal pole cell and into the blastocoel, where a

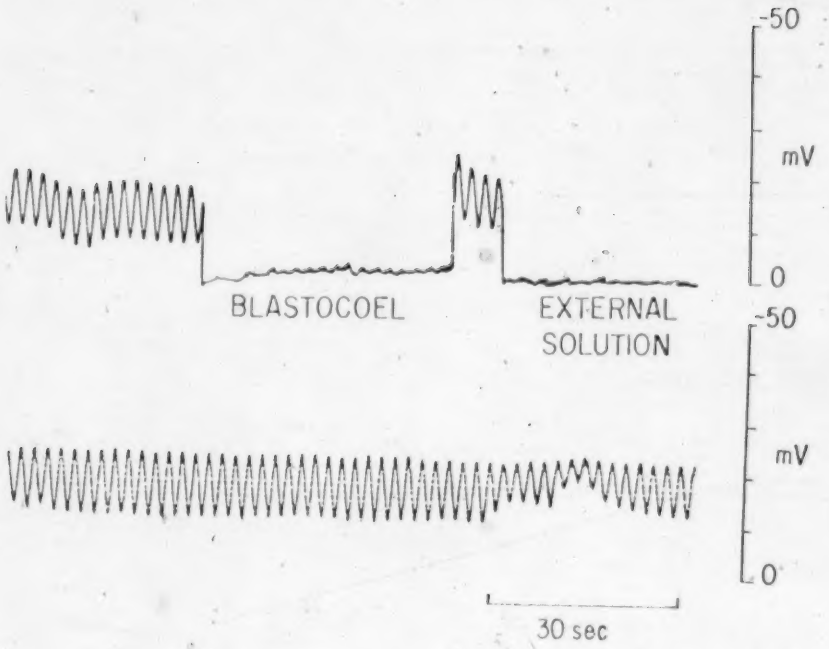

Fig. 8.10 Measurement of blastocoel potential. The upper trace is from the recording microelectrode driven by the microdrive through an animal pole cell, then into the blastocoel, and then withdrawn from the embryo. The bottom trace is from a recording microelectrode in the cell diagonally opposite the cell shown in the top trace.

potential identical to that of the external solution was recorded with no sinusoidal modulation present due to the injected current. The blastocoel was therefore at ground potential and unable to act as a common node electrically interconnecting the blastomeres.

In order to confirm the assumption that the recording electrode had penetrated the blastocoel, the embryo was fixed immediately after the experiment and later critically point dried. The embryo was then split into two hemispheres and prepared for scanning electron microscopy so that the blastocoel could be inspected. Fig. 8.11 shows scanning electron micrographs of each half of the embryo. It can be seen that a diffuse substance is present in one side of the blastocoel, which was not found to be present in control embryos. Fig. 8.12 shows two scanning micrographs of the blastocoel region and the presence of yolk platelets in the blastocoel indicates that the diffuse material is cytoplasm. The conclusion is therefore that the penetration of the microelectrode into the blastocoel had allowed some leakage of cytoplasm into the cavity.

In other experiments the recording electrode was not immediately withdrawn after penetrating the blastocoel but was instead advanced further until a cell membrane potential was recorded. The distance required to advance the electrode through the region of 0 volts was approximately 150 μ, which is in good agreement with the size of the blastocoel observed with scanning electron microscopy (DiCaprio *et al.*, 1974; see Appendix II).

8.8 *Conclusions:*

The electrical behaviour of the junctional and non-junctional membrane in *Xenopus* embryos during the first cleavage may be accounted

Fig. 8.11 Scanning electron micrographs of the eight-cell embryo used in the experiment of Fig. 8.10. In one half of the embryo (top) the blastocoel (B) can be seen as a cavity. In the bottom picture the blastocoel (B) is seen to be filled with a diffuse substance which is presumed by to cytoplasm.

B
200μ
B

Fig. 8.12 Two higher power views of the half embryo shown at the bottom of Fig. 8.11. The blastocoel contains cytoplasm as indicated by the presence of yolk platelets.

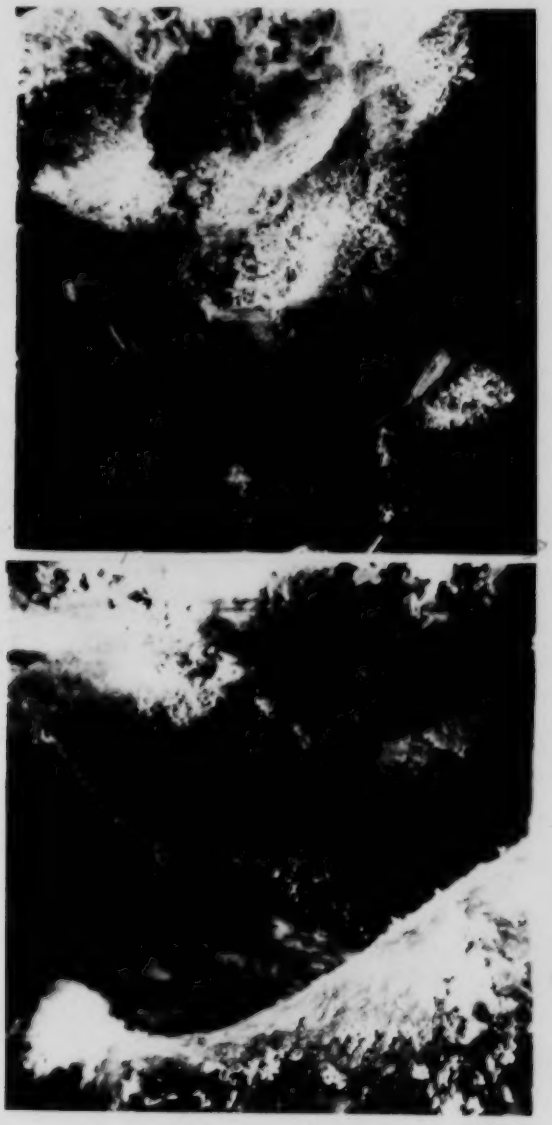
50μ
20μ

for by a model having the following properties: (1) new membrane is added to the cleavage furrow at a constant rate, (2) the new membrane has identical specific resistance to the original membrane, (3) the 'old' surface membrane is folded, thereby increasing the effective surface area, (4) the furrow and primitive blastocoel are electrically connected to the perivitelline space, (5) electrical coupling between daughter cells occurs through specialized junctions which are functional at the time of cytoplasmic separation.

The diffusion of dye into the blastocoel and the direct electrical measurements of the blastocoel potential strongly support a model in which the furrow and primitive blastocoel are in direct contact with the perivitelline space. They also preclude electrical coupling of the cells via flow of current through the perivitelline space. Although it was not possible to perform these two experiments on two- or four-cell embryos, evidence obtained by Singal and Sanders (1974), who demonstrated that the entire furrow was accessible to lanthanum ions applied during fixation, supports the hypothesis that the furrow is not sealed. The presence of a sealing ring of tight junctions would prevent the penetration of these ions into the furrow (Revel and Karnovsky, 1967).

The changes in cell membrane resistance and capacitance observed during the first cleavage are also compatible with the assumption of an open furrow and blastocoel, if the effects of surface membrane folding are taken into account. One factor which has not been considered in these calculations is the effect of the relatively thick coat of surface material in the furrow membrane, as compared with the non-furrow membrane (Singal and Sanders, 1974). This material is stained

by lanthanum ions and is thought to bind electrostatically to surface charges (Martinez-Palomo, 1970). The resulting separation of charges across the membrane could account for the lower value of membrane capacitance as compared with the predicted value.

Similar measurements of embryonic input resistance and capacitance and membrane potential were made on *Rana pipiens* by Woodward (1968). His experimental results were variable with large fluctuations being observed in all parameters as opposed to the smooth changes reported here. In addition, Woodward reported large increases in input resistance which contrasts with the steady decline reported here and by de Laat and Bluemink (1974), while his measured capacitance for a single cell was about twice that given here, although this may be due to a species difference. The increase in membrane capacitance of only 3% obtained by Woodward during first cleavage is also different from the large change noted here. Woodward's suggestion that these observed changes are caused by the electrical isolation of the blastocoel caused by the cable-like properties of the cleavage furrow is not supported by the direct measurements of the blastocoel potential.

Both Slack and Warner (1973) and de Laat and Bluemink (1974) contend that the new membrane which lines the cleavage furrows and blastocoel is of a lower specific resistance than the old surface membrane and that the low permeability of this membrane and the presence of tight junctions sealing the periphery of the embryo are the mechanism responsible for the intercellular communication. However, although intimate intercellular contacts have been demonstrated in early embryos of *Triturus* (Selman and Perry, 1970) and *Xenopus* (Kalt, 1971b; Singal and Sanders,

1974), there is no evidence that they form a complete sealing ring which electrically isolates the blastocoel from the perivitelline space. Indeed, it would be hard to explain how the resistance changes which have been observed here and by de Laat and Bluemink could occur if the furrow region was electrically isolated.

Evidence for a difference between the properties of old and new membrane has been presented for *Rana pipiens* embryos growing in hypertonic solutions (Woodward, 1968) and for *Xenopus* embryos growing in the absence of the vitelline membrane or in the presence of Cytochalasin-B (de Laat and Bluemink, 1974). The changes in membrane resistance with time in these preparations may be suspect as the effects of the modifying agents are incompletely understood. Bluemink and de Laat (1974) noted that removal of the vitelline membrane or addition of Cytochalasin-B not only caused eversion of the cleavage furrow but also altered the rate of membrane formation and the total amount of new membrane formed during cleavage. The removal of the vitelline membrane is a delicate procedure which may easily disturb specialized membrane junctions which may be responsible for intercellular communication. The incomplete sealing of these junctions or any other wounds incurred during the procedure may also account for the lower membrane resistance measured during these experiments.

CHAPTER 9

EFFECTS OF CALCIUM ION CONCENTRATION ON COUPLING

9.1 *Introduction:*

In many electrically-coupled systems the degree of coupling has been found to be sensitive to the concentration of free calcium ions both in the external medium and inside the cells (Rose and Loewenstein, 1971, 1975a, b; Oliveira-Castro and Loewenstein, 1971; Penn and Loewenstein, 1967). The effect of Ca^{++} concentration was investigated in early *Xenopus* embryos using two methods, first by placing the embryo in a saline solution containing a controlled amount of free Ca^{++} and secondly by the iontophoresis of Ca^{++} into the embryo using a microelectrode.

Low calcium solutions were prepared using Mg^{++} free Steinberg's solution plus EGTA with the following composition: NaCl, 3.3 g; KCl, 50 mg; $NaNO_3$, 43 mg; Na_2SO_4, 16 mg; TRIS, 560 mg; and EGTA, 380 mg (for 1 liter of solution). The desired amount of free calcium was obtained by adding $CaCl_2$ to the stock solution according to the formula:

$$x = \frac{200\,n^2 + 201\,n}{1 + 200\,n}$$

where x is the amount of Ca^{++} required given a 1 liter solution containing 1 mM EGTA and n mM free Ca^{++}. This formula was obtained from the expression:

$$\frac{[Ca - EGTA]}{[Ca^{++}][EGTA]} = k$$

where k = 200.

For intracellular calcium iontophoresis, glass microelectrodes were filled with 0.1 M solutions of both $CaCl_2$ and KCl, yielding resistances in the range of 20-40 MΩ. Three intracellular electrodes were used in the same way as for other experiments.

9.2 *Effects of low external free calcium concentration:*

Table VI summarizes the experiments performed on 24 embryos placed in Steinberg's solution containing varying amounts of free Ca^{++}. The normal calcium concentration in Steinberg's solution is 3.4×10^{-4} M, and when a solution containing 10^{-4} M free Ca^{++} was used, no effect on membrane potential, embryonic input resistance or coupling ratio was observed. For a free calcium ion concentration in the range 3×10^{-6} M to 8×10^{-6} M the membrane potential remained stable in the first few minutes of the experiment, the input resistance dropped to less than 20% of normal values during the experiment and the coupling ratio was unaffected. In addition, the magnitude of the membrane potential decreased during the course of these experiments. The plasma membrane of embryos maintained at this concentration deteriorated, allowing the escape of cytoplasm from the cells and eventual collapse of the embryo.

An external calcium ion concentration of 10^{-5} M had a variable effect on the membrane properties of the embryo and on the coupling ratio. In four out of eight experiments at this concentration, the coupling ratio decreased below normal levels and in three of these experiments the coupling ratio dropped to below 0.2. In all experiments where the coupling ratio decreased the input resistance also decreased

TABLE VI

SUMMARY OF RESULTS OBTAINED FROM EXPERIMENTS PERFORMED IN SOLUTIONS CONTAINING LOW FREE CALCIUM

$[Ca^{++}]_{ext}$	Number of Experiments	Membrane Potential	Input Resistance	Coupling Ratio
10^{-4} M	5	All normal	All normal	All normal No change
3×10^{-5} M	2	All normal	All normal	All normal No change
10^{-5} M	8	2 decreased 6 normal	6 decreased 2 normal	3 uncoupled cr<.2 1 low .4<cr<.6 4 normal
8×10^{-6} M	5	All decreased	All decreased	All normal No change
5.5×10^{-6} M	2	All decreased	All decreased	All normal No change
3×10^{-6} M	2	All decreased	All decreased	All normal No change

during the experiment. The data from an experiment performed at 10^{-5} M external calcium ion concentration is shown in Fig. 9.1. The peak-to-peak amplitudes of the modulated intracellular voltages and the coupling ratio are plotted against the time from the instant when the embryo was placed into the low Ca^{++} medium. The normal sealing process was seen to occur at the beginning of the intracellular voltage record and after 8 minutes the amplitude of the modulation in both cells decreased while the value of the coupling ratio did not drop until approximately the 11th minute. After 30 minutes the coupling ratio had decreased to below 0.2 from an initial value of approximately 0.95. During the course of the experiment the input resistance, which is proportional to the voltage in cell 1, dropped to 40% of its initial value. The experiment shown in Fig. 9.2 gives a similar result for an external calcium ion concentration of 10^{-5} M, although the magnitudes of the changes are not as great. The coupling ratio decreased from 0.9 to 0.4 in 24 minutes and the input resistance decreased to 65% of the initial value.

The concentration of free external calcium ions also affected the time required for the membrane to seal around the electrodes after they were placed into a cell. Fig. 9.3 illustrates the sealing rates for embryos in 10^{-4}, 10^{-5} and 10^{-6} M Ca^{++} solutions where the sealing rate is given by the rate of change of the intracellular voltage after penetration of the cell by the recording microelectrode. As the free external calcium was decreased, the rate of sealing decreased, indicating that the non-junctional membrane was also affected by the change in Ca^{++} concentration. In most of the experiments performed in solutions

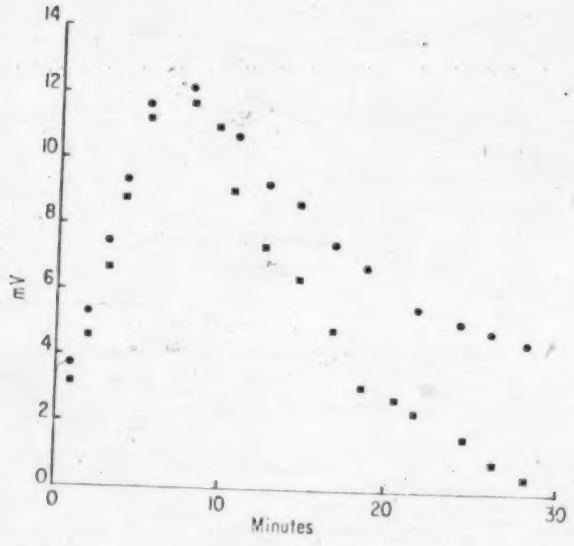

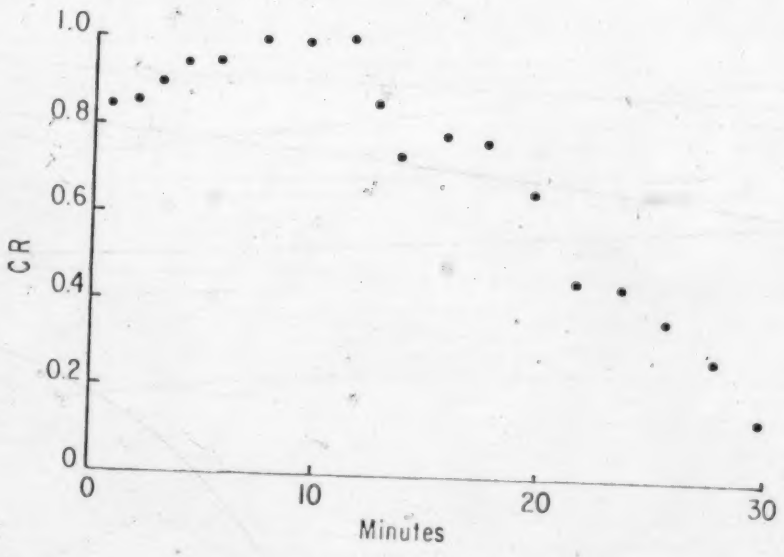

Fig. 9.1 Effect of 10^{-5} M free external calcium on intracellular voltage and coupling ratio. Data is from a four-cell embryo. ●, voltage in cell containing the current injection electrode, ■, voltage in adjacent cell.

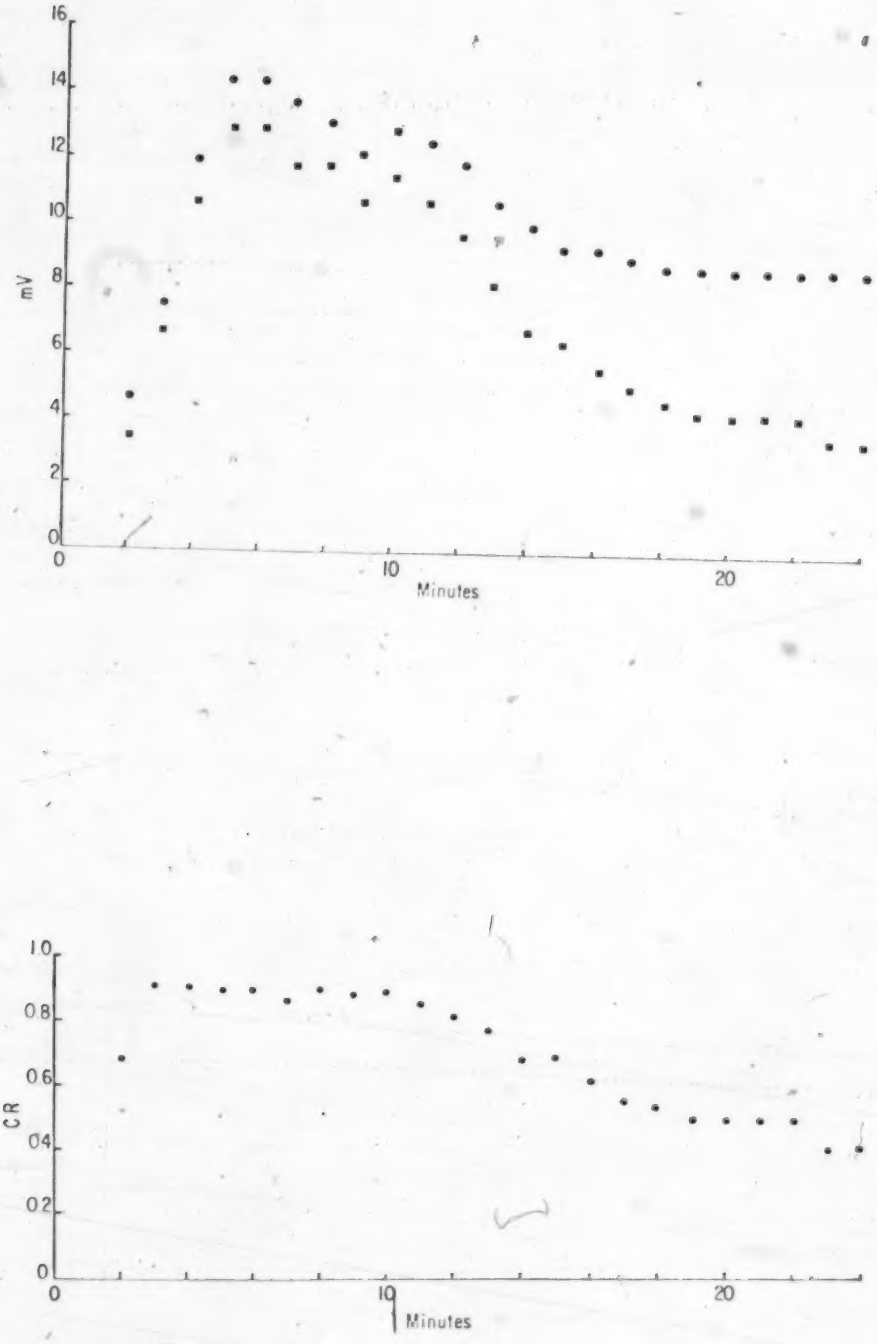

Fig. 9.2 Effect of 10^{-5} M free external calcium on intracellular voltage and coupling ratio. Data is from a four-cell embryo. ●, voltage in cell containing the current injection electrode, ■, voltage in adjacent cell.

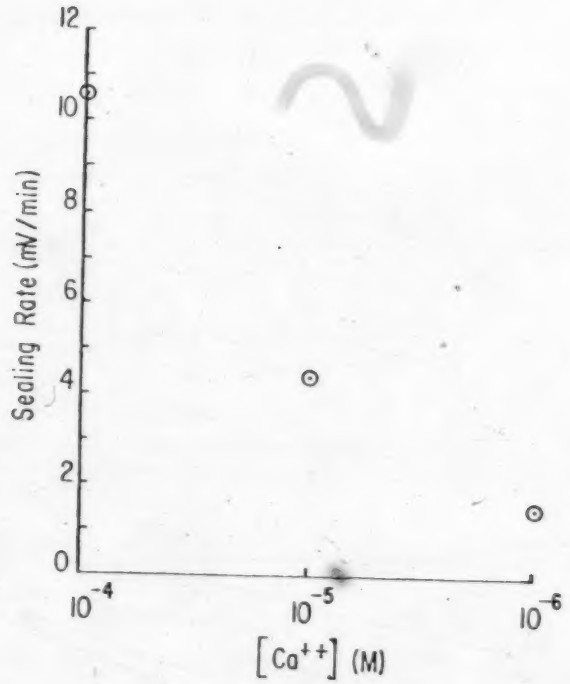

Fig. 9.3 Effect of varying external free calcium concentration on sealing rate.

containing less than 10^{-5} M free Ca^{++}, a pigment ring did not form around the electrodes, which also suggests that normal sealing had not occurred.

9.3 *Effects of intracellular calcium injection:*

In an attempt to achieve reproducible uncoupling of blastomeres, calcium ions were injected iontophoretically with a microelectrode into individual cells. This technique has been used to produce local uncoupling in *Chironomus* salivary gland cells with success (Loewenstein, Nakas and Socolar, 1967; Rose and Loewenstein, 1975a, b). The experiments were performed on four-cell embryos using microelectrodes filled with 0.1 M KCl and 0.1 M $CaCl_2$ for calcium iontophoresis (Loewenstein *et al.*, 1967). The external free Ca^{++} concentration was maintained at 5×10^{-5} M in all experiments using Mg^{++} free Steinberg's solution plus EGTA. In three experiments where Ca^{++} was injected using current pulses of 0.5 sec duration, at a rate of 1 pulse/sec with an amplitude of 10^{-8} amps, no measureable effects on membrane potential, input resistance or coupling ratios were observed for a total injection period of 45-50 minutes. The total amount of Ca^{++} injected in this time was about 2×10^{-11} mole[1].

9.4 *Conclusions:*

The reduction of free calcium ion concentration in the extra-

1 This was estimated from the expression: $m_{Ca} = \frac{nIt}{2F}$ where I is the current; t, total duration of injection; F, Faraday's constant; and n, the transference number. See Loewenstein *et al.*, 1967.

cellular medium appears to reduce the electrical coupling between blastomeres of early *Xenopus* embryos. These results are quite similar to those obtained using different preparations, for example, nerve cells (Penn and Loewenstein, 1966; Pappas *et al.*, 1971) and epithelial cells (Nakas, Higashino and Loewenstein, 1966), where uncoupling occurred using Ca^{++} concentrations in the range of 10^{-4} to 10^{-5} M. The main problems associated with using this technique to interrupt the electrical coupling in *Xenopus* are that the effect is variable in that the same degree of uncoupling is not always produced using the most effective Ca^{++} concentration of 10^{-5} M and that the permeability of the non-junctional membrane is also effected. As the experimental objective with this type of preparation would be to investigate the effect of uncoupling on embryonic development, this second effect cannot be tolerated. This effect has also been noted in uncoupling experiments performed on *Chironomus* salivary gland cells (Nakas *et al.*, 1966). The measured decrease in embryonic input resistance may not be due to a general increase in membrane permeability but could possibly be caused by the failure of the structures responsible for the electrical coupling to seal after they have been disrupted. In the experiments performed using free Ca^{++} concentrations of less than 10^{-5} M, no uncoupling was detected but any changes in junctional resistance could have been masked by the rapidly increasing permeability of the non-junctional membrane during the course of the experiment. In some embryos which were maintained at these concentrations for approximately 30 minutes, the cell membrane deteriorated to such an extent that excessive leakage of cytoplasm occurred, followed by the collapse of

the embryo.

Attempts to uncouple a single cell from the others in the embryo by increasing the level of intracellular Ca^{++} were also unsuccessful. Given the large volume of the cells at the stage used (approximately 2.7×10^{-4} ml) the concentration was increased by about 7×10^{-5} M during the injection period. In early experiments on *Chironomus* salivary gland cells (Loewenstein *et al.*, 1967) an increase in free internal Ca^{++} of 10^{-4} M was sufficient to produce uncoupling. It is therefore possible that, due to the large volume of the *Xenopus* cells, it was not possible to inject sufficient calcium to cause uncoupling. It is also possible that the Ca^{++} was sequestered in the cell as it was injected. It has been shown that a level of free Ca^{++} in the range of 5×10^{-5} to 8×10^{-5} M is necessary at the junctional site in order to uncouple *Chironomus* salivary gland cells (Rose and Loewenstein, 1975a). It has also been shown that when these cells are treated with ruthenium red to block the uptake of Ca^{++} by mitochondria, the diffusion of injected Ca^{++} to the junctional membrane is facilitated, which causes a rapid uncoupling of the cells (Rose and Loewenstein, 1975b).

CHAPTER 10

DISCUSSION

The main goal of this work was to determine the pattern of electrical coupling between cells of early *Xenopus* embryos and to measure the electrical properties of the embryonic membranes during the early cleavages. The use of linear systems analysis, in conjunction with standard electrophysiological techniques, allowed a description of the system which included their time-varying dynamic properties. This information, which is not available from the conventional direct current measurements, was useful in determining the patterns of connectivity between the cells, as well as providing accurate measurements of capacitance. In the analysis of the eight-cell embryo, for example, D.C. measurements of coupling ratio alone would have shown that the cells were closely coupled, but these measurements would not have indicated that the cells were coupled pairwise to each other. Another important advantage of spectral analysis was the relatively short time required for each experiment. This rapidity of measurement allowed several experiments to be performed on each batch of embryos, even though the developmental stages are quite transient.

Earlier studies of the electrical properties of non-junctional membranes in early *Xenopus* embryos have produced results similar to those reported here (Palmer and Slack, 1970; de Laat and Bluemink, 1974). However, the measurements made by Palmer and Slack used direct current and the only parameter obtained was total embryonic input resistance. Their range for this parameter was from approximately 0.3 to 1.0 MΩ

during the first three cleavages. Although the value of the total input resistance, R_I, was not stated explicitly in Chapters 5 and 6, the range of R_I obtained in the present experiments and subsequently used to calculate R_M and R_J was consistent with Palmer and Slack's data. However, they reported that there was no voltage drop across the intercellular junctions, which is in contrast to the values of 0.77 and 0.80 for the coupling ratios in the two- and four-cell embryos measured here. De Laat and Bluemink did not report a value of coupling ratio as their measurements were made before the termination of first cleavage, although their value of specific membrane resistance of 0.043 $M\Omega cm^2$ (no correction for surface folding) is in excellent agreement with the value of 0.041 $M\Omega cm^2$ determined from measurements made on two-cell embryos (Chapter 5). The specific membrane resistance of *Xenopus* embryos is also within the range of specific resistances (0.025 to 0.10 $M\Omega cm^2$) determined by Woodward (1968) for early *Rana pipiens* embryos. Woodward reported a value of specific capacitance for *Rana* embryos of 1.0 to 1.16 $\mu f/cm^2$ for the uncleaved embryo, whereas the value of specific membrane capacitance of an uncleaved *Xenopus* embryo was 0.83 $\mu f/cm^2$ (both values uncorrected for membrane folding). These differences could be due to Woodward's technique which was to measure the time constant of the intracellular voltage rise when a current pulse was injected, and was probably not as accurate as the frequency response measurements. In addition, there may be a species difference. No determination of membrane capacitance was made by de Laat and Bluemink.

Both Woodward (1968) and de Laat and Bluemink (1974) measured

the change in non-junctional membrane resistance during first cleavage although both studies failed to measure the change in junctional resistance, R_J, simultaneously. The results presented here and by Woodward both show a decrease in R_M occurring throughout the course of first cleavage, with the total change in R_M being 40% to 60% of the initial value. This is in sharp contrast to the data presented by de Laat and Bluemink, which showed that the change in R_M does not occur until 6-8 minutes after the start of first cleavage followed by a drop of approximately 50% occurring in the next 10 minutes, after which R_M remains constant for over 20 minutes. There is no obvious reason for this difference.

Other studies of electrically coupled systems have generally assumed that the junctional elements are purely resistive (Loewenstein *et al.*, 1965, 1967; Payton *et al.*, 1969). In many cases where the geometry of the coupled system is complex, for example in epithelial tissues where there is a large array of coupled cells, only measurements of coupling ratios can be obtained. In experiments performed on chains of coupled cells (Loewenstein and Kanno, 1965; Loewenstein *et al.*, 1967) estimates may be made of the specific resistance of the junctional membrane based on a cable model of the cell system and measurements of junctional membrane area from electron micrographs of the tissue. Estimates of junctional membrane specific resistance of *Chironomus* salivary gland cells are in the range 0.3 to 12 Ωcm^2. It was not possible to make such a calculation for *Xenopus* embryos as the junctional area is not known.

The different possible arrangements of junctional electrical

elements have already been discussed in Chapter 5 and no firm conclusions can be made on this matter since it is currently impossible to make any electrical measurements in the middle of an electrical junction. Any resistance from the junction to ground is therefore undetectable and the values of any shunt or series capacitances in the junctional structures were too small to be detected with the present techniques. In a study of electrical coupling using linear analysis techniques between Retzius cells in the leech, coupling ratios were found to be much lower (0.3) than in *Xenopus* and the value of lumped junctional resistance much higher (34 MΩ) (French and DiCaprio, 1975). There was also no evidence in this study of any significant junctional capacitance.

The mechanism of electrical coupling in amphibian embryos has not yet been determined. De Laat and Bluemink (1974) and Woodward (1968) have suggested that coupling may be caused by current flow through new membrane of low resistivity formed in the cleavage furrows. Slack and Warner (1973) have also suggested that the primitive blastocoel is isolated from electrical ground, thereby providing a common electrical pathway between all cells. De Laat and Bluemink (1974) determined the specific resistance of the cleavage furrow membranes in *Xenopus* to be 1.8 KΩcm^2, while Woodward obtained a value of 0.950 Ωcm^2 for *Rana* embryos. Both of these calculations were based on the assumptions that the specific resistance of the "old" membrane remains constant while the "new" membrane in the cleavage furrow is of lower specific resistance, that the flow of current in the cleavage furrow is prevented or restricted, and that the changes in membrane resistance measured after the cleavage furrow is everted are due to this low resistance membrane being exposed

to the external solution. These assumptions may be criticized on various grounds. Ultrastructural studies of early cleavage stages in *Xenopus* show that there is no sealing ring of tight junctions around the periphery of the cleavage furrow which would provide the required electrical isolation (Bluemink and de Laat, 1973; Singal and Sanders, 1974). Woodward has offered an alternate explanation for the sealing of the furrow by contending that current flow out of the furrow region is limited by the close apposition of the furrow membranes. His calculations indicated that the furrow would have an input impedance of approximately 0.4 MΩ. A resistance of this magnitude would have been easily detectable during the direct measurement of potential in the blastocoel, and the finding that the blastocoel is electrically connected to the external solution contradicts the above assumptions. Finally, the procedures employed to expose new membrane to the external solution, namely the application of Cytochalasin-B, removal of the vitelline membrane (de Laat and Bluemink, 1974), or treatment with hypertonic solutions (Woodward, 1968), may themselves damage the cell membranes or alter their permeability, thereby causing the observed decreases in membrane resistance.

It has been shown that electrical coupling may be mediated by small regions of closely apposed membrane which have a low resistivity (Bennett and Auerbach, 1969; Heppner and Plonsey, 1970). If membranes with a resistivity of approximately 1 Ω/cm^2 were separated by an intercellular cleft of 200 Å it was calculated that the two cells would show a significant degree of electrical coupling. However, Bennett (1973) has also stated that when the electrical coupling is found to be "very

close" it is unlikely to be mediated by such apposed but separated low resistance membrane. Tracer experiments using fluorescent dyes or other molecules can be performed on coupled cells to determine whether coupling occurs via specialized junctions or through the extracellular space. In *Fundulus* embryos, for example, electrical coupling has been found to be mediated by specialized junctions and through the extracellular space due to the segmentation cavity being sealed off from the exterior by a high resistance barrier (Bennett and Trinkaus, 1970).

In other electrically coupled systems where ultrastructural studies have been performed, the presence of gap junctions has been closely correlated with electrical coupling (Payton, Bennett and Pappas, 1969; Gilula, Reeves and Steinbach, 1972; Azarnia, Larsen and Loewenstein, 1974). Gap junctions are characterized in thin electron microscopic sections by the presence of a 20 Å space between the two apposed membranes. When the specimens are exposed to lanthanum ions, subunits are outlined in the intercellular gap, with diameters of 70-75 Å (Revel and Karnovsky, 1967). When gap junctions have been studied using the freeze fracturing technique, they have been characterized by closely-packed hexagonal arrays of particles with a center-to-center spacing of 90-100 Å (McNutt and Weinstein, 1970; Goodenough and Revel, 1970). The available ultrastructural evidence on gap junction morphology suggests a structure in which a hexagonally shaped lattice of extracellular channels surrounds a hexagonal array of hydrophilic intercellular channels with diameters of approximately 15-25 Å (Goodenough and Gilula, 1974; McNutt and Weinstein, 1970; Pappas *et al.*, 1971). An excellent review of the morphology of intercellular junctions is available in McNutt and Weinstein (1973). A preliminary biochemical analysis of gap

junctions from mouse hepatocytes (Goodenough and Stoeckenius, 1972) has indicated that the primary phospholipids present are phosphatidylcholine with a small amount of phosphatidylethanolamine plus some neutral lipid. A single prominent protein with a molecular weight of 20,000 was also detected in the isolated junction fraction. In the same study, X-ray diffraction studies of the isolated gap junctions also revealed the same periodicity of the hexagonal lattice as that determined from electron microscopy.

Gap junctions have been detected between some embryonic cells (Goodenough *et al.*, 1968; Lentz and Trinkaus, 1971) but as yet have not been found in early *Xenopus* embryos, although Sanders and Zalik (1972) and Singal and Sanders (1974) have demonstrated the presence of cell contacts possessing an intercellular gap of 20-30 Å in the cleavage and the blastula stages of *Xenopus*. It seems probable therefore that gap junctions may mediate the electrical coupling in *Xenopus*.

Electrical measurements of intercellular communication only serve to indicate that one or more small ions can pass between the cells, but many small molecules have been found to cross the intercellular junctions in adult and embryonic tissues. In experiments using dye injection it was found that Fluorescein, Neutral red and Procion yellow all cross the intercellular junctions in the crayfish septate axon (Bennett, Dunham and Pappas, 1967; Payton, Bennett and Pappas, 1969). Fluorescein and Procion yellow pass between the coupled cells in *Chironomus* salivary glands (Rose, 1971). The largest of the tracer molecules (Procion yellow) has a molecular weight of about 625. In one study, molecules with molecular weights as high as 69,000 (serum albumin)

were reported to pass between coupled *Drosophila* salivary gland (Kanno and Loewenstein, 1969) but successful results with tracers as large as this have not been reported in other systems. Studies which use Fluorescein have also been criticized on the grounds that this dye can diffuse through cell membranes and would therefore not require specialized junctions to move between cells.

Junctions in *Xenopus* embryos do not seem to have permeabilities as high as in the adult tissues described above. Fluorescein does not pass between electrically coupled cells of early cleavage stages and early blastulae (Slack and Palmer, 1969), but it has been found to cross between reaggregated cells from blastula and larval stages (Sheridan, 1971). This difference may be important as the junctions may allow chemical intercellular communication, but only via molecules below a certain size.

Gap junctions have been shown to occur transiently in organisms during development. Lopresti, Macagno and Levinthal (1974) have shown that gap junctions form for a short time between the growth cone of optic nerve fibers and undifferentiated neuroblasts in *Daphnia*. The implication of this work is that intercellular communication is involved in the differentiation of neuroblast cells in this preparation. It is not clear if the cellular interaction serves to trigger a preset program of differentiation or whether the target cell is controlled by a series of signals from the communicating cell.

The absence of electrical coupling between cancerous cells in tissues which are normally coupled was thought to be closely correlated with the cancerous state. Examples of this uncoupling have been found

in liver (Loewenstein and Kanno, 1967), thyroid (Jamakosmanovic and Loewenstein, 1968), stomach tumours (Kanno and Matsui, 1968), cancerous strains in culture (Borek, Higashino and Loewenstein, 1969) and cultured fibroblasts (Azarnia and Loewenstein, 1971). The conclusions from these studies were that cellular interactions involving electrical coupling are important in the normal growth of cells and that the disruption of this communication can lead to the development of a cancerous state. In further work it was found that some cancerous cell lines were electrically coupled (Borek *et al.*, 1969; Sheridan, 1970) although it was impossible to determine from simple electrical measurements if the coupling was normal. It is possible in these cases that there are subtle defects in the structure of the junctions which may alter their permeability to some essential substance or that there are defects in intercellular communication which do not involve the junctions directly. There is also evidence that the formation of gap junctions and consequent electrical coupling may be controlled genetically (Azarnia, Larsen and Loewenstein, 1974). In this study, hybrid cells formed from an electrically coupled human cell line and a non-communicating mouse cell line were found to be electrically coupled. When the hybrid cell line lost the human chromosomes, their ability to form gap junctions and the electrical coupling was lost.

Electrical coupling has been found in a variety of embryos, for example, *Fundulus* (Bennett *et al.*, 1970), *Triturus* (Ito and Loewenstein, 1969), squid (Potter, Furshpan and Lennox, 1966), chick (Sheridan, 1966) and *Asterias* (Tupper and Saunders, 1971). There has been much speculation concerning the role that electrical junctions may

play in the control of embryonic development. However, it is quite possible that they function only to equalize intercellular ionic balance or nutrition, instead of being involved with the processes of induction or the movement of morphogenetic material (Potter, Furshpan and Lennox, 1966; Loewenstein, 1968; Crick, 1970; Bennett, 1973). A number of theoretical models for the control of differentiation make the assumption that intercytoplasmic exchange exists between cells (Loewenstein, 1968; Goodwin and Cohen, 1969; Wolpert, 1969). In many of these models, gradients of some substance which controls differentiation, also termed a morphogen, are established in the developing embryo from a site that produces the substance. The various cells in the embryo then take their developmental cues from the concentration of the morphogen at the position occupied by the cell. A recent model for the establishment of gradients of a hypothetical morphogen within developing systems without cellular partitions relies only on the free diffusion of a small ion (K^+) within the system (D.I. McLaren, personal communication). This model could easily be applied to the early *Xenopus* embryo, as the degree of connectivity found in the embryo would permit the flow of ions in a system that behaves as a continuum. If in the eight-cell embryo, for example, the coupling between distant cells was mediated by pathways through the intervening cells, the path differences present in this situation would alter the diffusion of material throughout the embryo and impose gradients due only to these differences. The finding that all cells up to the eight-cell stage are directly coupled, due to the specific alteration of cell shape and embryonic geometry, is important if development is in fact controlled by diffusion of material throughout the embryo.

This finding is also interesting in light of the work of Curtis (1962), who has shown that the grey crescent region of the early *Xenopus* embryo is capable of inducing the formation of a second embryonic axis when transplanted into an uncleaved embryo. However, Curtis also found that transplants of the grey crescent region to the eight-cell embryos did not induce another embryonic axis. It is therefore possible that a gradient established in the uncleaved egg cannot be disrupted after the formation of cell membranes and that the coupling between these cells plays some secondary role in the regulation or control of development by restricting the flow of certain substances.

It would be of interest in further studies of coupling in *Xenopus* to determine the size range of substances which can pass through the electrical junctions. It would then be possible to investigate the developmental effects of varying concentrations of ions and small molecules which are able to pass through the junctions. Another interesting possibility would be to find an agent that could selectively uncouple one cell from its neighbors and to study the effects of such separation on development. Techniques that have been used so far, such as altering cation concentrations, lowering the temperature or the use of metabolic inhibitors, probably have substantial effects on other cellular processes. The study of connectivity between cells after the eight-cell stage would also be interesting, although the use of linear analysis techniques for embryos of 16 or more cells would be quite time-consuming. A more profitable approach might be to investigate the gross electrical coupling between groups of cells at later stages.

APPENDIX I

The *F*ocal *C*ircuit *A*nalysis *P*rogram (FCAP) was divided into two programs for ease of operation. The first portion, FCAPI (*FCAPI*nput) is used to enter the specifications of the network to be analyzed and to store them on the PDP 11/40 disc memory. The nodes of the circuit are numbered (node zero = ground) and the position of all circuit branch elements are specified by their input and output nodes. The valid circuit elements are independent voltage sources, resistors, capacitors and inductors. The number of nodes and branches in the network is only limited by the amount of the computer core memory available and the time required to perform the computations.

The second program, *FCAPCO* (*FCAPC*omputation, *O*utput) uses the data file constructed by *FCAPI* for its input and will compute the frequency response between any two nodes. If node Ø is specified as the input node, then voltage source 1 is assumed to be the input voltage. The frequency response is plotted in the form of a Bode plot directly on an X-Y chart recorder controlled by the PDP 11/40.

FCAPI

```
C - BOSS FOCAL

  1.01 E;X FCON(1);S J=0
  1.02 A "BRANCHES",B1;A "NODES",N1
  1.03 X FDAT(1,0,0,B1)+FDAT(1,0,1,N1)
  1.05 T !,"NUMBER,INPUT,OUTPUT,TYPE,VALUE",!
  1.06 I(J-B1)1.08,1.07,1.07
  1.07 Q
  1.08 A B2,S1,S2,T1,V1;T !;D 2;D 3
  1.09 GOTO 1.06

  2.70 S J=J+1
  2.80 I(T1-0R)2.81,2.90
  2.81 I(T1-0L)2.82,2.90
  2.82 I(T1-0C)2.83,2.90
  2.83 I(T1-0V)2.84,2.93
  2.84 T!,"ILLEGAL VALUE IN BRANCH ";X FCHR(48+B2)
  2.85 A B2,S1,S2,T1,V1;T !;G 2.80
  2.90 R
  2.93 T !,"PHASE ANGLE OF VOLTAGE SOURCE ";X FCHR(48+B2);A V2
  2.94 X FDAT(1,J,5,V2);T !;S B1=B1+1

  3.10 X FDAT(1,J,0,B2)+FDAT(1,J,1,S1)+FDAT(1,J,2,S2)
  3.14 X FDAT(1,J,3,T1)+FDAT(1,J,4,V1)
```

```
1.02 X FCON(1)
1.03 S B1=FDAT(1,0,0);S N1=FDAT(1,0,1);S N2=N1+1
1.04 S K=0
1.08 F J=1,B1;D 2
1.10 G 8.01

2.70 S K=K+1
2.72 S B2=FDAT(1,K,0);S S1=FDAT(1,K,1);S S2=FDAT(1,K,2)
2.74 S T1=FDAT(1,K,3);S V1=FDAT(1,K,4)
2.76 S N(B2)=S1;S M(B2)=S2
2.80 I(T1-0R)2.91,2.90
2.81 I(T1-0L)2.82,2.91
2.82 I(T1-0C)2.93,2.92,2.93
2.90 S Y(B2)=1/V1;S T(B2)=T1;R
2.91 S L(B2)=1/V1;S T(B2)=T1;R
2.92 S C(B2)=V1;S T(B2)=T1;R
2.93 S V2=FDAT(1,K,5)
2.94 I(B2-1)2.96,2.95,2.96
2.95 S Z1=V1;S Z2=V2
2.96 S V2=V2*.01745;S E(B2,1)=V1*FCOS(V2)
2.97 S E(B2,2)=V1*FSIN(V2);S J=J-1

3.01 F J=1,N1;F K=1,N2;S R(J,K)=0;S X(J,K)=0
3.02 F J=1,B1;D 4
3.08 F J=1,B1;S O(J,1)=Y(J)*E(J,1)-(C(J)+W-L(J)*W1)*E(J,2)-R(J,1)
3.10 F J=1,B1;S O(J,2)=Y(J)*E(J,2)+(C(J)+W-L(J)*W1)*E(J,1)-R(J,2)
3.16 F J=1,B1;D 18

4.01 S I=N(J);S H=M(J)
4.02 I(I)4.03,4.21
4.03 I(H)4.37,4.20,4.37
4.20 S H=I
4.21 I(T(J)-0R)4.22,4.30
4.22 I(T(J)-0L)4.26,4.34
4.26 S X(H,H)=X(H,H)+W*C(J);R
4.30 S R(H,H)=R(H,H)+Y(J);R
4.34 S X(H,H)=X(H,H)-W1*L(J);R
4.37 I(T(J)-0R)4.38,4.50
4.38 I(T(J)-0L)4.39,4.58
4.39 S S1=W*C(J);S X(I,I)=X(I,I)+S1
4.40 S X(I,H)=X(I,H)-S1;S X(H,I)=X(H,I)-S1;G 4.26
4.50 S R(I,I)=R(I,I)+Y(J);S R(I,H)=R(I,H)-Y(J)
4.57 S R(H,I)=R(H,I)-Y(J);G 4.30
4.58 S S1=W1*L(J);S X(I,I)=X(I,I)-S1
4.59 S X(I,H)=X(I,H)+S1;S X(H,I)=X(H,I)+S1;G 4.34

5.01 F M=1,N1;D 13
5.02 F LL=1,N1;S L=N1-LL+1;D 15
```

```
 6.01 S S4=S1;S S1=FSQT(S1^2+S2^2)
 6.02 S S2=FATN(S2/S4)/3.14159
 6.03 I(-S4)6.04;S S2=S2-FSGN(S2)
 6.04 S S2=S2*180

 7.01 F Y=2,9;D 9

 8.01 T !," IN NODE,OUT NODE,INIT FREQ,STEP,FINAL FREQ"
 8.02 A P(1),P(2),X1,C,S3
 8.04 S V9=X1/C;S A=0
 8.05 S V9=V9*C;I(V9-S3)8.06,8.12,8.12
 8.06 S W=V9*6.2831;S W1=1/W;S A=A+1;D 10
 8.10 G 8.05
 8.12 S GM=G(1);S GN=G(1)
 8.14 F X=1,A;D 16
 8.16 S D=GM-FSGN(GN)*FABS(GN);S M=FITR(D/5+.5)
 8.18 S M=FITR(M/5+1)*5;X FPLT(.6,.5,0);I(M)8.19,8.19,8.20
 8.19 S M=1
 8.20 F Y=0,4;X FPLT(.6,Y+.5,1)+FPLT(.7,Y+.5,1)+FPLT(.6,Y+.5,1)
 8.21 X FPLT(.6,5,0)
 8.22 F Y=5,10;X FPLT(.6,Y,1)+FPLT(.7,Y,1)+FPLT(.6,Y,1)
 8.23 S X2=FITR(FEXP(2.303*FITR(FLOG(X1/.999))))
 8.24 S M1=FITR(FLOG(V9/X2)+.5);S M2=FITR(12/M1)
 8.26 X FPLT(1.6,.3,0)
 8.27 S M3=FITR(GM/M-1000)+1000
 8.28 F X=1.6,M2,14;X FPLT(X,.3,1)+FPLT(X,.4,1)+FPLT(X,.3,1);D 7
 8.30 X FPLT(FLOG(X1/X2)*M2+1.6,10-(M3*M-G(1))/M,0);S V9=X1/C
 8.32 F X=1,A;S V9=V9*C;X FPLT(FLOG(V9/X2)*M2+1.6,10-(M3*M-G(X))/M,1)
 8.34 X FPLT(FLOG(X1/X2)*M2+1.6,2.5+PH(1)/90,0)
 8.36 S V9=X1/C
 8.38 F X=1,A;S V9=V9*C;X FPLT(FLOG(V9/X2)*M2+1.6,2.5+PH(X)/90,1)
 8.42 F X=0,5;X FIG(.1,9.85-X,M3*M-X*M)
 8.44 F X=0,4;X FIG(.1,4.4-X,180-X*90)
 8.46 S Y=-1;F X=1.6,M2,14;S Y=Y+1;X FIG(X,0,FLOG(X2/.999)+Y)
 8.60 Q

 9.02 S YY=FLOG(Y)*M2+X
 9.03 I(13-X)9.05
 9.04 X FPLT(YY,.3,1)+FPLT(YY,.35,1)+FPLT(YY,.3,1)
 9.05 R

10.02 D 3;D 5
10.04 I(P(1))10.06,10.40
10.06 F YY=1,2;D 11
10.08 S G(A)=20*FLOG(V(2,1)/V(1,1));S PH(A)=V(2,2)-V(1,2);R
10.40 S S1=0(P(2),1);S S2=0(P(2),2);D 6
10.42 S G(A)=20*FLOG(S1/Z1);S PH(A)=S2-Z2
```

```
11.02 S S1=0(P(YY),1);S S2=0(P(YY),2)
11.04 D 6;S V(YY,1)=S1;S V(YY,2)=S2

12.01 S S1=0;S S2=0;I(M-1)12.02,12.04
12.02 F K=1,M-1;S S1=S1+R(N,K)*R(K,M)-X(N,K)*X(K,M)
12.03 F K=1,M-1;S S2=S2+R(N,K)*X(K,M)+X(N,K)*R(K,M)
12.04 S R(N,M)=R(N,M)-S1
12.05 S X(N,M)=X(N,M)-S2

13.01 F N=M,N1;D 12
13.02 S P1=1/(R(M,M)^2+X(M,M)^2)
13.04 S I1=-X(M,M)*P1;S P1=R(M,M)*P1
13.06 F N=M+1,N2;D 14

14.02 S S1=0;S S2=0;I(M-1)14.04,14.10
14.04 F K=1,M-1;S S1=S1+R(M,K)*R(K,N)-X(M,K)*X(K,N)
14.06 F K=1,M-1;S S2=S2+R(M,K)*X(K,N)+X(M,K)*R(K,N)
14.10 S S1=R(M,N)-S1;S S2=X(M,N)-S2
14.12 S R(M,N)=P1*S1-I1*S2
14.14 S X(M,N)=S1*I1+S2*P1

15.01 S S1=0;S S2=0;I(L-N1)15.02,15.10
15.02 F K=L+1,N1;S S1=S1+O(K,1)*R(L,K)-O(K,2)*X(L,K)
15.03 F K=L+1,N1;S S2=S2+O(K,1)*X(L,K)+O(K,2)*R(L,K)
15.10 S O(L,1)=R(L,N2)-S1
15.12 S O(L,2)=X(L,N2)-S2

16.02 I(GM-G(X))16.03,16.04,16.04
16.03 S GM=G(X)
16.04 I(G(X)-GN)16.06;R
16.06 S GN=G(X)

18.02 S I=N(J);S H=M(J)
18.04 I(I)18.06,18.10,18.06
18.06 S R(I,N2)=R(I,N2)-O(J,1)
18.08 S X(I,N2)=X(I,N2)-O(J,2)
18.10 I(H)18.12,18.16,18.12
18.12 S R(H,N2)=R(H,N2)+O(J,1)
18.14 S X(H,N2)=X(H,N2)+O(J,2)
18.16 R
```

APPENDIX II

MORPHOLOGY

The micrographs in this appendix were prepared by Dr. E.J. Sanders and reproduced here with his kind permission.

The material presented in Fig. 1 was prepared for electron microscopy using procedures described previously (Sanders and Zalik, 1972). The light micrograph in Fig. 3 was taken from 2 μm sections obtained from glutaraldehyde fixed and araldite embedded material and were stained with a mixture of equal volumes of 1% methylene blue and 1% azure B in 0.5% borax solution. Embryos used for light microscopy in Fig. 8 were fixed overnight in the mixed aldehyde solution of Kalt and Tandler (1971) which contains 3% glutaraldehyde, 2% formaldehyde, 1% acrolein, and 2.5% dimethyl sulphoxide. The material was dehydrated in ethanol, cleared in benzene, embedded in paraffin wax, and serially sectioned at 5 μm thickness. Sections were stained with 35% alcoholic eosin solution and micrographs were made using a Leitz Orthoplan microscope (E. Leitz, Inc., Rockleigh, N.J.) and Panatomic-X film (Eastman, Kodak Co., Rochester, N.Y.)

Several techniques were used in preparing embryos for scanning electron microscopy (SEM), such that they could be manually split apart along the plane of cleavage furrows. Singal and Sanders (1973) had found that freeze drying allowed them to be broken in this manner. The appearance of blastomeres prepared in this way was similar to the appearance of the living cells by light microscopy and of the corresponding regions of sectioned cells by transmission electron

microscopy (Singal and Sanders, 1974). The close correlation of cell appearance after several preparative procedures has been used as a criterion to judge the quality of preservation of tissue for SEM (Porter *et al.*, 1973). At the low magnifications used in the present work, the freeze drying technique is considered satisfactory. Successfully split embryos were coated with a carbon and gold conducting layer and examined using a Cambridge S4 scanning electron microscope (Kent Cambridge Ltd., Willowdale, Ontario).

Fig. 1 Electron micrograph of a section through the cortical region of a *Xenopus laevis* embryo showing the vitelline membrane (VM) *in situ*, the perivitelline space (PS) and the plasma membrane (PM). The width of the perivitelline space may vary according to the region and the method of preparation for electron microscopy.

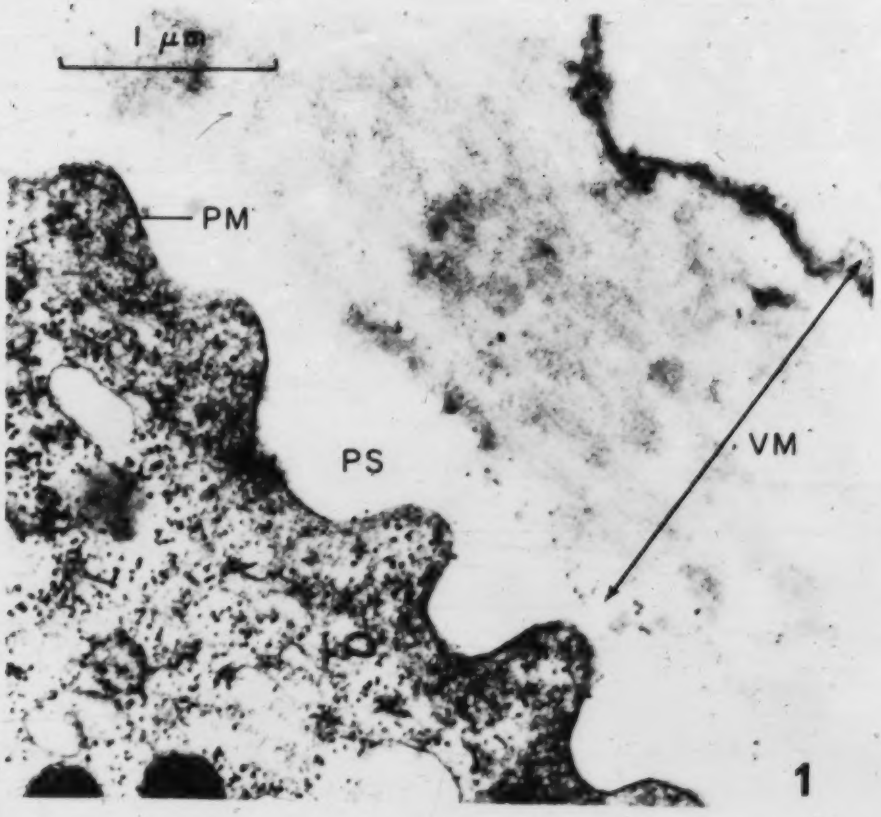

1

Fig. 2 Scanning electron micrograph of the animal pole of a four-cell embryo. Note the area of close apposition of two diagonally opposite cells which causes separation of the other diagonal pair.

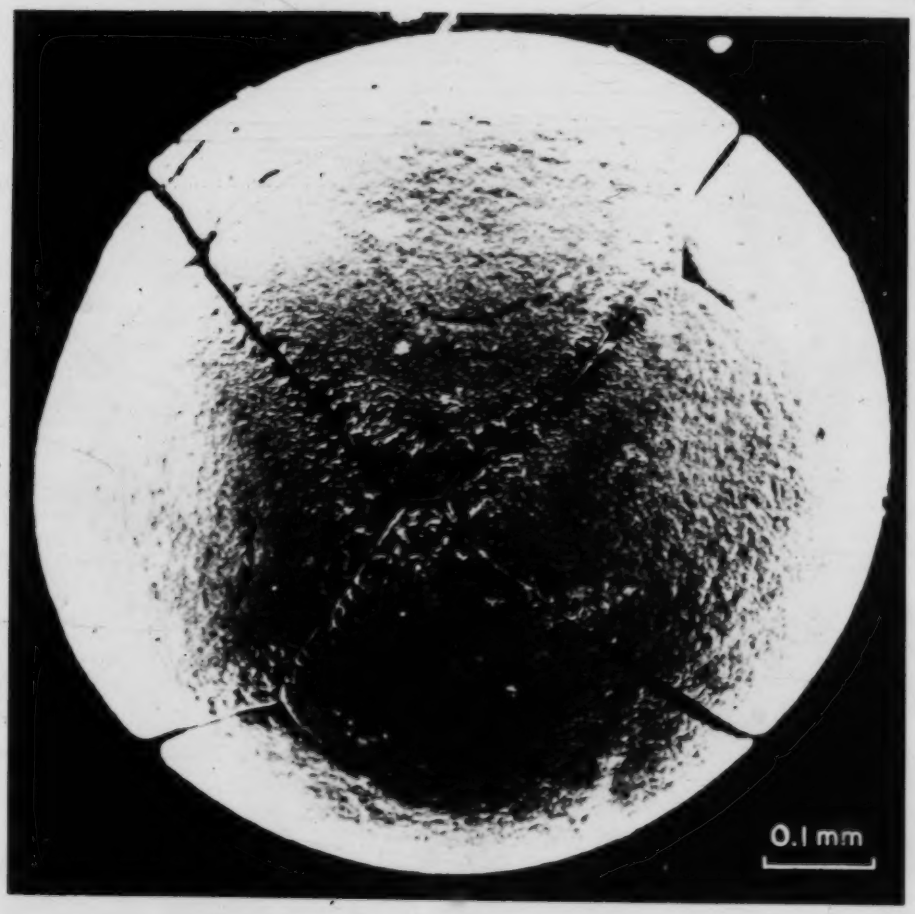

2

Fig. 3 : Light micrograph of a section through the vegetal hemisphere of a four-cell embryo. The cells are numbered 1-4. Close apposition of one pair of diagonal cells is indicated by the arrow.

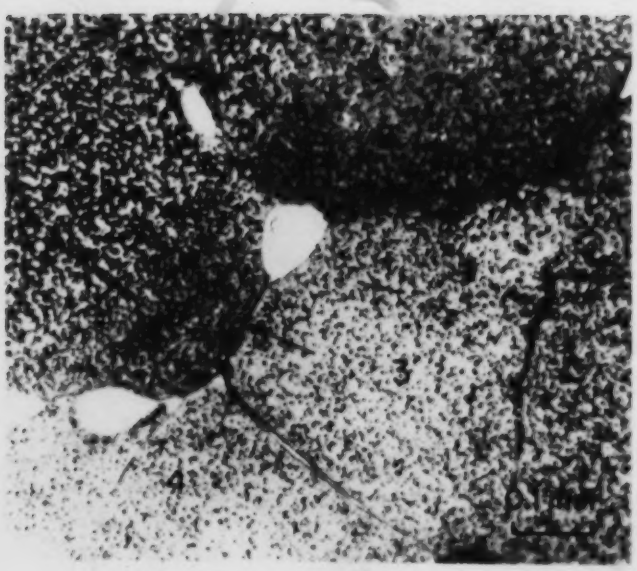

3

Fig. 4 Scanning electron micrograph of an eight-cell embryo from which one cell has been removed. If the missing cell is arbitrarily assigned the number 1, then contact faces are directly visible between the following pairs of cells: 1 to 2, 1 to 4, 1 to 5, 1 to 6, 1 to 8. These faces are identifiable as flattened surfaces and also in Fig. 5, which shows the removed cell. The faces seen in these figures all possess intact membrane surfaces as judged by the absence of yolk platelets when the specimen was observed at high magnification. In cases where the plasma membrane was damaged, these organelles were exposed. x125

Fig. 5 Scanning electron micrograph of the cell which was removed from the embryo in Fig. 4. This cell shows faces which correspond to those of the remaining cells of the embryo. x132

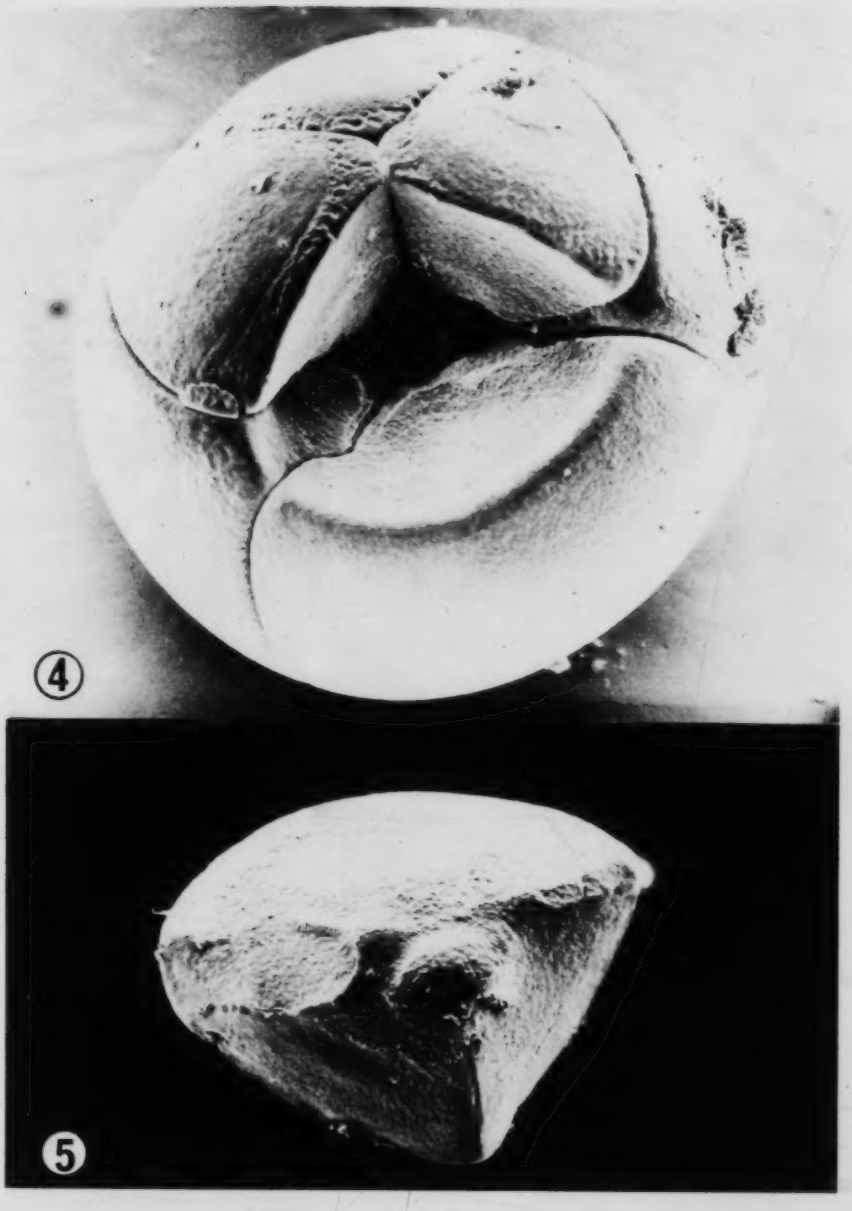

④

⑤

Fig. 6 An enlargement of the blastocoel cavity of Fig. 4 which shows a number of cytoplasmic processes issuing from the surfaces lining the blastocoel. It is not possible to decide from which cells these processes originate but some appear to be in a position to make contact with the removed cell 1. It is probably that further processes have been broken during the removal of cell 1, since several stumps are visible. The finest processes observed by scanning electron microscopy were approximately 10-15 μm in diameter. x258

Fig. 7 Scanning electron micrograph of vegetal pole cells of an eight-cell embryo showing a process from one cell (arrow) making contact with two other cells by pushing between them. The upper surface shows blunt surface projections. x248

⑥

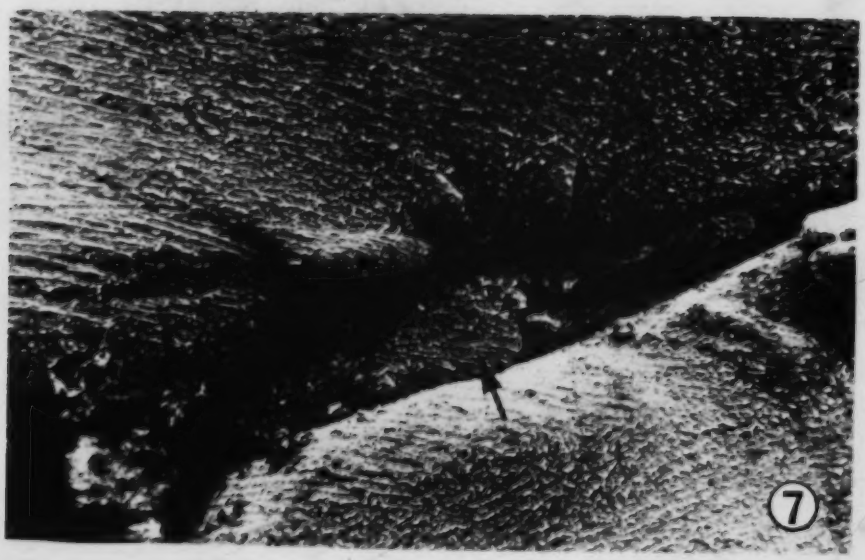

⑦

Fig. 8 A-L Light micrographs of sections through an eight-cell embryo, cut in a vertical plane. Figures 8A and 8L are sections from near the extremities while 8B through 8K are serial sections from the center of the embryo. The cells are numbered according to the scheme of Fig. 7.1. The series illustrates the way in which cells make contact with more remote cells by means of processes. Cell 8 can be seen to have extended a process (arrow in Fig. 8G) which has insinuated itself between processes from cells 3 and 5. x 31

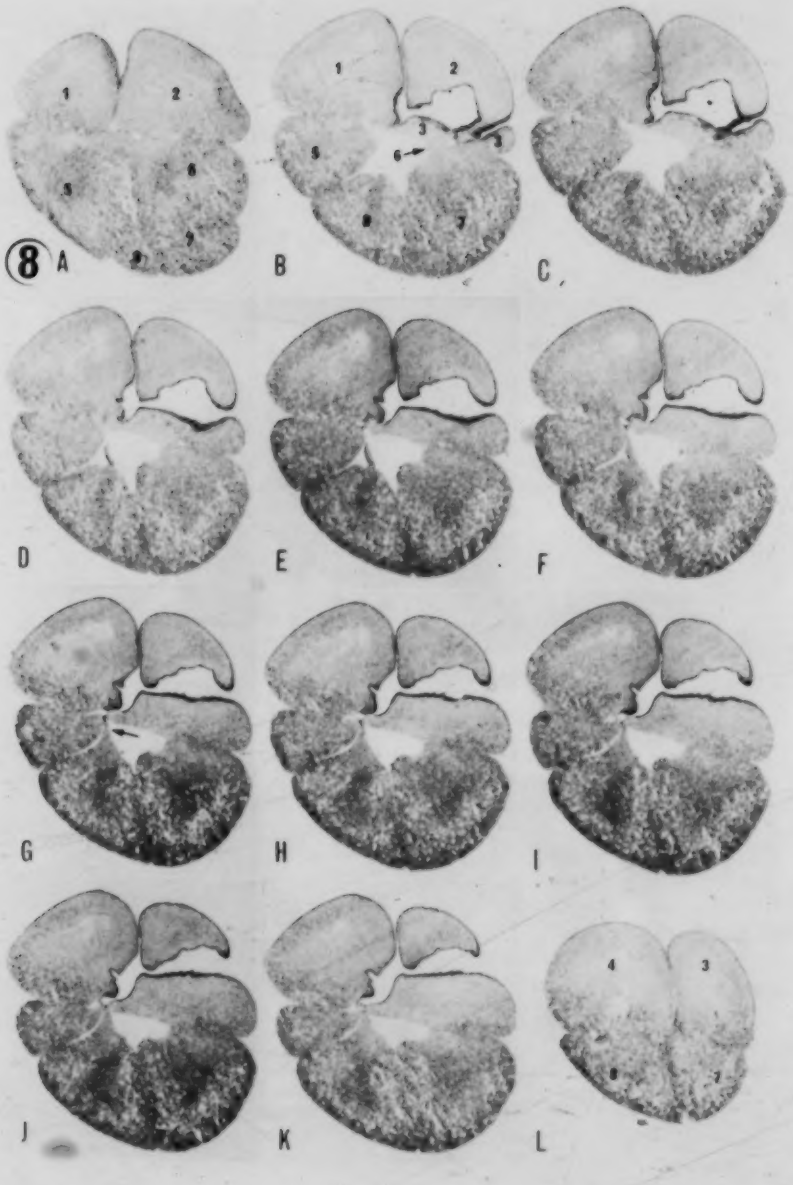
8
A
B
C
D
E
F
G
H
I
J
K
L

BIBLIOGRAPHY

ASADA, Y., and M.V.L. BENNETT. 1971. Experimental alteration of coupling resistance at an electrotonic synapse. *J. Cell Biol. 49*: 159.

ASHMAN, R.F., Y. KANNO, and W.R. LOEWENSTEIN. 1964. Intercellular electrical coupling in a forming cell membrane junction of a dividing cell. *Science 145*: 602.

AUERBACH, A.A., and M.V.L. BENNETT. 1969. A rectifying electrotonic synapse in the CNS of a vertebrate. *J. Gen. Physiol. 53*: 211.

AZARNIA, R., W.J. LARSEN, and W.R. LOEWENSTEIN. 1974. The membrane junctions in communication and noncommunicating cells, their hybrids, and segregants. *Proc. Natl. Acad. Sci. U.S. 71*: 880.

AZARNIA, R., and W.R. LOEWENSTEIN. 1971. Intercellular communication and tissue growth. V. A cancer cell strain that fails to make permeable junctions with normal cells. *J. Mem. Biol. 6*: 368.

BAKER, R., and R. LLINAS. 1971. Electrotonic coupling between neurons in rat mesencephalic nucleus. *J. Physiol., London 212*: 45.

BARR, L., M.M. DEWEY, and W. BERGER. 1965. Propagation of action potentials and the structure of the nexus in cardiac muscle. *J. Gen. Physiol. 48*: 797.

BENDAT, J.S., and A.G. PIERSOL. 1966. *Measurement and Analysis of Random Data*. John Wiley: New York.

BENNETT, M.V.L. 1966. Physiology of electrotonic junctions. *Ann. N.Y. Acad. Sci. 137*: 509.

BENNETT, M.V.L. 1972. A comparison of electrically and chemically mediated transmission. In: *Structure and Function of Synapses*, edited by G.D. Pappas and D.P. Purpura. Raven: New York. 221.

BENNETT, M.V.L. 1973. Function of electrotonic junctions in embryonic and adult tissues. *Fed. Proc. 32*: 65.

BENNETT, M.V.L., and A.A. AUERBACH. 1969. Calculation of electrical coupling of cells separated by a gap. *Anat. Record 163*: 152.

BENNETT, M.V.L., P.B. DUNHAM, and G.D. PAPPAS. 1967. Ion fluxes through a "tight junction". *J. Gen. Physiol. 50*: 1094.

BENNETT, M.V.L., M.E. SPIRA, and G.D. PAPPAS. 1972. Properties of electrotonic junctions between embryonic cells of *Fundulus*. *Develop. Biol. 29*: 419.

BENNETT, M.V.L., and J.P. TRINKAUS. 1970. Electrical coupling between embryonic cells by way of extracellular space and specialized junctions. *J. Cell Biol. 44*: 592.

BENNETT, M.V.L., S.G. WAXMAN, and G.D. PAPPAS. 1969. Occulomotor neurons in fish: electrotonic coupling and multiple sites of impulse initiation. *Science 166*: 520.

BLUEMINK, J.G. 1971. Effect of Cytochalasin-B on surface contractility and cell junction formation during egg cleavage in *Xenopus laevis*. *Cytobiologie 3*: 176.

BLUEMINK, J.G. 1972. Cortical wound healing in the amphibian egg. *J. Ultrastruct. Res. 41*: 95.

BLUEMINK, J.G., and S.W. de LAAT. 1973. New membrane formation during cytokinesis in normal and Cytochalasin-B-treated eggs of *Xenopus laevis*. I. Electron-microscopical observations. *J. Cell Biol. 59*: 89.

BOREK, C., S. HIGASHINO, and W.R. LOEWENSTEIN. 1969. Intercellular communication and tissue growth. IV. Conductance of membrane junctions of normal and cancerous cells in culture. *J. Mem. Biol. 1*: 274.

CARLSON, A.B. 1968. *Communication Systems. An Introduction to Signals and Noise in Electrical Communication*. McGraw-Hill: New York.

COOLEY, J.W., and J.W. TUKEY. 1965. An algorithm for the machine calculation of complex Fourier series. *Math. Comput. 19*: 297.

CRICK, F. 1970. Diffusion in embryogenesis. *Nature 225*: 420.

CURTIS, A.S.G. 1962. Morphogenetic interactions before gastrulation in the amphibian, *X. laevis*. The cortical field. *J. Embryo. Exp. Morph. 10*: 410.

d'AZZO, J.J., and C.H. HOUPIS. 1966. *Feedback Control System Analysis and Synthesis*. McGraw-Hill: New York.

de LAAT, S.W., and J.G. BLUEMINK. 1974. New membrane formation during cytokinesis in normal and Cytochalasin-B treated eggs of *Xenopus laevis*. II. Electrophysiological observations. *J. Cell Biol. 60*: 529.

de LAAT, S.W., R.J.A. BUWALDA, and A.M.M.C. HABETS. 1974. Intracellular ionic distribution, cell membrane permeability and membrane potential of the *Xenopus* egg during first cleavage. *Exp. Cell Res. 89*: 1.

de LAAT, S.W., D. LUCHTEL, and J.G. BLUEMINK. 1973. The action of Cytochalasin-B during egg cleavage in *Xenopus laevis*: Dependence on cell membrane permeability. *Dev. Biol. 31*: 163.

DEWEY, M.M., and L. BARR. 1964. A study of the structure and distribution of the nexus. *J. Cell Biol. 23*: 553.

DiCAPRIO, R.A., A.S. FRENCH, and E.J. SANDERS. 1974. Dynamic properties of electrotonic coupling between cells of early *Xenopus* embryos. *Biophys. J. 14*: 387.

DiCAPRIO, R.A., A.S. FRENCH, and E.J. SANDERS. 1975. Intercellular connectivity in the eight-cell *Xenopus* embryo. Correlation of electrical and morphological investigations. *Biophys. J. 15*: 373.

FARQUHAR, M.G., and G.E. PALADE. 1963. Junctional complexes in various epithelia. *J. Cell Biol. 17*: 375.

FARQUHAR, M.G., and G.E. PALADE. 1965. Cell junctions in amphibian skin. *J. Cell Biol. 26*: 263.

FRENCH, A.S. 1973. Automated spectral analysis of neurophysiological data using intermediate magnetic tape storage. *Comput. Prog. Biomed. 3*: 45.

FRENCH, A.S. 1974. Synthesis of low-frequency noise for use in biological experiments. *IEEE Trans. Biomed. Eng. BME-21*: 251.

FRENCH, A.S., and R.A. DiCAPRIO. 1975. The dynamic electrical behaviour of the electrotonic junction between Retzius cells in the leech. *Biol. Cybernetics 17*: 129.

FRENCH, A.S., and A.V. HOLDEN. 1971a. Alias-free sampling of neuronal spike trains. *Kybernetik 8*: 165.

FRENCH, A.S., and A.V. HOLDEN. 1971b. Frequency domain analysis of neurophysiological data. *Comput. Prog. Biomed. 1*: 219.

FRENCH, A.S., A.V. HOLDEN, and R.B. STEIN. 1972. The estimation of the frequency response function of a mechanoreceptor. *Kybernetik 11*: 15.

FURSHPAN, E.J., and D.D. POTTER. 1959. Transmission at the giant motor synapse of the crayfish. *J. Physiol., London 145*: 289.

FURSHPAN, E.J., and D.D. POTTER. 1968. Low resistance junctions between cells in embryos and tissue culture. In: *Current Topics in Developmental Biology*, edited by A.A. Moscona and A. Monroy. Academic Press: New York, Vol. 3: 95.

FURUKAWA, T., and E.J. FURSHPAN. 1963. Two inhibitory mechanisms in the Mauthner neurons of goldfish. *J. Neurophysiol. 26*: 140.

GILULA, N.B., O.R. REEVES, and A. STEINBACH. 1972. Metabolic coupling, ionic coupling and cell contacts. *Nature 235*: 262.

GOODENOUGH, D.A., and J.-P. REVEL. 1970. A fine structural analysis of intercellular junctions in the mouse liver. *J. Cell Biol. 45*: 272.

GOODENOUGH, D.A., and N.B. GILULA. 1974. The splitting of hepatocyte gap junctions and zonulae occludentes with hypertonic disaccharides. *J. Cell Biol. 61*: 575.

GOODENOUGH, D.A., S. ITO, and J.-P. REVEL. 1968. Electron microscopy of early cleavage stages in *Arbacia punctulata*. *Biol. Bull. 135*: 421.

GOODENOUGH, D.A., and W. STOECKENIUS. 1972. The isolation of mouse hepatocyte gap junctions. Preliminary chemical characterization and X-ray diffraction. *J. Cell Biol. 54*: 646.

GOODWIN, B.C., and M.H. COHEN. 1969. A phase shift model for the spatial and temporal organization of developing systems. *J. Theoret. Biol. 25*: 49.

GOSHIMA, K. 1969. Synchronized beating and electrotonic transmission between myocardial cells mediated by heterotypic strain cells in monolayer culture. *Exp. Cell Res. 58*: 240.

GOSHIMA, K. 1970. Formation of nexuses and electrotonic transmission between myocardial cells and Fl cells in monolayer culture. *Exp. Cell Res. 63*: 124.

HAGIWARA, W., and H. MORITA. 1962. Electrotonic transmission between two nerve cells in leech ganglion. *J. Neurophysiol. 25*: 721.

HAMBURGER, V. 1960. *A Manual of Experimental Embryology*. University of Chicago Press, Chicago, Illinois.

HEPPNER, D.B., and R. PLONSEY. 1970. Simulation of electrical interaction of cardiac cells. *Biophys. J. 10*: 1057.

ITO, S., and N. HORI. 1966. Electrical characteristics of *Triturus* egg cells during cleavage.

ITO, S., and W.R. LOEWENSTEIN. 1969. Ionic communication between early embryonic cells. *Dev. Biol. 19*: 228.

JAMOKOSMANOVIC, A., and W.R. LOEWENSTEIN. 1968. Intercellular communication and tissue growth. III. *J. Cell Biol. 38*: 556.

JENKINS, G.M., and D.G. WATTS. 1968. *Spectral Analysis and Its Applications*. Holden-Day: San Francisco.

JOHNSON, R.G., and J.D. SHERIDAN. 1971. Junctions between cancer cells in culture: ultrastructure and permeability. *Science 174*: 717.

KANNO, Y., and W.R. LOEWENSTEIN. 1966. Cell-to-cell passage of large molecules. *Nature 212*: 629.

KANNO, Y., and H. MATSUI. 1968. Cellular uncoupling in cancerous stomach epithelium. *Nature 218*: 775.

KALT, M.R. 1971a. The relationship between cleavage and blastocoel formation in *Xenopus laevis*. I. Light microscope observations. *J. Embryol. Exp. Morph. 26*: 37.

KALT, M.R. 1971b. The relationship between cleavage and blastocoel formation in *Xenopus laevis*. II. Electron microscope observations. *J. Embryol. Exp. Morph. 26*: 57.

KALT, M.R., and B. TANDLER. 1971. A study of fixation of early amphibian embryos for electron microscopy. *J. Ultrastruct. Res. 36*: 633.

KENEKO, A. 1971. Electrical connexions between horizontal cells in the dogfish retina. *J. Physiol., London 213*: 95.

KUFFLER, S.W., and D.D. POTTER. 1964. Glia in the leech central nervous system: physiological properties and neuron-glia relationship. *J. Neurophysiol. 27*: 290.

LATHI, B.P. 1965. *Signals, Systems and Communications*. John Wiley: New York.

LOEWENSTEIN, W.R. 1967. Cell surface membranes in close contact. Role of calcium and magnesium ions. *J. Colloid Interface Sci. 25*: 34.

LOEWENSTEIN, W.R., and R.D. PENN. 1967. Intercellular communication and tissue growth. II. Tissue regeneration. *J. Cell Biol. 33*: 235.

LOEWENSTEIN, W.R., M. NAKAS, and S.J. SOCOLAR. 1967. Junctional membrane uncoupling. Permeability transformations at a cell membrane junction. *J. Gen. Physiol. 50*: 1865.

LOEWENSTEIN, W.R. 1966. Permeability of membrane junctions. *Ann. N.Y. Acad. Sci. 137*: 441.

LOEWENSTEIN, W.R. 1967. On the genesis of cellular communication. *Dev. Biol. 15*: 503.

LOEWENSTEIN, W.R. 1968. Communication through cell junctions. Implications in growth control and differentiation. *Dev. Biol., Suppl. 2*: 151.

LOEWENSTEIN, W.R., S.J. SOCOLAR, S. HIGASHINO, Y. KANNO, and N. DAVIDSON. 1965. Intercellular communication: renal, urinary bladder, sensory and salivary gland cells. *Science 149*: 295.

LOEWENSTEIN, W.R., and Y. KANNO. 1964. Studies on an epithelial (gland) cell junction. I. Modifications of surface membrane permeability. *J. Cell Biol. 22*: 565.

LOEWENSTEIN, W.R., and Y. KANNO. 1967. Intercellular communication and tissue growth. I. Cancerous growth. *J. Cell Biol. 33:*

LEITZ, T.L., and J.P. TRINKAUS. 1971. Differentiation of the junctional complex of surface cells in the developing *Fundulus* blastoderm. *J. Cell Biol. 48*: 455.

LOPRESTI, V., E.R. MACAGNO, and C. LEVINTHAL. 1974. Structure and development of neuronal connections in Isogenic organisms: Transient gap junctions between growing optic axons and lamina neuroblasts. *Proc. Natl. Acad. Sci. U.S. 71*: 1098.

MARTINEZ-PALOMO, A. 1970. The surface coats of animal cells. *Int. Rev. Cytol. 29:* 29.

McCALLA, W.J., and D.O. PEDERSON. 1971. Elements of computer-aided circuit analysis. *IEEE Trans. Circuit Theory CT-18*: 14.

McNUTT, N.S., and R.S. WEINSTEIN. 1970. The ultrastructure of the nexus. A correlated thin section and freeze cleave study. *J. Cell Biol. 47*: 666.

McNUTT, N.S., and R.S. WEINSTEIN. 1973. Membrane ultrastructure at mammalian intercellular junctions. *Prog. Biophys. Mol. Biol. 26*: 45.

MICHALKE, W., and W.R. LOEWENSTEIN. 1971. Communication between cells of different types. *Nature 232*: 121.

NAKAS, M., S. HIGASHINO, and W.R. LOEWENSTEIN. 1966. Uncoupling of an epithelial cell membrane junction by calcium ion removal. *Science 151*: 89.

NICHOLS, J.G., and D. PURVES. 1970. Monosynaptic chemical and electrical connections between sensory and motor cells in the central nervous system of the leech. *J. Physiol., London 209*: 647.

OLIVEIRA-CASTRO, G.M., and W.R. LOEWENSTEIN. 1971. Junctional membrane permeability. Effects of divalent cations. *J. Mem. Biol. 5*: 51.

PALMER, J.F., and C. SLACK. 1970. Some bio-electric parameters of early *Xenopus* embryos. *J. Embryol. Exp. Morph. 24*: 535.

PAPPAS, G.D., Y. ASADA, and M.V.L. BENNETT. 1971. Morphological correlates of increased coupling resistance at an electrotonic synapse. *J. Cell Biol. 49*: 173.

PAYTON, B.W., M.V.L. BENNETT, and G.D. PAPPAS. 1969. Temperature dependence of resistance at an electrotonic synapse. *Science 165*: 594.

PENN, R.D., and W.R. LOEWENSTEIN. 1966. Uncoupling of a nerve cell membrane junction by calcium-ion removal. *Science 151*: 88.

PORTER, K.R., G.J. TODARO, and V. FONTE. 1973. A scanning electron microscope study of surface features of viral and spontaneous transformants of mouse Balb/3T3 cells. *J. Cell Biol. 59*: 633.

POTTER, D.D., E.J. FURSHPAN, and E.S. LENNOX. 1966. Connections between cells of the developing squid as revealed by electrophysiological methods. *Proc. Natl. Acad. Sci. Y.S. 55*: 328.

REVEL, J.-P., and M.J. KARNOVSKY. 1967. Hexagonal array of subunits in intercellular junctions of the mouse heart and liver. *J. Cell Biol. 33*: C7.

ROSE, B. 1970. Junctional membrane permeability: Restoration by repolarizing current. *Science 169*: 607.

ROSE, B. 1971. Intercellular communication and some structural aspects of membrane junctions in a simple cell system. *J. Mem. Biol. 5*: 1.

ROSE, B., and W.R. LOEWENSTEIN. 1971. Junctional membrane permeability. Depression by substitution of Li for extracellular Na^+, and by long-term lack of Ca^{++} and Mg^{++}: Restoration by cell repolarization. *J. Mem. Biol. 5*: 20.

ROSE, B., and W.R. LOEWENSTEIN. 1975a. Permeability of cell junction depends on local cytoplasmic calcium activity. *Nature 254*: 250.

ROSE, B., and W.R. LOEWENSTEIN. 1975b. Calcium ion distribution in cytoplasm visualized by aequorin: Diffusion in cytosol restricted by energized sequestering. *Science 190*: 1204.

SANDERS, E.J., and P.K. SINGAL. 1973. Visualization of the outer and interblastomeric surface of early *Xenopus laevis* by scanning electron microscopy. *Micron 4*: 156.

SANDERS, E.J., and S.E. ZALIK. 1972. The blastomere periphery of *Xenopus laevis*, with special reference to intercellular relationships. *Wilhelm Roux' Arch. Entwicklungsmech. Org. 171*: 181.

SELMAN, G.G., and M.M. PERRY. 1970. Ultrastructural changes in the surface layers of the newt's egg in relation to the mechanism of its cleavage. *J. Cell Sci. 6*: 207.

SHERIDAN, J.D. 1966. Electrophysiological study of special connections between cells in the early chick embryo. *J. Cell Biol. 31*: C1.

SHERIDAN, J.D. 1968. Electrophysiological evidence for low-resistance intercellular junctions in the early chick embryo. *J. Cell Biol. 37*: 658.

SHERIDAN, J.D. 1970. Low resistance junctions between cancer cells in various solid tumors. *J. Cell Biol. 45*: 91.

SHERIDAN, J.D. 1971. Dye movement and low-resistance junctions between reaggregated embryonic cells. *Dev. Biol. 26*: 627.

SINGAL, P.K., and E.J. SANDERS. 1974. An ultrastructural study of the first cleavage of *Xenopus* embryos. *J. Ultrastruct. Res. 47*: 433.

SLACK, C., and J.F. PALMER. 1969. The permeability of intercellular junctions in the early embryo of *Xenopus laevis*, studied with a fluorescent tracer. *Exp. Cell Res. 55*: 416.

SLACK, D., and A.E. WARNER. 1973. Intracellular and intercellular potentials in the early amphibian embryo. *J. Physiol., London 232*: 313.

SOTELLO, C., and R. LLINAS. 1972. Specialized membrane junctions between neurons in the vertebrate cerebellar cortex. *J. Cell Biol. 53*: 271.

TERZUOLO, C.A. (editor) 1969. *Systems Analysis Approach to Neurophysiological Problems*. Univ. Minnesota, Minneapolis.

TUPPER, J.T., and J.W. SAUNDERS. 1971. Intercellular permeability in the early *Asterias* embryo. *Dev. Biol. 27*: 546.

WARNER, A.E. 1973. The electrical properties of the ectoderm in the amphibian embryo during induction and early development of the nervous system. *J. Physiol., London 235*: 267.

WATANABE, A., and A. GRUNDFEST. 1961. Impulse propagation at the septal and commissural junctions of crayfish giant axons. *J. Gen. Physiol. 45*: 267.

WILSON, D.M. 1961. The connections between the lateral giant fibers of earthworms. *Comp. Biochem. Physiol. 3*: 274.

WOLPERT, L. 1969. Positional information and the spatial pattern of cellular differentiation. *J. Theoret. Biol. 25*: 1.